8-2016

Dynamic Modeling and Renewable Integration Studies on the U.S. Power Grids

Gefei Kou
University of Tennessee, Knoxville, gkou@vols.utk.edu

To the Graduate Council:

I am submitting herewith a dissertation written by Gefei Kou entitled "Dynamic Modeling and Renewable Integration Studies on the U.S. Power Grids." I have examined the final electronic copy of this dissertation for form and content and recommend that it be accepted in partial fulfillment of the requirements for the degree of Doctor of Philosophy, with a major in Electrical Engineering.

<div align="right">Yilu Liu, Major Professor</div>

We have read this dissertation and recommend its acceptance:

Kevin Tomsovic, Hector Pulgar, Charles Collins

<div align="right">Accepted for the Council:
Dixie L. Thompson</div>

<div align="right">Vice Provost and Dean of the Graduate School</div>

(Original signatures are on file with official student records.)

Dynamic Modeling and Renewable Integration Studies on the U.S.
Power Grids

A Dissertation Presented for the
Doctor of Philosophy
Degree
The University of Tennessee, Knoxville

Gefei Kou
August 2016

Acknowledgements

This thesis is the culmination of five years of research on power system dynamics modeling and simulation. The completion of the work cannot be made possible without the support from many mentors and colleagues. My greatest debt is to my major advisor, Dr. Yilu Liu, who was the primary investigator on the projects and continuously offered academic mentorship and research directions. Her strategic thinking and openness to new ideas are always the source of inspiration.

The graduation committee, which includes Dr. Kevin Tomsovic, Dr. Hector Pulgar, and Dr. Charles Collins, offered invaluable technical suggestions and feedback. Their critiques are insightful and helped improve the quality of the work.

I also owe Stanton Hadley with the Oak Ridge National Laboratory a big thanks for managing the three year wind penetration study on the Eastern Interconnection. It was an enjoyable working experience to collaborate with the best talents at the national laboratory.

I was also privileged to work with a few great mentors, who have been a positive impact on my professional career. Dr. Chien-fei Chen invited me to join the Student Leadership Center (SLC) at the CURENT engineering research center and it was a lifetime learning experience. From the organizing of professional and social activities, I learned the courage to proactively take initiative and make a difference. Dr. Yanzhu "Kelly" Ye, Dr. Lang Chen, Dr. Penn Markham, Dr. Ye "Zoe" Zhang, and Dr. Yong "Frank" Liu provided a lot of help and gave me a jump start in the beginning of the Ph.D program. My colleagues are my most valuable treasure and constant source of new ideas.

Abstract

Wind and solar generation have gained a significant momentum in the last five years in the United States. According to the American Wind Energy Association, the installed wind power capacity has tripled from 25,410 MW in early 2009 to 74,472 MW as of the end of 2015. Meanwhile, solar photovoltaic (PV) is reported that its capacity has skyrocketed from 298 MW in 2009 to 7,260 MW in 2015 by the Solar Energy Industries Association. Despite the fact that wind and solar only make up 4.4% and 0.4% , respectively, of total electricity generation in 2014, the nation is right on its track to the Department of Energy (DOE)'s goal of 20% wind and 14% solar by year 2030. The future of renewable energy is aspiring.

The rapid growth in renewable generation results in an urge to studying the reliability implication of renewable integration. For this purpose, two DOE projects were funded to the University of Tennessee, Knoxville, and the Oak Ridge National Laboratory. The first project, Grid Operational Issues and Analyses of the Eastern Interconnection (EI), is aimed at studying the dynamic stability impact of high wind penetration on the U.S. EI system in year 2030. The second project, Frequency Response Assessment and Improvement of Three Major North American Interconnections due to High Penetrations of Photovoltaic Generation, concentrates on the influence of high solar penetration on primary frequency response.

This thesis documents the efforts of the above-mentioned two projects. Chapter 1 gives an introduction on power system dynamic modeling. Chapter 2 describes the process of dynamic models development. Chapter 3 discusses the adoption of synchro-

phasor measurement for system-level dynamic model validation and the impact of turbine governor deadband on system dynamic response. Chapter 4 presents a stability impact study of high wind penetration on the U.S. Eastern Grid. Chapter 5 documents the modeling and simulation of the EI system under high solar penetration. Chapter 6 summaries two dynamic model reduction studies on the EI system. Conclusions, a summary of the major contribution of the Ph.D. work, and a discussion of possible future work are given in Chapter 7.

Table of Contents

List of Tables

List of Figures

I.   Introduction

1.1 Power System Dynamic Simulation

Power system dynamic simulation is a prevailing tool in system planning and operation. It is widely used in the industry and academia to identify potential system stability risks, set operation transfer limits, evaluate dynamic system performance, and so forth. Because of its effectiveness, the North American Electric Reliability Corporation (NERC) mandates thorough and comprehensive dynamic simulation studies in transmission planning (TPL) and modeling (MOD) standards. In fact, dynamic simulation is the only tool that can verify the stability impact of a future build-out before it is physically implemented. Dynamic simulation can tackle numerous stability problems, including transient stability, frequency stability, oscillatory stability, and voltage stability. Depending on the concerned dynamics, simulation time frame can range from several cycles to several minutes. The main topic of this thesis is to explore the stability impact of wind and solar generation on the U.S. Eastern Interconnection (EI). Dynamic simulation is used to study power system frequency response, rotor angle stability, and inter-area oscillation stability.

1.2 The Eastern Interconnection Planning Collaborative

The Eastern Interconnection Planning Collaborative (EIPC) is a U.S. Department of Energy (DOE) funded project starting in 2010. The objective of this project is to model the impact on the grid of various policy options. Nineteen major planning authorities in the EI, including PJM Interconnection, Tennessee Valley Authority (TVA), ISO-New England, Midcontinent ISO, and New York ISO, participated in the project. The project

builds upon the current local and regional transmission planning processes within the entire EI system. The project contains two phases. In Phase 1, eight futures plus multiple sensitivities per future, for a total of 80 model runs, were developed for the EI 2030 grid based on Charles River Associates' (CRA) Multi-Region National (MRN) macroeconomic model and their North American Electricity and Environment Model (NEEM). The future scenarios include Business as Usual (BAU), National Carbon Constraint–National Implementation, National Carbon Constraint–Regional Implementation, Aggressive Energy Efficiency/Demand Response/Distributed Generation/Smart Grid, National Renewable Portfolio Standard–National Implementation, National Renewable Portfolio Standard–Regional Implementation (RPS/R), Nuclear Resurgence, and Combined Federal Climate and Energy Policy (CO2+). While the eight future scenarios are intended to represent distinct future grid development under various energy and environmental policy drives, sensitivities represent minor variations on each future scenario. Typical sensitivities can be load growth and natural gas prices. At the end of Phase 1, three final scenarios, considered to be balanced in terms of policy goals, levels of implementation, transmission build-outs, and total cost, were selected for transmission studies, reliability analysis, and production cost analysis in Phase 2. In Phase 2, the EI system was modeled at a very detailed level (70,000+ buses, 8,000+ generators) in the PSS/E model for a peak hour and off-peak hour in each case (only the peak hour in the BAU case). Variable generation levels were set at the average values for those blocks. The members of EIPC, in consultation with their stakeholder steering committee, first created a one-line diagram of the EI from their

respective long-range plans with some modifications. They then added the generators, loads, lines, and substations that they projected would be needed to approximately match the results from the Phase 1 cases for 2030. These models were run through PSS/E to first solve with all lines. Once the models gave a solution, various levels of NERC contingency criteria were applied and additional modifications were added to meet the criteria. This resulted in three peak hour and two off-peak hour steady-state PSS/E models covering the three scenarios. The resulting build-outs of the transmission system in these scenarios were then used to model the EI in the General Electric (GE) MAPS model run by CRA [1] [2].

To complement the steady-state study by the EIPC and understand the stability impact of high renewable on the EI system, the research team at the University of Tennessee, Knoxville, (UTK) and the Oak Ridge National Laboratory (ORNL) looked at building the dynamic counterpart, which can shed insights onto the following aspects:

- Transient stability: Transient stability is also referred as large-disturbance rotor angle stability. It is concerned with the ability of the power system to maintain synchronism when subjected to a severe disturbance. Instability is in the form of aperiodic angular separation due to insufficient synchronizing torque, manifesting as first swing stability. Instability may also occur in the form of increasing angular swings of some generators leading to their loss of synchronism with other generators. The time frame of interest is usually 3 to 5 seconds [3].

- Small signal stability: Small signal stability is concerned with the ability of the power system to maintain synchronism under small disturbances. The disturbances

are considered to be sufficiently small that linearization of system equations is permissible for purposes of analysis. Small signal stability is usually associated with insufficient damping of oscillations. The time frame of interest in small signal stability studies is on the order of 10 to 20 seconds following a disturbance [3].

- Frequency response: Frequency response, or primary frequency control, is designed to arrest and stabilize frequency in response to frequency deviations [4]. It plays an important role in system reliability that unsatisfactory frequency response can lead to involuntary under-frequency load shedding, damages on equipment, and even blackouts.

Wind generators profoundly differ from traditional synchronous units in the sense that they are asynchronous to the power grid and coupled through power electronics converters (Types 3 and 4). As a consequence, wind generators do not contribute to inertial response, which is the first line of defense that prevents frequency from large deviation. Higher wind penetration could result in higher rate of change of frequency and thus lower frequency nadir. Additionally, wind generators normally have governor response functions disabled and do not react during an under-frequency event. The non-responsiveness translates into reduced system frequency response and deteriorates system stability.

To evaluate the impact of wind generation on the EI system's performance on frequency response, rotor angle stability, and inter-area oscillatory stability, the research team spent three year since 2012 on the EI 2030 dynamic modeling project. The project started off by developing EI dynamic models based on the power flow models from the

EIPC project. Then, to make sure the baseline models are accurate in reflecting the real system's behavior, synchro-phasor measurements are utilized for model validation. With proper model tuning and calibration, the validated baseline models achieve satisfactory accuracy levels. At the final stage of the project, simulation studies were conducted to compare the high wind case against the baseline case on three aspects: frequency response, synchronous generator transient stability margins, and inter-area oscillation damping. The model building, validation, and analysis are documented in Chapters 2, 3, and 4.

1.3 The SunShot Initiative Project

The SunShot initiative is a research program managed by the U.S. DOE Solar Energy Technologies Office. The mission of the program is to make solar energy fully cost-competitive against traditional energy sources by 2020. The targeted goal is to drive down the cost of solar electricity to $0.06 per kilowatt-hour (kWh) or $1 per watt (W) for utility-scale photovoltaics (PV) systems, $1.25/W for commercial rooftop PV, $1.50/W for residential rooftop PV, and $3.60/W for concentrating solar power (CSP) systems with up to 14 hours of thermal energy storage capacity. All costs do not include incentives.

The SunShot Vision Study provides an in-depth assessment of the potential for solar technologies to meet a substantial percentage of electricity generation in the U.S. over the next two to four decades [5]. The study assumes the price of solar technologies declines by about 75% between 2010 and 2020, which is in line with the U.S. DOE SunShot Initiative's target. The study uses the National Renewable Energy Laboratory's (NREL)

Regional Energy Deployment System and Solar Deployment System models to build and evaluate future scenarios. By factoring in key parameters, including solar resource quality, cost of electricity, transmission requirements, reserve requirements, variability impacts, and projected fuel prices, it is projected that solar generation, both PV and CSP, will satisfy roughly 14% (11% PV + 3% CPS) of the nation's electricity demand by 2030 and 27% (19% PV + 8% CPS) by 2050. It is also concluded that the envisioned level of solar deployment poses significant but not insurmountable technical challenges with respect to grid integration and could require substantial changes to system planning and operation practices.

One of the major technical challenges in operation lies on power system frequency regulation. Unlike conventional generation like gas and hydro, solar generation does not have inherent inertial response and its governor response is normally disabled. Therefore, the increasing level of solar generation and the de-commissioning of conventional plants will result in wider or even extreme frequency excursions after sudden large power mismatch and thus put system stability into risks.

In response to the frequency response degradation issue, the joint research team at UTK, ORNL, NREL, and General Electric (GE) has been conducting a SunShot National Laboratory Multiyear Partnership project since early 2016. The goal of the project is to estimate primary frequency response performance at higher PV penetration levels of the three major North American power grids, i.e. EI, WECC, and ERCOT, identify potential frequency stability risks, and propose and verify PV based mitigation measures. The study is based on dynamic simulation studies on interconnection-level power system

models. The stability impact of PV generation is represented by modeling PV panels and converters at the plant level. The accuracy of the simulation study is ensured by building upon measurement validated baseline models and using the GE PV plant dynamic model. The model development, validation, and preliminary analysis are documented in Chapter 5.

II.   Development of Power System Dynamic Models

In order to predict a power system's dynamic response to a disturbance, modeling the dynamic behavior of synchronous generators, excitation systems, turbine governors, and many other dynamic components is necessary. In dynamic simulation, the dynamics are described using differential and algebraic equation. Depending on physical design and control logic, a specific component can be represented by a built-in dynamic model type, such as the salient pole synchronous generator model (GENSAL) or the generic thermal turbine governor model (TGOV1). Sometimes, a dynamic component cannot be represented by any off-the-shelf model types and thus has to be modeled by a user-defined model. Besides the model type, a set of model parameters has to be prepared to adequately depict a component's dynamic characteristics. Depending on the model, the parameter set can include design parameters like machine reactance or control parameters like excitation transient gain. A valid dynamic file contains both component model types and parameter sets of any online dynamic equipment. However, the availability of the dynamic file is solely the minimum requirement for a successful dynamic run.

This effort described in this chapter is to solve a specific problem: How to build the dynamic model for a given power flow case without dynamic parameters or with partial dynamic parameter sets. The model development process involves power flow tuning, creating generic dynamic component models, and integrating real dynamic parameters. Special attentions are given to generic parameter selection, convergence check, and model validation. This dynamic model development effort was stimulated by the EI 2030 project. Since stability studies were out of the EIPC's study scope, the high wind and

BAU scenarios came without corresponding dynamic component models and parameters. The EI model is used below to demonstrate the principle of the process. But this process is generic and can be, and was, used in many other power flow models.

2.1 The U.S. Eastern Interconnection (EI)

The Eastern Interconnection is one of the three major alternating current (AC) power grids. The EI system reaches from Central Canada eastward to the Atlantic coast (excluding Québec), south to Florida and west to the Rockies, as shown in Figure II-1. All of the electric utilities in the EI are electrically synchronized during normal system conditions. The projected peak total internal demand for summer 2016 is 613,581 MW [6]. With over 70,000 buses and 8,000 generators, the EI power flow and dynamic models are known for its sheer volume and complexity.
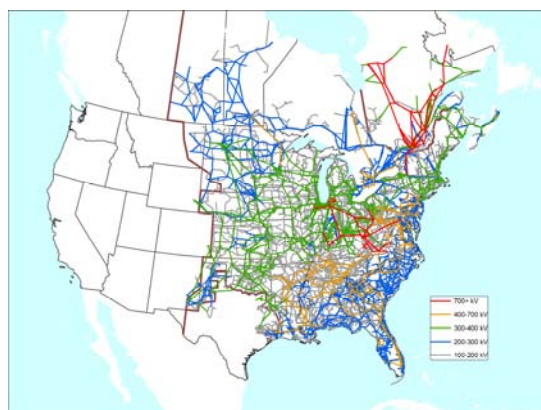
Figure II-1 EI Transmission Network

The interconnection-level EI transmission planning models are developed by the Eastern Interconnection Reliability Assessment Group (ERAG) Multiregional Modeling Working Group (MMWG). The group includes direct representation from the regions in

the EI and is charged with the responsibility for developing and maintaining a series of power flow and dynamics base cases for the benefit of ERAG members. Each case provides detailed steady state and dynamic representation of the bulk electric system behavior for a specific planning scenario. The interconnection of regional networks is realized by the development of a technique to merge selected portion of several power flow models. This allows each group of systems to function independently when preparing a power flow model. Regional coordinates are responsible for submitting dynamics data for their member systems. The overarching goal of MMWG is to provide power flow and dynamics simulation cases that can realistically simulate steady state and dynamic bulk electric system behavior. With accurate model representations, the performance of the EI system can be evaluated [7].

2.2 Power Flow Tuning

The EI 2030 power flow models, including the BAU, high wind high build-out, and mid wind mid build-out scenarios, were prepared by the EIPC study group and have no dynamics data. For the purpose of simulating dynamic behaviors, generic dynamics parameters along with real dynamics parameters were prepared as described below. It was noticed that the correctness of power flow data could have a determining influence on the success of dynamic simulation. Below records some best practices that can improve the successful initialization and numerical integration convergence.

2.2.1   High Voltage Direct Current (HVDC)

Forty High-Voltage Direct Current(HVDC) transmission lines have been modeled

connecting to Hydro Quebec, Western Electricity Coordinating Council(WECC), Electric

Reliability Council of Texas (ERCOT), and within the EI. As the HVDC and its control

are out of scope at the first stage, HVDC is equivalent to positive and negative constant

power load on the sending and receiving ends, respectively.

2.2.2   Switched Shunt

There are 6396 switched shunts in the model. However, due to the poor convergence

of the switched shunt dynamic model, they are assumed to be locked. Locked switched

shunts have constant capacitance/inductance during the dynamic simulation.

2.2.3   Machine Rating - MBase

MBase is a variable that represents the machine capacities in MVA. Its value does not

affect a steady-state power flow run and so was not validated in the original EIPC runs.

However, all machine-related dynamic models, including generator, exciter, turbine

governor, and power system stabilizers (PSS), use MBase as their base for power. In

other words, per unit values of the machine-related dynamic model are based on MBase.

Therefore, a random MBase can cause inaccurate simulation results.

MBase should be set about the same as the machine capacity. However, a random

value may have been assigned inadvertently during the EIPC static analysis. In some

situations in the EI 2030 model the MBase is smaller than the actual machine power

output. To ensure the correctness of simulation results, the original MBase is replaced

with the value equal to 1.1 times that of the machine's apparent power output. This gives a good estimation of the actual machine capacity.

2.2.4 Machine Sub-transient Reactance - X_{source}

X_{source} is the machine internal reactance. It does not affect static power flow results. In dynamic simulations, when GENCLS is used, X_{source} is the equivalent voltage source reactance. When other detailed generator models are used, X_{source} should be equal to sub-transient reactance X''. Therefore, attention should be paid to ensure $X_{source} = X''$.

2.2.5 Converting Machines to Negative Load

In some cases, the generator cannot stabilize in a flat run. It is suggested that GENCLS be used as the generator model or that the machine be converted into a negative load.

2.2.6 Identification of Generator Types

In a static power flow, a specific type of generating unit (including the models for its generator, exciter, turbine governor, and PSS) is not needed. As a result, the EIPC did not specify the technology (hydro, steam, combustion turbine, wind, etc.) for every generator in the model. We matched the names of units from the model to those in various databases available (e.g., MMWG or Multiregional Modeling Working Group) cases from Energy Visuals, EIA Form 860 data from Energy Information Administration) in order to assign technology types. Many plants did not exist in these databases since they were added specifically for the EIPC 2030 cases. Some information in the EIPC case files helped to identify the plants; others required engineering judgment based on size, capacity factor, and location. As part of this effort, latitude and longitude estimates were

set for each generating unit and all buses above 200 kV. These data are useful for

geographical visualization when data is ported to the PowerWorld simulator.

2.2.7   Load Conversion

To build a valid power flow case, HVDCs and unstable machines are converted to

equivalent load. MBase and X_source are adjusted. A power flow run is recommended

even if the case is already solved. Afterwards, the load conversion is performed. A

typical load composite is 50% constant current and 50% constant impedance. Finally, the

switched shunt control mode is changed to the locked mode.

2.3 Generic Dynamics Model Type

The transient simulation process integrates three steps: first, differential algebraic

equations (DAEs), describing the dynamic behavior of physical devices and the

transmission network, are formulated. Second, a set of constant and variable parameters

that describe the detailed condition of the physical components are determined. Initial

conditions of DAEs are obtained by the power flow solution. Next, numerical integration

methods are applied to the DAEs formulated in the first step along with the parameters

and initial conditions determined in the second step [8]. The general form of transient

response calculation can be expressed in the following form [9]:

$$\dot{x} = f(x,V) \tag{2-1}$$

$$I = Y \cdot V \tag{2-2}$$

Where x is the state variable of synchronous generators, excitation, turbine governors,

wind machines, HVDC, and other dynamic devices. V and I are node voltage and current

vectors. Y is the node admittance matrix of the network structure. Equations (2-1) and (2-

2) can be solved either by a partitioned-solution approach or a simultaneous-solution approach [10].

The commercial-grade transient simulation solvers, such as PSS/E by Siemens PTI, PSLF by GE, and TSAT by Powertech, facilitate the automated formulation of the system dynamic equations, integration of power flow solutions, and numerical computations. To enable a successful transient simulation run, the user only needs to choose the appropriate dynamic model and determine a set of model parameters required by the model. Note that the dynamic model parameters are not necessary for power flow solutions and need to be obtained either from manufactures' data or by field tests.

When constructing the EI 2030 dynamic model, no dynamic parameters were readily available. Even if some current model parameters were accessible, there is no guarantee of data accuracy for a system with more than 70,000 buses and 8,000 machines, let alone the infrastructure to be built in the future. Therefore, our attempt is to create the dynamic model with generic parameters so that the future grid can be simulated as closely as possible. To this end, a software framework is built to automatically create the dynamic model based on power flow solutions. A trial-and-error process is adopted to continuously tune the model parameter so that the simulated frequency responses match with the measurement.

The actual EI grid contains an enormous amount of dynamic components, such as generators, excitation systems, turbine governors, and load. To accurately simulate the system response to any perturbation, efforts have been made to model the variations within each model category. The following section lists the dynamic models used in the

EI 2030 model. It should be mentioned that the models comply with the PSS/E nomenclature [8]. The round rotor generator model (GENROU) for thermal plants and the salient pole generator model (GENSAL) for hydro plants are represented. The voltage-behind-reactance model (GENCLS) is also used in case successful machine initialization cannot be reached.

The excitation system serves the function of voltage and reactive power control. The types of excitation system installed fall into a broad range of categories, including DC excitation systems, AC excitation systems, and static excitation systems [11] [12]. DC excitation systems have given way to the other two, characterized by fast acting and high gain. To capture the principal dynamic features of modern excitation systems while not being limited to the detailed design, the simplified excitation system mode (SEXS) is adopted [8]. Excitation time constant T_E, gain K, over-excitation limit E_{max} set by generator field winding thermal constraint, and under-excitation limit E_{min} set by the stability constraint or the stator core end-region heating limit provide a general depiction of the excitation system. The compensator provides a transient gain reduction of T_A/T_B, which allows satisfactory performance on the full frequency spectrum. The control diagram is shown in Figure II-2.
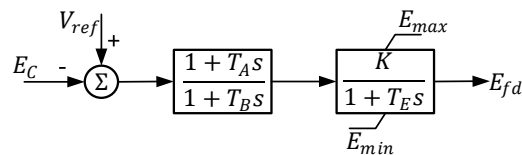
Figure II-2 Control Diagram of the Simplified Excitation Model (SEXS)

The turbine governor system is essential to real power and frequency control. The dynamic performance may differ vastly depending on the type of turbines, including steam, hydro, and gas. To represent variations in turbine governor systems, several types of turbine governor models are considered. TGOV1 is a simplified representation of steam turbine governors (Figure II-3). Governor action, re-heater time constant, and the ratio of high-pressure turbine are recognized in this model. IEEE type 1 (IEEEG1) turbine governor model is used to represent steam turbines in a wide range of designs including non-reheat, tandem compound, and cross-compound types (Figure II-4). The hydro turbine governor is represented by HYGOV, which models the penstock with unrestricted head race and tail race, but no surge tank. GAST is used to characterize gas turbine-governor systems. References [8], [11], and [13] give detailed descriptions of the models aforementioned.

It has been observed that the measured frequency governing response in the EI system is considerably less than that of simulated response [14] [15]. In [16], it is argued that governor deadband can contribute to the decline of governor response. To take into account the governor deadband, the IEEE type 1 turbine governor model with deadband, WSIEG1 [8], is adopted for extended frequency response studies. Its control diagram is illustrated in Figure II-5.

Constant admittance/current/power (ZIP) load modeling approach is widely used in industry practice [17]. However, ZIP load assumes a static (algebraic) correlation between load power and bus voltage, which apparently neglects the dynamics of component devices such as induction motors, discharge lighting, and saturated
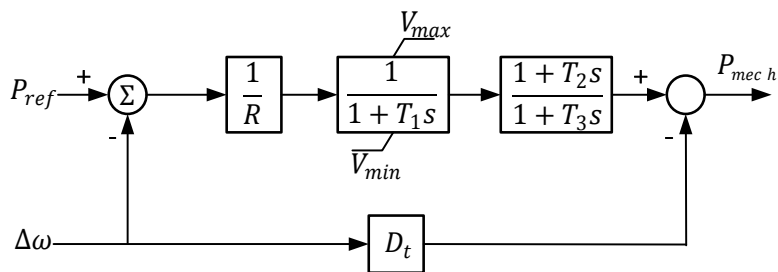
Figure II-3 Control Diagram of TGOV1
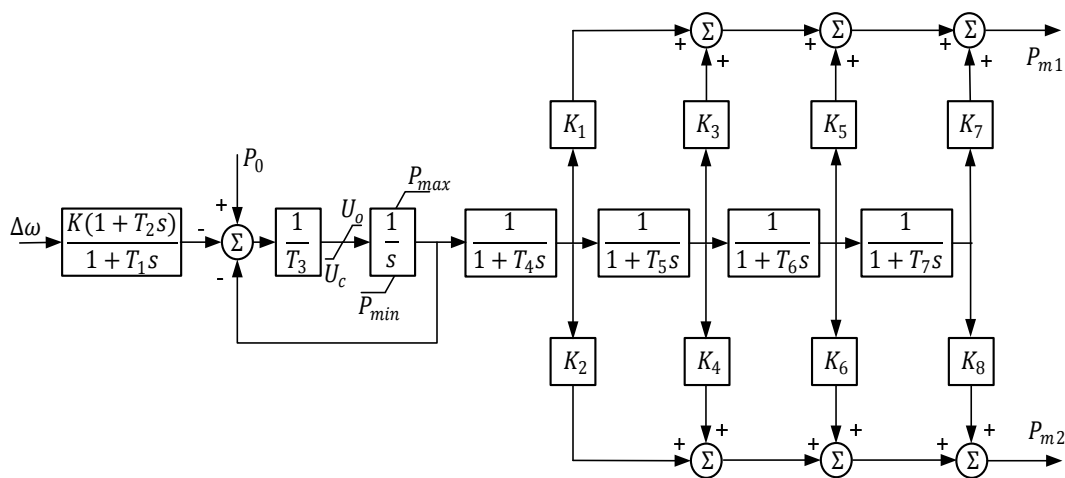
Figure II-4 Control Diagram of IEEEG1
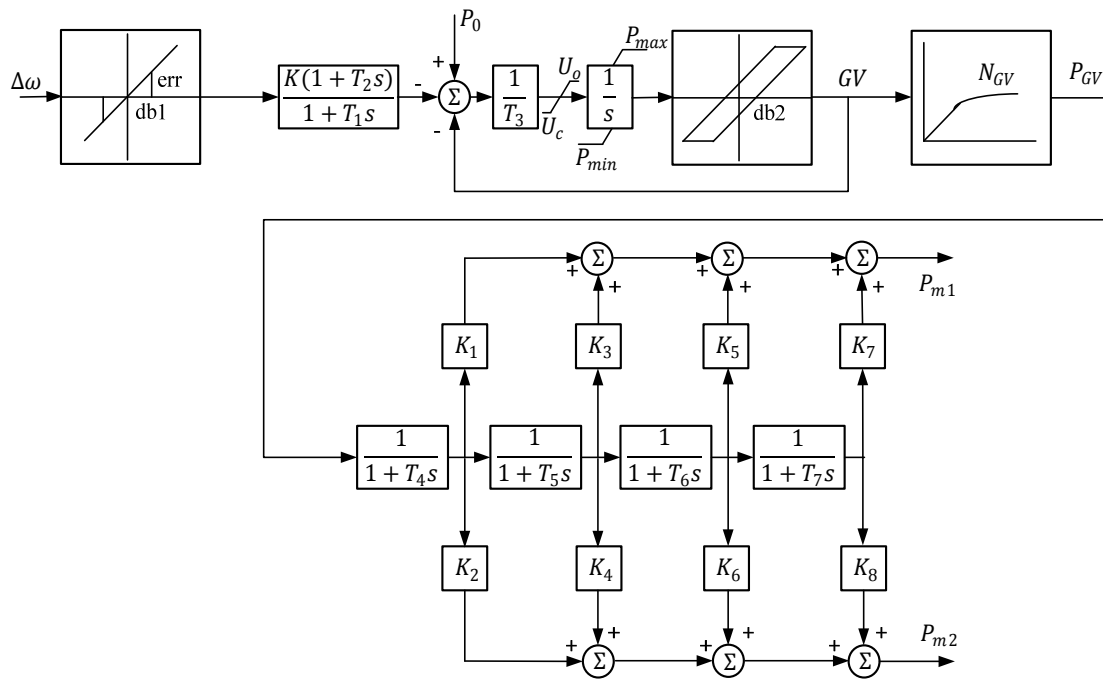
Figure II-5 Control Diagram of WSIEG1

transformers. It is reported that detailed dynamic load modeling approaches render more accurate simulation results than the static modeling approaches [18] [19]. Therefore, the EI 2030 dynamic model adopts both a ZIP load model and complex load model (CLOD [8]), which represents motors, discharging lighting, saturated transformers, and static load (Figure II-6). It should be noted that the models used above help build the base case. To represent the system in greater details, more comprehensive models can be added.

$$\frac{R + jX}{P_o}$$

| M | M | Discharge Lighting | Transformer Saturation | Constant MVA | $P = P_{ro} \cdot V^{K_p}$ $Q = Q_{ro} \cdot V^2$ |

Large Motors   Small Motors   Remaining Loads
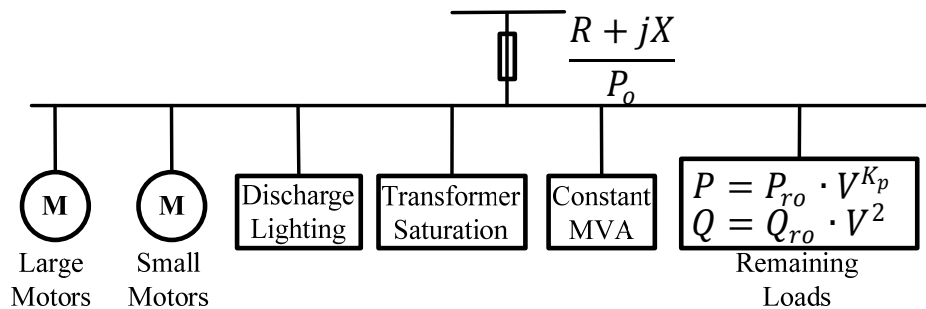
Figure II-6 CLOD Model

2.4 Generic Dynamics Model Parameter

Another issue that had to be addressed is the model parameters. Credible model parameters are indispensable to the fidelity of simulation results. However, most model parameters are either unavailable or nonexistent for future infrastructures. To resolve this issue, the generic parameter approach is adopted.

According to References [9] and [11], the generators' parameters fall into a narrow range. References [12] and [13] provide typical parameters on excitation and turbine governor systems. A statistic study is conducted to survey the variations in dynamic parameters from the current EI dynamics model.

It is concluded that most dynamic parameters converge to a typical value with a small amount of outliers. Figure II-7, Figure II-8, and Figure II-9 present variations of some common machine parameters. It is observed that the design parameters like machine reactance tend to fall in a small value range, while control parameters, which are determined by field tests, may vary. However, even though the generic model approach may not simulate the real system in a perfect match, it is useful to establish a reasonable starting point for dynamic simulation and integrating real parameters. A set of typical dynamics parameters for GENROU, SEXS, and TGOV1 is given in Table II-1, Table II-2, and Table II-3.

2.5 GenDyn Framework

Transient simulation requires the dynamic parameter set. Therefore, a computer program is necessary to realize the following functions.

• Read and parse power flow solution: collect static components that require a dynamic model in transient simulation; and correct erroneous data.

• Assign dynamic models and generic parameters to dynamic components.

• Output the dynamic parameter file in certain format, for example, .dyr in PSS/E.

Additionally, it is desirable that the program features modularity, which allows parsing and writing data in different formats and extending of model libraries. To this end, a computer program named GenDyn is created in Python and adopts an object-oriented programming (OOP) approach. Additional information is available in [20] regarding the application of OOP to power system modeling.
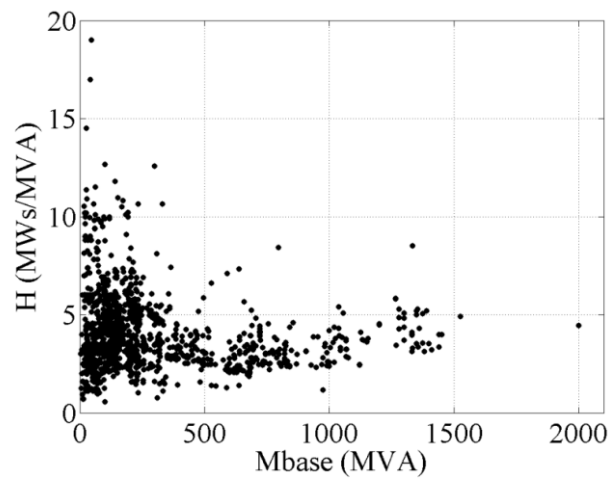
Figure II-7 Machine Inertia Variation
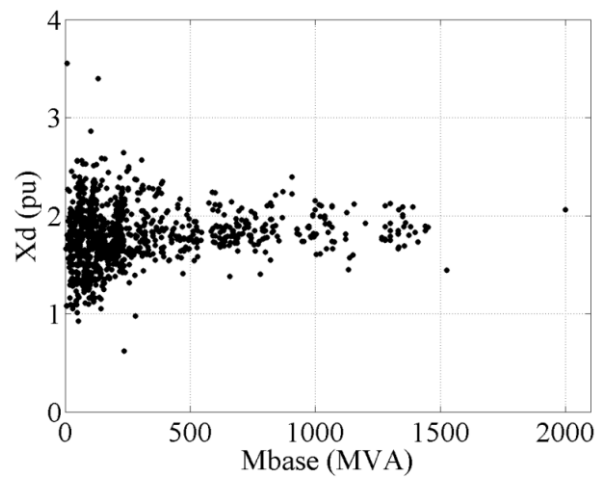
Figure II-8 Machine *d*-axis Synchronous Reactance Variation
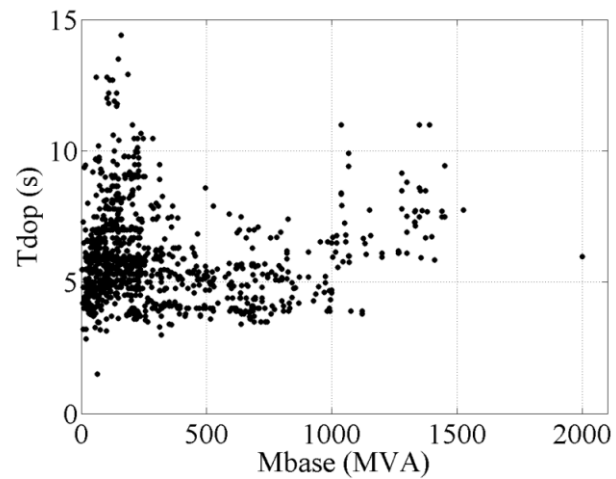
Figure II-9 Machine *d*-axis Open Circuit Transient Time Constant Variation

Table II-1 Typical GENROU Parameters

Parameter	Value
T'_{do} (sec)	6.0
T''_{do} (sec)	0.5
T'_{qo} (sec)	1.0
T''_{qo} (sec)	0.05
H, Inertia	3.94
D, Speed damping	0.0
X_d	1.4
X_q	1.35
X'_d	0.3
X'_q	0.6
$X''_d = X''_q$	0.2
X_l	0.1
$S_{(1.0)}$	0.03
$S_{(1.2)}$	0.4

Table II-2 Typical SEXS Parameters

Parameter	Value
T_A/T_B	0.1
T_B (>0) (sec)	10.0
K	100.0
T_E (sec)	0.1
E_{MIN} (pu on E_{FD} base)	-4.0
E_{MAX} (pu on E_{FD} base)	5.0

Table II-3 Typical TGOV1 Parameters

Parameter	Value
R	0.05
T_1 (sec)	0.5
V_{MAX}	1.0
V_{MIN}	0.0
T_2 (sec)	6.0
T_3 (sec)	6.0

Figure II-10 illustrates the framework of GenDyn. It first reads the power flow data through the data parser and feeds the generator class with machine identifiers, power generation, power limits, and other operation data. The generator class also stores the machine, exciter, turbine governor, and power system stabilizer (PSS) model. By default, GENROU, SEXS, and TGOV1 are assumed. A separate input file changes the default models for generators that require non-default settings. For instance, the hydro units are represented with GENSAL and HYGOV. Afterwards, the dynamic component class is created to each type of dynamic model. The dynamic component class stores machine identifiers, assumed dynamic parameters, and static operation data if necessary. Finally, the dynamic parameters are output in a specific format.
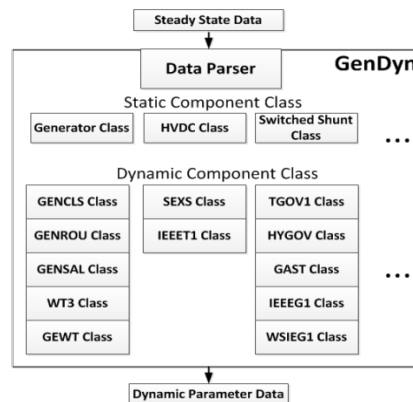
Figure II-10 GenDyn Framework

2.6 Convergence Check

Numerical divergence is the enemy of smooth dynamic simulations. To ensure that the built case is not suffering from numerical issues and provides valid results, a 20-second no-disturbance simulation is performed on each case. As no disturbance applies,

the system is supposed to stay static such that any variable is constant. However, if erroneous data exist and cause numerical issues, the system will drift from the steady state.

2.7 Integrating Real Dynamic Parameters

The EI 2030 grid is modeled at a very detailed level with a size of 70,000+ buses and 8,000+ generators. The power plants are broadly categorized in fuel types and generation technologies. In each type of power plant, the corresponding dynamic models, including generator, exciter, and turbine governor models can vary in complexity. Figure II-11, Figure II-12, and Figure II-13 show the MMWG dynamics models that can be mapped into the EI 2030 model, whose generation capacity of 560 GW and 60% of the generation units can be associated with real dynamic data.

The real dynamic data has to be verified and corrected in order to reach a successful simulation run. The data verification process can be grouped into two categories, i.e. the erroneous data correction and the operating limit relaxation.

The erroneous data result from various sources, such as the misunderstanding of the dynamic parameter and human mistakes. The consequences range from dynamic simulation initialization failures to inaccurate simulation results. To eliminate erroneous data, the data scanning and parameter out-of-range check is performed. For design parameters, such as the machine reactance, the exciter time constant, and the steam turbine re-heater time constant, the values stay in a narrow range. Typical values are replaced if any violation occurs.
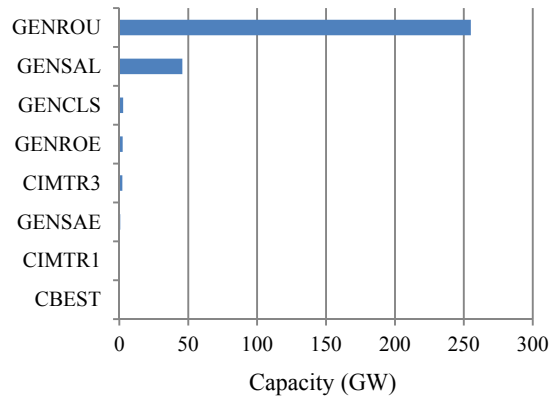
Figure II-11 Generator Model Type
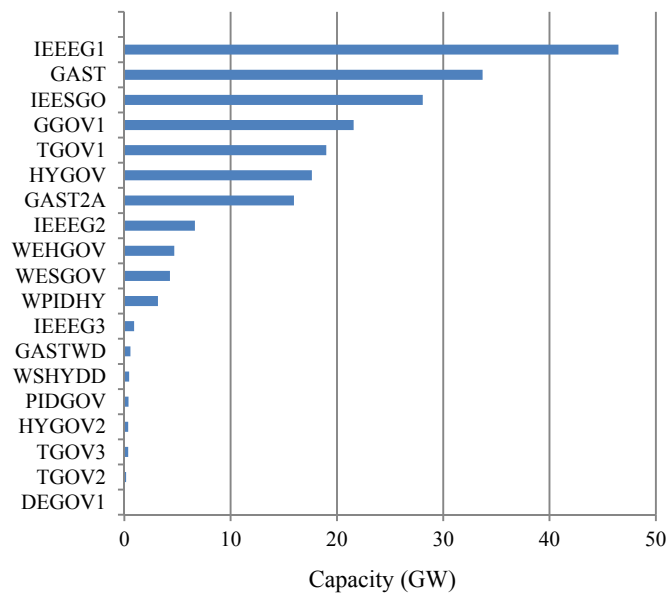
Figure II-12 Turbine Governor Model Types
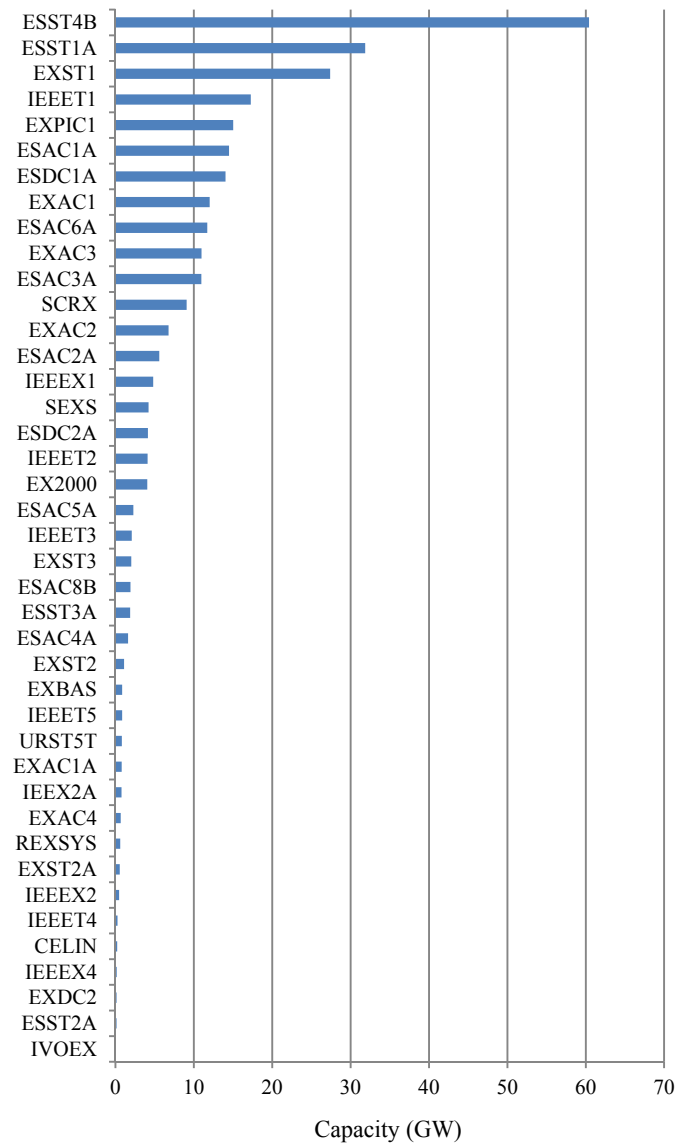
Figure II-13 Exciter Model Types

In addition, proper relationships have to be held between parameters. For instance, the inequality (2-3) cannot be violated for the machine reactance. Otherwise, numerical divergence could happen. For control parameters, such as the exciter phase compensation shown in Figure II-14, additional attentions have to be put on the parameter relationship. In the case of the exciter phase compensation, the transient gain reduction T_{lead}/T_{lag} has to be smaller than unity. Violation can result in unstable generator response as shown in Figure II-15. The assumed value of 0.1 is used when violations happen.

$$X_d > X_d' > X_d'' \tag{2-3}$$
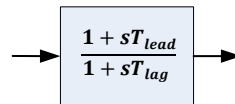
Figure II-14 The Exciter Phase Compensation Block

The data correction is closely related to the specific dynamic model and it is beyond the scope of this paper to document detailed checking criteria for every dynamic model. Table II-4 andTable II-5give examples on typical parameter ranges and proper relations. Additional information can be found in [8].

The exciters and turbine governors have physical limits in providing the field voltage and the mechanical power, respectively. The limits are represented by the upper and lower limit in the corresponding dynamic model. Since the generators in the EI 2030 grid could be re-dispatched and operating in a different loading condition, it happens that the same generator violates the original limits.
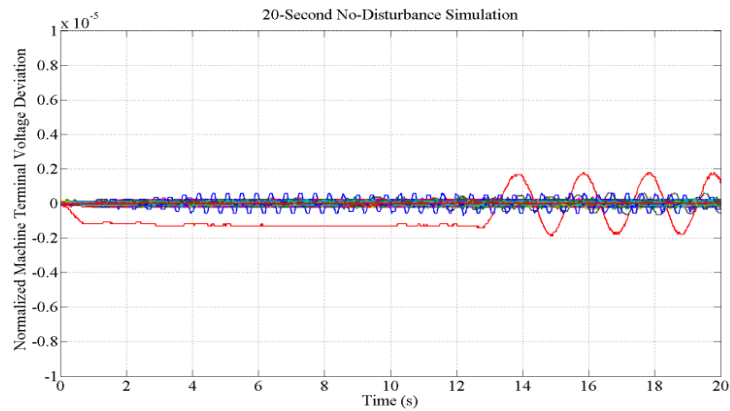
Figure II-15 Unstable voltage response in the flat run caused by $\frac{T_{lead}}{T_{lag}} > 1.0$

Table II-4 Typical Parameter Ranges

Model	Parameter	Typical Range
GENROU	X_d	0.90 - 2.60
SEXS	T_E	0.00 - 0.60
TGOV1	T_3	0.50 - 10.00

Table II-5 Proper Relations between Parameters

Model	Proper conditions	Correction if violated
GENROU	$X_d{}' > X_d{}''$	$X_d'' = 0.6 \cdot X_d{}'$
EXAC1	$T_{lead}/T_{lag} < 1.0$	$T_{lead} = 0.1 \cdot T_{lag}$
TGOV1	$T_2/T_3 \leq 1.0$	$T_2 = 0.4 \cdot T_3$

Another scenario is that since the limits are in per unit and normally rated at the machine MVA capacity, if the plant is expanded or partially de-committed, the machine loading condition will violate operating limits. The operating limit violation will result in simulation initialization failures.

To eliminate the operating limit violation, a pre-initialization process is conducted to calculate the loading condition. The loading condition is compared with the operating limits. If violations happen, a pre-set value of limits is assumed. Table II-6 gives an example on assumed operating limits.

Table II-6 Assumed Operating Limits when Violations Occur

Model	Parameter	Corrected value
IEEEG1	P_{max}	1.0
IEEEG1	P_{min}	0.3 or 0.0
SEXS	E_{max}	5.0
SEXS	E_{min}	0.0 or -3.0

For future plants, including wind farms that make up 17% of generation, the generic model approach is adopted. The exciter is represented by the simplified excitation model (SEXS), which captures the major characteristics of modern fast-acting high gain excitation systems. Steam turbine governors are represented by TGOV1 and IEEEG1, which recognize the governor droop and re-heater dynamics. Hydro and gas turbine governors are represented by HYGOV and GAST. The generic type 3 wind model and the GE wind model are used to represent wind machines. All generic models assume typical parameters.

A computer program, ParseDyn, is coded to automate the following functions:

- Read MMWG dynamic parameters.

- Scan the raw data and perform error data correction.

- Output the dynamic data file.

The framework of the program is shown in Figure II-16. The dynamic data parser first reads the raw dynamic data and feeds into each dynamic model class. The dynamic model class stores the parameter set for each type of dynamic models as well as the steady state parameters, such as the generator rating and the real power generation. Within each dynamic model class, methods are created to perform data scanning and correction. The dynamic data file is produced once all dynamic parameters are checked and refined.
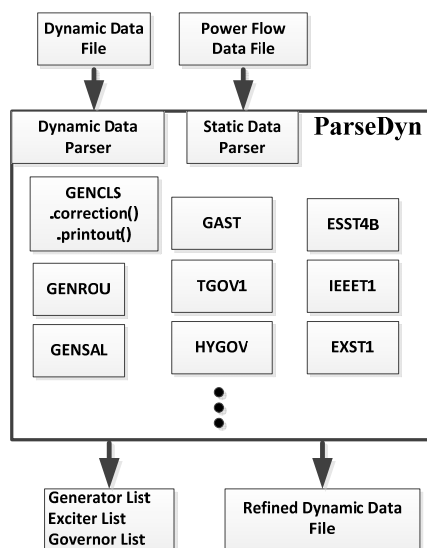
Figure II-16 ParseDyn Framework

The dynamic data for generic models is separately prepared by another program named GenDyn.

2.8 Initial Testing Simulation

The developed dynamic model is verified through three stages. In the first stage, the 20-second no-disturbance simulation (the flat run) is performed. The machine speed deviation and the machine terminal voltage are observed. The speed and voltage variations should be bounded under non-disturbance conditions. A satisfactory flat run are presented in Figure II-17 and Figure II-18. It is noted that the magnitude of variation is within the order of 10^{-6}. An unstable flat run indicates that the dynamic model is subjected to numerical instability or that the system is unstable. If the system shows stable response during the 20-second flat run, the second step is to apply typical contingencies system-wide, including generation trips, line faults, and bus faults. The purpose is to examine if the system can respond to the disturbance in the expected manner and to identify local unstable control loops. A generation trip example is graphed in Figure II-19. In order to build a realistic case, the constructed model is validated against the synchronized phasor measurement collected by the Frequency Monitoring Network (FNET/GridEye) [21]. Three major system parameters, i.e., the fraction of generation providing governor response (defined as K_t in [22]), the machine inertia, and the load composite ratio, are adjusted to resemble the real system dynamic behavior. Note that since the current EI system has very low wind penetration level, the EI 2030 model is indirectly validated against the current system by displacing the wind machines with conventional generators.
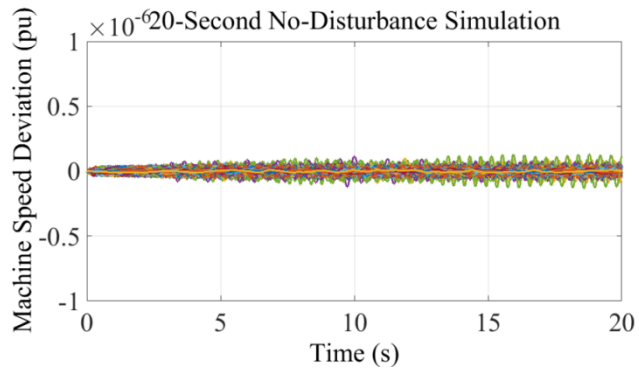
Figure II-17 Acceptable Machine Speed in Flat Run
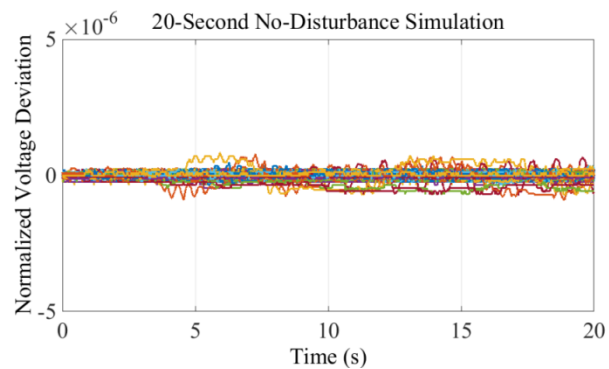
Figure II-18 Acceptable Machine Terminal Voltage Deviation in Flat Run
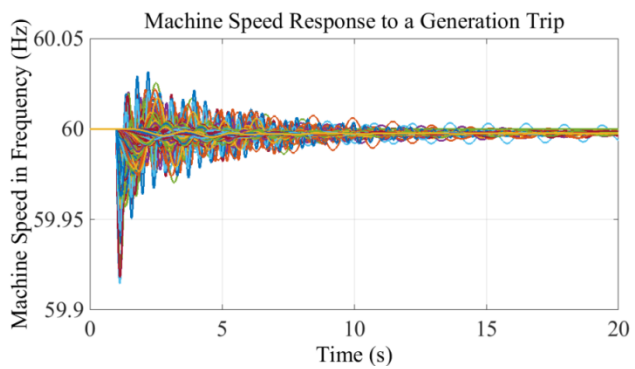
Figure II-19 System Response to a Generation Trip

The fraction of generation providing governor response (K_t) is the dominant factor on the settling frequency after the generation loss. In the MMWG models, most plants are modeled with providing governor response. In reality, nuclear plants and large fossil fuel plants are base-loaded and will not react to the frequency excursion. To simulate the correct settling frequency in the EI 2030 model, large steam turbine governors are turned off.

The system inertia is the sum of the kinetic energy stored in the rotating mass and determines the initial rate of frequency change. For the EI 2030 model, the system inertia can be expressed in (2-4), where subscript i indicates machines with real dynamic data and subscript j indicates machines with generic dynamic data. To resemble the inertial response, the inertia H of the generic model is uniformly adjusted.

$$The\ System\ Inertia\ (MW \cdot s) = \sum_i H_i \cdot MBase_i + \sum_j H_j \cdot MBase_j \qquad (2\text{-}4)$$

The load composite ratio is the fraction of constant power, constant current, and constant admittance load in real and reactive power, respectively. The load composite ratio plays a significant role in the system damping and therefore is tuned at the zonal and area level to reflect the system damping as close as possible. Figure II-20 illustrates the case study for a 1200 MW generation loss in North Carolina. The simulation result from the EI 2030 model shows acceptable resemblance to the measurement in terms of the settling frequency, the inertial response, and oscillation frequency.

2.9 Summary

Preparing dynamics models for a large scale power system can be a challenging task. Parameter unavailability or problematic data set makes dynamic simulation vulnerable to

unsuccessful runs and inaccurate simulation results. The contribution of the work in this

chapter is to develop a systematic method to prepare dynamics models for large scale

systems in an automatic manner so that converged dynamic simulation can be achieved.

However, there is no warranty that developed dynamics models are able to truly reflect

the system's behavior unless measurement based model validation is conducted. The

details on model validation are discussed in the next chapter.
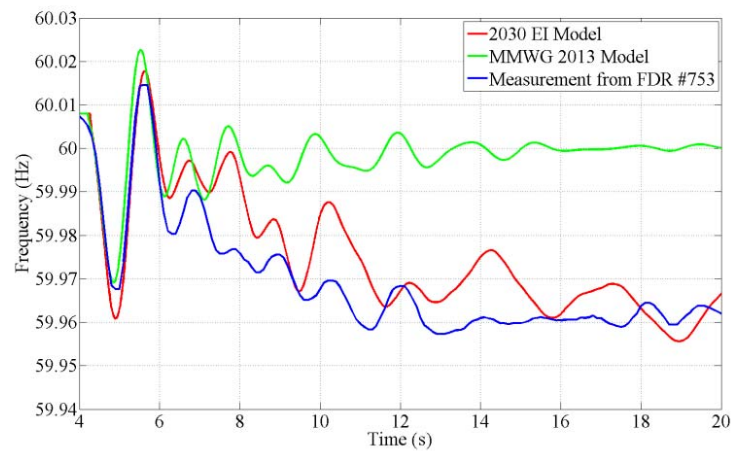
Figure II-20 Preliminary Model Validation Result

III.   Dynamic Model Validation of EI Dynamic Models

Power system operation and planning are heavily reliant on power flow and dynamic models. The operation models are used to perform contingency analysis and establish safe operating limits, while the planning models are employed to study grid expansion and resource integration. Lack of accurate simulation results lead to poor awareness of risks [23-25]. Therefore, the accuracy of power system models is of extreme importance to the reliable and economic operation of the power grid in both the short and long terms. To this end, the U.S. Federal Energy Regulatory Commission (FERC) directs in Order No. 693 Paragraph 1211 that the models shall be validated against actual system responses and if the model output is not within the accuracy required, the model shall be modified to achieve the necessary accuracy [26]. To improve model accuracy and address the FERC directives, the North American Electric Reliability Corporation (NERC) proposed and adopted several standards. MOD-026-1 requires the verification of the generator excitation control system model and the model parameters used in dynamic simulations through a staged test or a measured system disturbance [27]. MOD-027-1 requires verification of the turbine governor model and the model parameters used in dynamic simulation through tests or a system disturbance [28]. While MOD-032-1 requires submission of steady-state, dynamics, and short circuit data for interconnection-wide model construction, MOD-033-1 exists in conjunction with MOD-032-1 and requires every planning coordinator to compare simulated performance to actual system behavior in both power flow and dynamic models on a periodic basis [29, 30]. Those four standards have been approved by FERC and will be enforced in the near future. Thus,

there is a need to develop an effective model validation process [31, 32]. The Western

Electricity Coordinating Council (WECC) has put in considerable effort on model

validation studies after the 1996 Western America blackouts. The effort substantially

refines the dynamic model and its parameters of major system elements, including

generators, turbine governors, HVDC, and loads. Recent studies have proven that the

correlation between model and measurement has improved immensely [16, 23, 24, 33-

37]. One major finding by the WECC is that generating units running at fixed valve

opening or at load limit are not responding to frequency change. Units with load

controllers slowly reset output power after a frequency excursion. Both operating modes

result in withdrawn system-wide frequency response compared to active governing mode

[16, 36].

Power system dynamic model validation involves three components: the power

flow model, the dynamic models and their parameters, and actual event recordings. The

power flow model represents the real system's pre-disturbance condition. The solved

nodal voltage angle, magnitude, and tie-line flow should be in good agreement with those

obtained by the state estimator. The dynamic models are composed of the design and

control parameters of every dynamic component, including generators, exciters, turbine

governors, power system stabilizers (PSS), HVDC and its controls, FACTS, and loads.

The accuracy of the dynamic models and their parameters has to be verified in order to

reach a converged solution and credible simulation accuracy [38]. As for actual event

recordings, measurement with synchronized time index and high resolution is desirable.

This study employs the synchrophasor measurements collected by FNET/GridEye [39].

The measurement unit, called a Frequency Disturbance Recorder (FDR), is a single-phase

PMU installed at the distribution network. The FDR measures voltage magnitude, angle,

and frequency, and transmits the GPS time-synchronized data to the central phasor data

concentrator (PDC) via the Internet. The synchrophasor features a reporting rate of ten

points per second, which adequately captures electromechanical behaviors of a power

grid. A map of current FDR locations in North America is shown in Figure III-1.
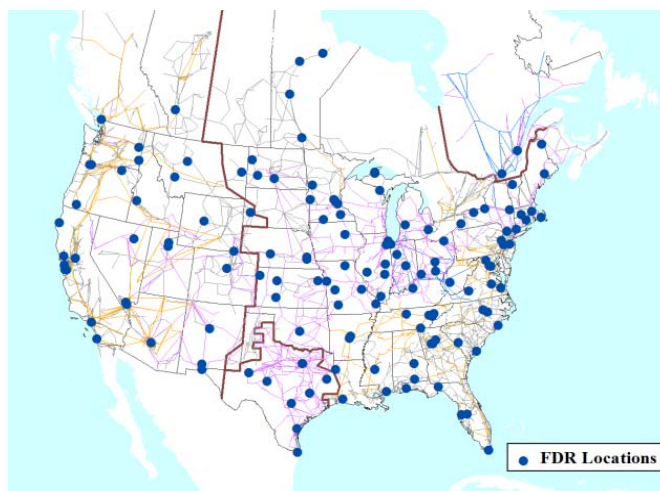
Figure III-1 FDR Deployment Map with Transmission Networks

3.1 Frequency Response Mismatch

It has been observed that there is a constant mismatch between simulation and

measurement of the frequency response in the EI system: the simulation always shows

faster frequency recovery [4, 14, 15, 40]. One example is illustrated in Figure III-2. The

disconnection between modeling and reality raises serious concerns over the fidelity of

the EI dynamic models used for operation and planning studies. The models with faster

frequency recovery could also result in under-estimated Interconnection Frequency

Response Obligation (IFRO), which is the minimum amount of frequency response that must be maintained by an interconnection [4]. In addition, possible consequences include unexpected load shedding and optimistic prediction of frequency response when considering renewable integration.
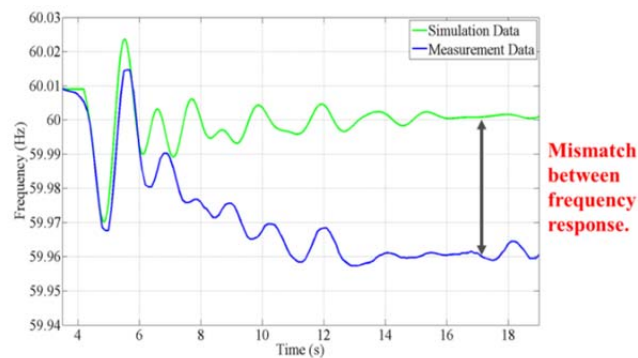
Figure III-2 Frequency Mismatch between Measurement and Simulation in the EI System

3.2 Frequency Response Sensitivity Study

To sort out the primary contributors to the frequency response mismatch, a sensitivity study is passed through the factors described below. Two EI dynamic models are used in this paper. The original MMWG-TVA model has 16,000+ buses and 3,000+ machines with a total capacity of 591 GW. 45.42% generation capacity (268.43 GW) is attached with active governors. Figure III-3 charts the dominant governor types in the original model. The top four types are steam (IEEEG1, IEESGO, and TGOV1) and gas (GAST) turbine governors, which make up 92.06% of the total active governor capacity.

The second model is the MMWG-TVA model base case, or simply the base case. In order to represent governor deadband, the most dominant four types of turbine governors

are equivalent to WSIEG1 (Figure III-4), which is an augmented version of the IEEE

type 1 turbine governor model. The conversion equations are listed in Section 3.3. The

remaining turbine governor models, which make up 7.94% of total active governing

capacity, are omitted. In other words, the base case has a total active governor capacity of

247.12 GW. In the base case, the governor deadband is set to 0 mHz. This facilitates

comparison among various factors. The following paragraphs introduce a series of factors

that possibly have profound effects on frequency response, particularly on the settling

frequency. An actual 1100-MW generation trip event at McGuire Unit 1 in North

Carolina (NC) is replicated. The observation is made around 300 km away from the

power plant.
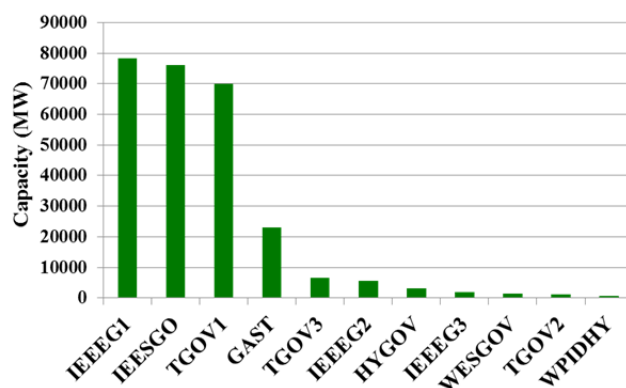
Figure III-3 Turbine Governor Model Types

As defined in [41], the fraction of capacity providing governing response, Kt, is a

major factor of system frequency response. Several features in turbine control and

operation cause that many synchronized units do not respond to under-frequency events:

nuclear and large fossil fuel plants dispatched at their maximum power output; gas

turbines at exhaust temperature limits; and steam units in pure sliding pressure mode [42]. Therefore, a substantial amount of generating units modeled with active governing response is not arresting frequency excursion in reality. As fewer governors are active than expected, the measurement shows diminished frequency response [40]. Figure III-5 shows the impact of reduced active governor capacity. The fraction of active governor capacity is 41.91% for the base case, comparing with 12.30% for the case with reduced governor capacity. Apparently, in order to approximate the actual settling frequency, the fraction of active governors is below one tenth, which is not realistic [4].
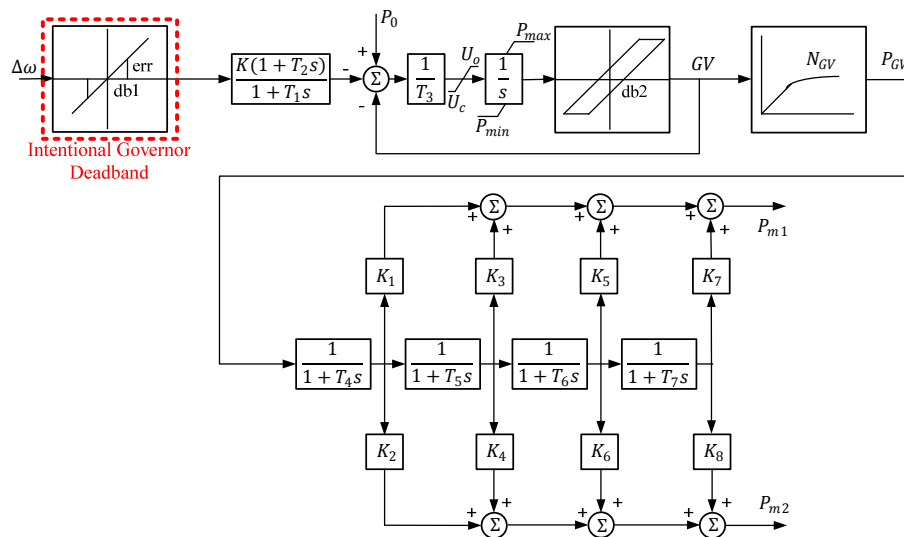
Figure III-4 WSIEG1 Block Diagram

The power mismatch within a synchronized grid will cause frequency to deviate from the nominal value. Until a new balance is met, frequency will continuously drift away. In a large synchronized electric grid, the governor droop control is employed so that speed

governors respond to the shaft speed error by adjusting the turbine mechanical output and in the meanwhile prevent the system frequency from experiencing a large excursion. An example of the droop curve is shown in Figure III-6. The slope of the curve is represented by the speed regulation R, which is defined in (3-1). ΔPmech and Δω are per-unit values and based on machine MVA rating and nominal frequency, respectively. By adopting the per-unit value, the total power mismatch is equally divided to machines based on their capacity.
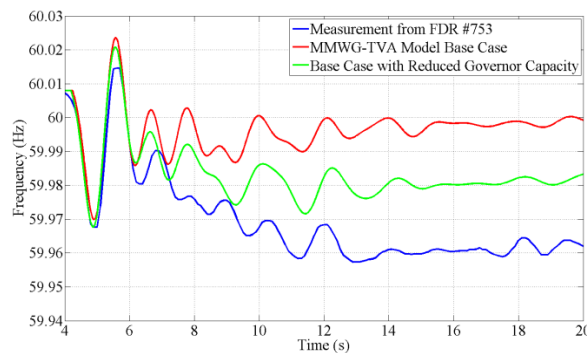
Figure III-5 Impact of the Fraction of Active Governor Capacity

The speed regulation R has a typical range of 3% - 5% [43], and a smaller value of R means a stronger governor response. The simulation in Figure III-7 evaluates the sensitivity of R. Two extreme values are implemented system widely: 2% and 10%. It is observed that there is a considerable gap between the measurement and the simulation with $R = 10\%$.

$$\frac{1}{R} = -\frac{\Delta P_{mech}}{\Delta \omega}$$

(3-1)
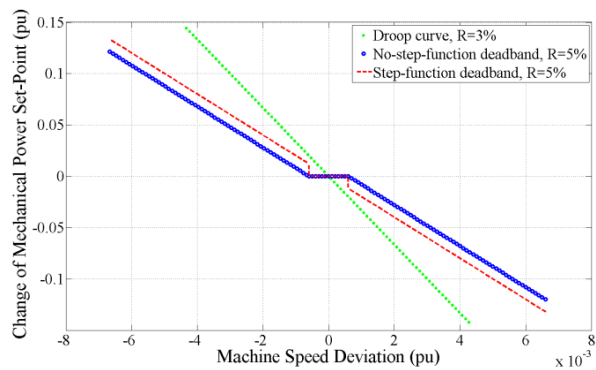
Figure III-6 Governor Droop Curve
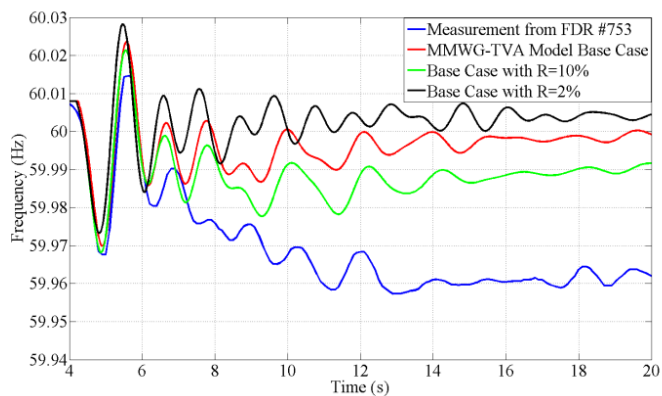
Figure III-7 Impact of Governor Speed Regulation

Load composition could be another contributing factor to frequency response. The fact that end-user components at the distribution network are unknown in detail makes it challenging to build a credible aggregate load model at the transmission network level for dynamic analysis. Besides, the load component fractions, including single-phase motor, three-phase motor, and static load, are changing throughout year (and even day), making it difficult to keep the model database up-to-date. Therefore, the industry has adopted the practice of modeling the load with a combination of the ZIP load, induction motors, and distribution equivalent [44, 45].

For the ZIP load, the constant admittance and current components draw less power during voltage decline, and provide a relief effect on the grid. The constant power component, which is mainly comprised of data centers, consumer electronics, and variable frequency drives, consumes the same amount of power during transients. Generation loss often accompanies voltage drop. Thus, the fraction of constant power, current, and admittance load will dictate the absolute value of load after generation trip. However, due to the localized nature of reactive power and widely installed voltage regulation equipment, the impact of the ZIP load fraction on settling frequency may not be significant in a large interconnection. Figure III-8 shows the normalized generator terminal voltage response to the aforementioned event and indicates that the change of voltage magnitude after 10 seconds is within 0.5%. The simulation corresponds to the measurements in that the voltage magnitude at the distribution level is almost identical before and after generation trip system-wide [46]. Figure III-9 is the actual recording of voltage magnitude at the distribution network during the generation trip. To evaluate the
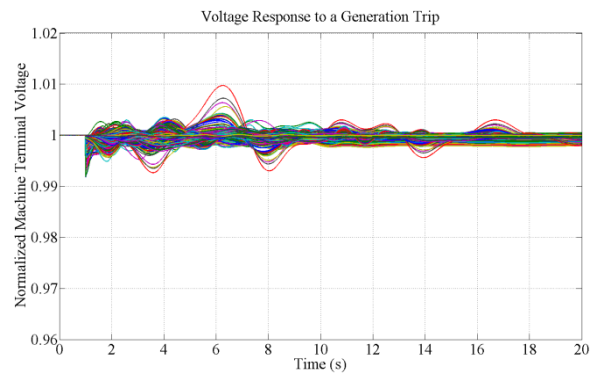
Figure III-8 Normalized Generator Terminal Voltage Response to the Generation Trip
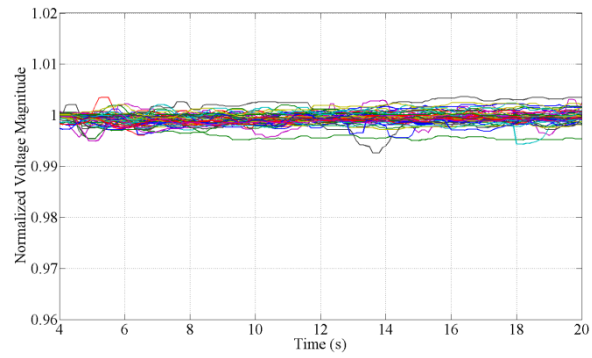
Figure III-9 Normalized Voltage Recording at the Distribution Network

impact of load voltage sensitivity on frequency response, two bounding cases are simulated: the constant admittance case has 100% constant admittance load for both active and reactive power; and the constant power case has 60% constant power and 40% constant current load for both active and reactive power. Figure III-10 clearly demonstrates that the settling frequency has a slight change regardless of the ZIP fraction.

The load frequency sensitivity also has an impact on frequency response. For example, direct-drive motors can contribute to inertial response and damping ratio [35].

To estimate the impact of load frequency sensitivity, the frequency-dependent load model (LDFR) is used. 50% of total loads are set dynamically proportional to the square of bus frequency. Simulation in Figure III-11 reveals that the change of settling frequency is relatively small.

The load controller (or the outer-loop control) is also a differentiating factor on frequency response. It is found by the WECC that a thermal unit with load controller would reset its output power after a disturbance. Consequently, the system would exhibit diminished frequency response [16]. The time scale for the resetting control is slow in relation to that of the governing loop. It is reported in [8] that a load controller may be able to completely cancel a deviation of output within as little as 30 seconds, while a reset time of a few minutes would be common in large steam plants. In [4], the withdrawal of primary response becomes effective after 45 to 60 seconds in EI. In the simulation study, the load control is represented by LCFB1 [8, 36]. 37.56% generating units are accompanied with load controllers. A relatively large value of $K_I = 0.05$ is adopted to simulate the fast withdrawal impact in Figure III-12.
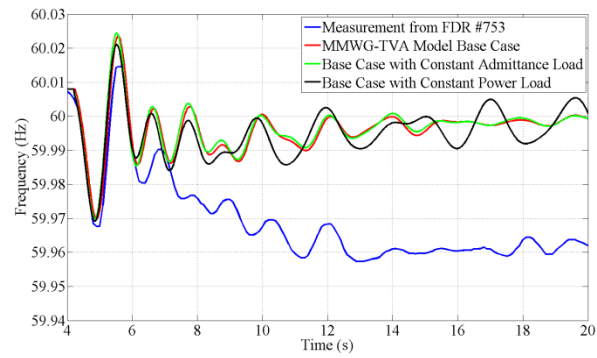
Figure III-10 Impact of Load Voltage Sensitivity
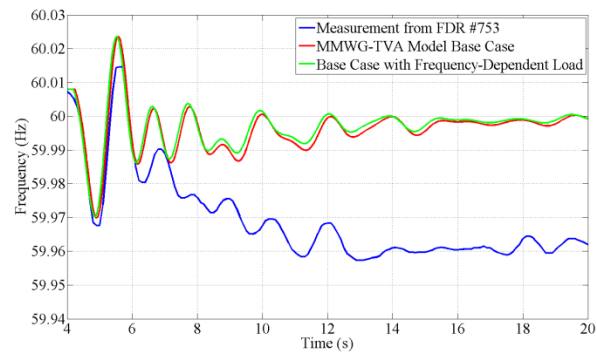
Figure III-11 Impact of Load Frequency Sensitivity
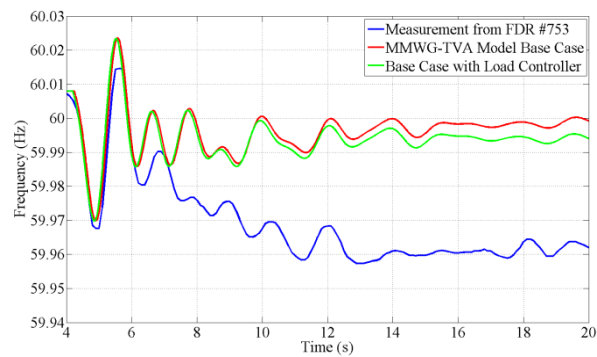
Figure III-12 Impact of Load Controllers

It is observed that the frequency trace of the load controller case starts to deviate from that of the base case after 10 seconds, largely due to the slow integration effect of the load controller. It is noticeable that within 20 seconds after the generation trip, the governing control is dominant despite an extremely fast power output withdrawal.

Deadband is generally categorized into unintentional and intentional deadband. The unintentional deadband is used to describe the inherent mechanical effect of a turbine-governor system, such as sticky valves, loose gears, and hydraulic system nonlinearity, which are un-avoidable and un-adjustable [47]. Intentional governor deadband is adopted in more modern governor designs to reduce excessive controller activities and turbine mechanical wear for normal power system frequency variations. Until the pre-set intentional deadband is reached, the turbine governor would not respond to system frequency excursion. Thus, governor deadband leads to an increased frequency deviation. There are two types of deadband implementation: step-function and no-step-function (Figure III-6). The first type results in a step change in mechanical set-point and consequently excessive stresses on mechanical parts and is thus undesirable [48]. In this study, only the intentional no-step-function implementation is considered.

Modeling the governor deadband is necessary for EI frequency response simulation. It is reported that governor deadband is widely implemented in the EI, with the smallest generating units having the lowest governor deadband, followed by the mid-size, and then the largest units [4]. As the EI system total capacity is relatively large (roughly 600 GW during peak hours) and frequency deviation small, the effect of governor deadband is not negligible: a typical size of deadband (the transition frequency deviation as shown in

Figure III-6), 36 mHz, is equivalent to 851 MW, given the average EI β value, i.e.

2363 MW/0.1 Hz. The other rationale is based on the fact reported in [4] that 'pre-

disturbance frequency (Value A) is another statistically significant contributor to the

variability of frequency response. The expected frequency response for events where

Value A is greater than 60 Hz is 2188 MW/0.1 Hz versus 2513 MW/0.1 Hz for events

where Value A is less than or equal to 60 Hz. This observation is attributed to the fact

that governor deadband is centered at the nominal frequency (60 Hz). If the pre-

disturbance frequency is larger than the nominal, it will cost more relative frequency

deviation to trigger the same amount of MW response. Therefore, it is justified to take

account of governor deadband in frequency response simulation.

In the sensitivity study, the width of the deadband is adjusted uniformly on every

turbine governor. Figure III-13 reveals that the recording settles above the ± 49 mHz case

and under the ± 30 mHz case.
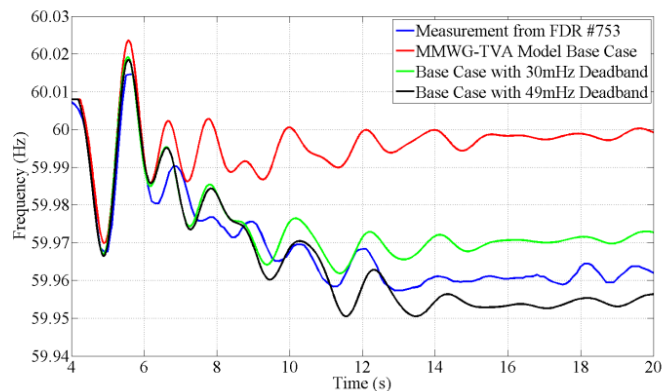
Figure III-13 Impact of Governor Deadband

3.3 Turbine Governor Modeling

To implement governor deadband modeling, the most dominant turbine governor

models, including TGOV1, IEESGO, IEEEG1, and GAST, are converted to WSIEG1

through parameter equivalence. The parameter conversion equations are listed below.

The left-hand side of the equations are the WSIEG1 parameters.

For TGOV1 (Figure III-14), the equations are listed from (3-2) to (3-6).

For IEESGO (Figure III-15), the equations are listed from (3-7) to (3-16).

WSIEG1 is an augmented version of IEEEG1 and therefore there is no need for

parameter conversion of IEEEG1 (Figure III-16).

For GAST (Figure III-17), due to the structural limitation of WSIEG1, the load limit

control loop in the gas turbine model cannot be represented through parameter

conversion. The load limit control serves as an upper limiter if the exhaust temperature

exceeds a certain value. The equations are listed from (3-17) to (3-20).
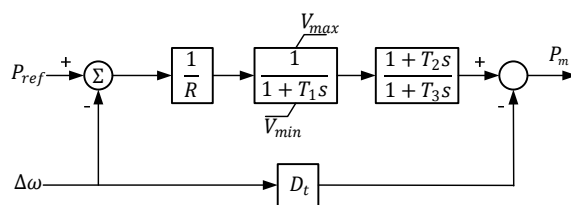
Figure III-14 TGOV1 Block Diagram

$$K = 1/R \tag{3-2}$$
$$T_3 = T_1 \tag{3-3}$$
$$K_1 = T_2/T_3 \tag{3-4}$$
$$K_3 = 1 - T_2/T_3 \tag{3-5}$$
$$T_5 = T_3 \tag{3-6}$$
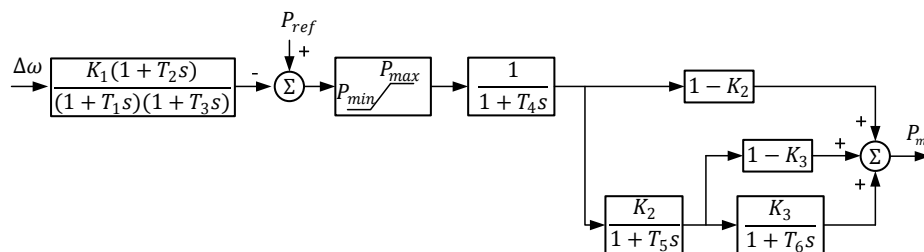
Figure III-15 IEESGO Block Diagram

$$K = K_1 \tag{3-7}$$
$$T_1 = T_1 \tag{3-8}$$
$$T_2 = T_2 \tag{3-9}$$
$$T_3 = T_3 \tag{3-10}$$
$$T_4 = T_4 \tag{3-11}$$
$$K_1 = 1 - K_2 \tag{3-12}$$
$$K_3 = K_2(1 - K_3) \tag{3-13}$$
$$K_5 = K_2 K_3 \tag{3-14}$$
$$T_5 = T_5 \tag{3-15}$$
$$T_6 = T_6 \tag{3-16}$$
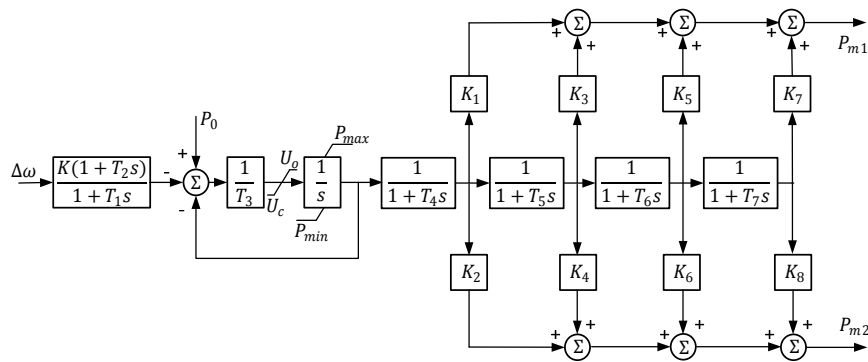
Figure III-16 IEEEG1 Block Diagram
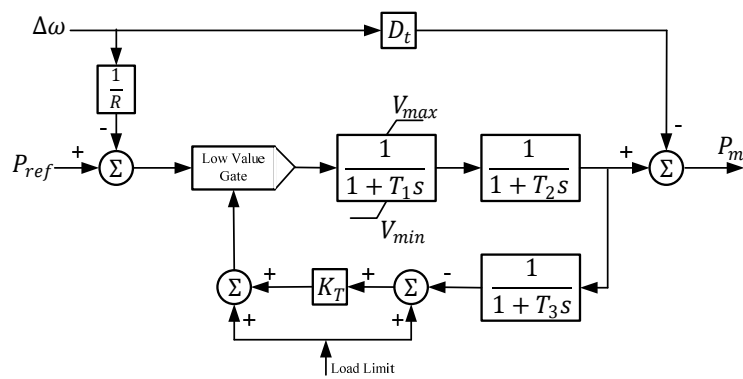
Figure III-17 GAST Block Diagram

$$K = 1/R \qquad\qquad (3\text{-}17)$$
$$T_3 = T_1 \qquad\qquad (3\text{-}18)$$
$$T_4 = T_2 \qquad\qquad (3\text{-}19)$$
$$K_1 = 1 \qquad\qquad (3\text{-}20)$$

As demonstrated in the sensitivity study, the governor deadband could be the major

parameter that accounts for the frequency mismatch between simulation and

measurement in the EI. To validate the proposition, simulations with deadband

represented are compared with FNET measurements at various locations. Figure III-18

illustrates the validation process. Since the governor deadband is not a standard

parameter widely modeled in the EI dynamic models and therefore not readily available,

the deadband is assumed uniform across the system. This assumption may change the

governor MW distribution, even though the total MW is kept the same. Since the

generator dispatch is variable, the governor deadband width in simulation is adjusted to

best match the actual event. A fixed deadband case (36 mHz) is also accompanied as a

reference.
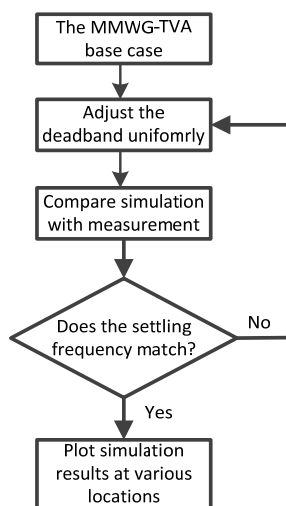
Figure III-18 Model Validation Flowchart

3.4 Model Validation Case Studies

Two case studies are presented in this section.

Case A (Figure III-19) is the 1100 MW generation trip event that happens at McGuire Unit 1, North Carolina, on 14:57:00 UTC, 2013-02-21. The WSIEG1 deadband width is ± 39 mHz. The comparison across the system is presented in Figure III-20, Figure III-21, Figure III-22, Figure III-23, Figure III-24, Figure III-25, and Figure III-26.

By modeling governor deadband, the simulated settling frequency goes from 60.00 Hz to 59.96 Hz and matches perfect with the measurements across the system. It also shows steeper inertial slope and resembles the real responses better.

Case B (Figure III-27) is the 1060 MW generation trip at Cook Unit 2, Michigan, that happened at 14:18:40 UTC, 2013-07-28. The WSIEG1 deadband width is ± 33 mHz. The comparison across the system is presented in Figure III-28, Figure III-29, Figure III-30, Figure III-31, Figure III-32, and Figure III-33.

Figure III-19 Case A Locations
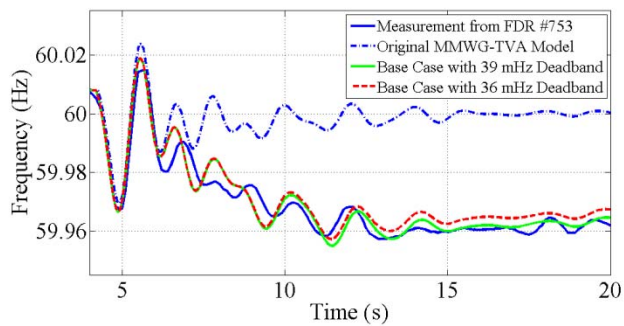
Figure III-20 Case A – Measurement in North Carolina
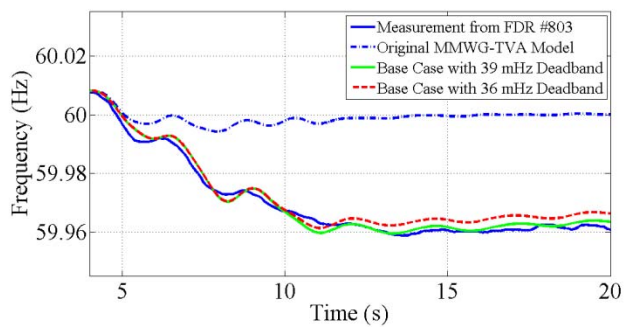
Figure III-21 Case A – Measurement in Ohio
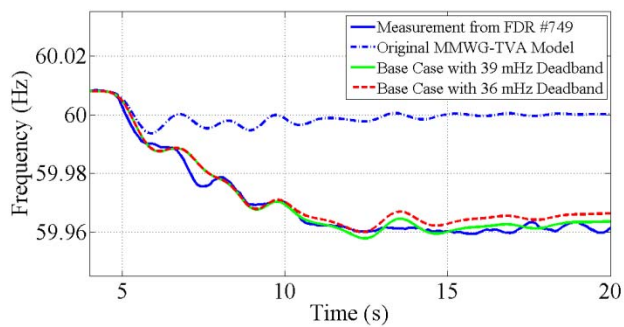
Figure III-22 Case A - Measurement in Missouri
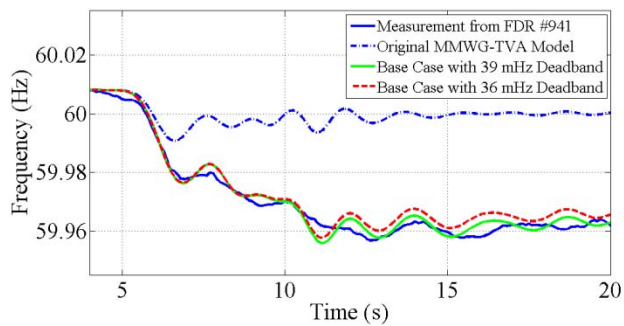
Figure III-23 Case A – Measurement in Kansas
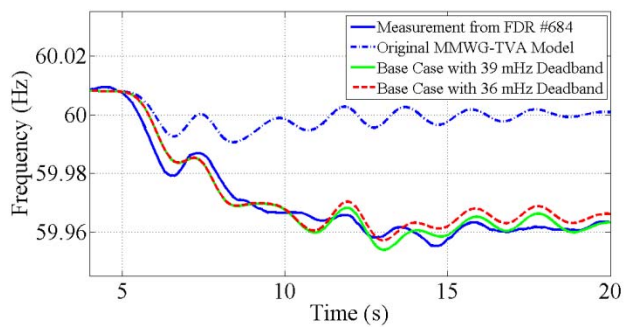
Figure III-24 Case A – Measurement in Massachusetts
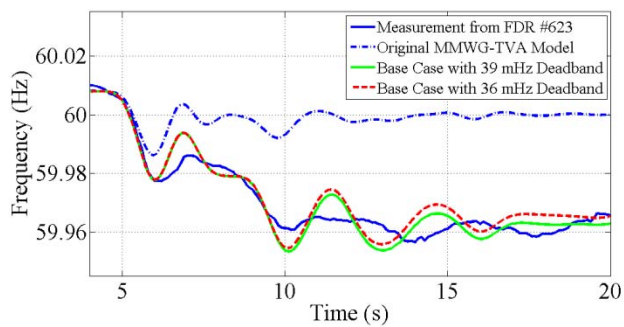
Figure III-25 Case A – Measurement in Florida
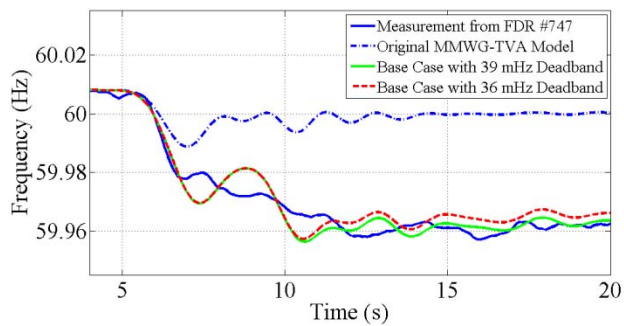
Figure III-26 Case A – Measurement in Minnesota

Figure III-27 Case B Locations
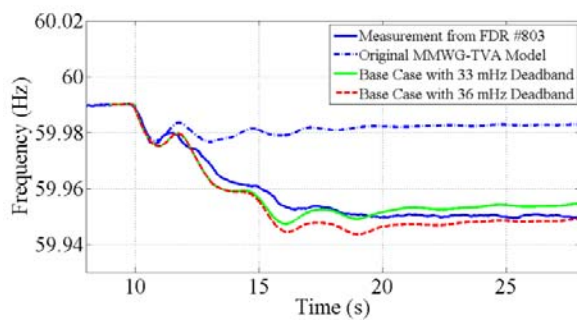
Figure III-28 Case B – Measurement in Ohio
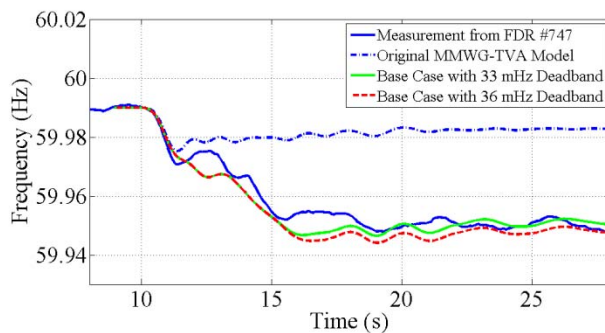
Figure III-29 Case B – Measurement in Minnesota
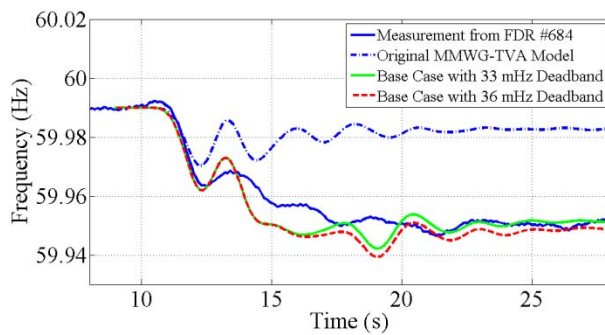
Figure III-30 Case B – Measurement in Massachusetts
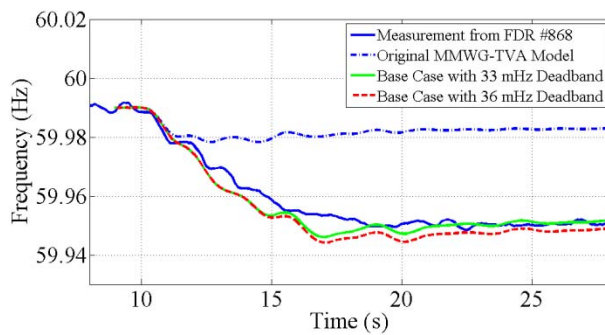
Figure III-31 Case B – Measurement in Tennessee
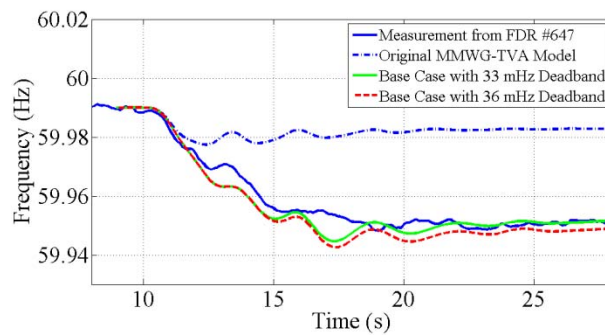
Figure III-32 Case B – Measurement in Arkansas
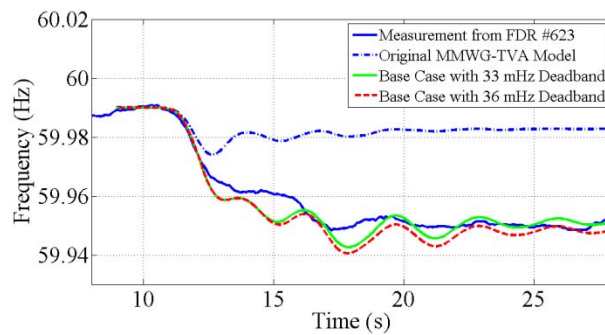
Figure III-33 Case B – Measurement in Florida

In Case B, the deadband decreases the simulated settling frequency from 59.983 Hz to 59.950 Hz. The original MMWG-TVA model shows a final deviation of 7.2 mHz, while the actual deviation is 40.3 mHz.

3.5 Summary

Based on the analysis and simulation, the following conclusions can be drawn:

- Frequency response is closely correlated to a myriad of factors, including the fraction of generation capacity providing governor response, the speed regulation, load composition, load controllers, and the governor deadband. The governor deadband has a significant frequency response, particularly on settling frequency. To build a credible dynamic model, all those factors and parameters should be set with caution.

- In the EI system, modeling the governor deadband greatly improves simulated frequency response in terms of settling frequency, inertial response, and frequency nadir.

- It is desirable that actual deadband data are collected for assembling an interconnection-wide dynamic model for better frequency response prediction. The deadband across the interconnection has a broad range (16 mHz to 300+ mHz) and can largely affect the MW response of individual machines. But as shown in simulations, even modeling deadband using a fixed value (36 mHz) may greatly improve the simulation accuracy, considering that system conditions are constantly changing.

- The deadband width largely contributes to settling frequency. A deadband centered at 60 Hz may have contributed to the observed β value difference above and below 60 Hz.

- Synchrophasors are valuable in calibrating power system dynamic models by providing high-definition recordings (compared to data from Energy Management Systems (EMS) with a resolution of 3-5 seconds) that capture major electromechanical behaviors.

Case A exhibits closer alignment than Case B partly due to the fact that Event A occurs during the winter season, which matches the Winter Peak model better. There is no denying that a power flow model that represents the pre-disturbance condition is most desirable to reflect actual system performance.

The simulation results from the deadband model still exhibit mismatch against the recordings and require further improvement in modeling. More inclusive load models, such as the WECC composite load model [45], should be employed. Synchrophasor-based methodologies on determining the load composition fraction at regional level are significantly valuable for system-wide dynamic model validation.

This study omits 21.21 GW gas (excluding GAST) and hydro governor capacity that cannot be converted to the WSIEG1 model. The limitation can be overcome by using GGOV1 (GE general purpose turbine-governor model) and WSHYDD (WECC double derivative hydro governor model) [8] or building user-defined governor models with deadband block. Based on the sensitivity study of active governor capacity, omitting such

a small portion of governor capacity (3.59%) does not exert a significant change in settling frequency and is therefore acceptable.

Due to practical limitations, this study could only use generic deadband parameters in the governor models. A comprehensive effort using true governor deadband parameters will require the involvement of all industry. This could be a major undertaking, but it should improve the EI dynamic model performance significantly.

IV.   Stability Impact of High Wind Generation on the EI 2030 Grid

Wind energy is one of the cleanest and most affordable energy sources available to reduce carbon dioxide emissions. It has become the fastest growing renewable energy resource for electricity generation in the last few years. According to the Global Wind Energy Council, the world-wide cumulative installed wind capacity has doubled from 2009 to 2013 to reach 318,105 MW [49]. In the United States, the total installed capacity has reached 65,879 MW as of the end of 2014 [50]. The nation is on track to realize the Department of Energy's target of 20% wind generation by 2030 [51]. Meanwhile, starting from April 2015, the Mercury and Air Toxics Standards are enforced to regulate emissions from coal-fired power plants. The U.S. Energy Information Administration (EIA) projects that a total of 60 GW will retire by 2020 [52]. The displacement of conventional synchronous generators is undoubtedly cutting back the national carbon footprint, but simultaneously results in numerous challenges in power system operation and planning.

This chapter is concentrating on studying the stability impact of the increasing level of wind generation on the EI system. The studies are made by comparing two dynamics models. The baseline model is built upon the EI 2030 high wind power flow model. MMWG dynamics models and parameters are used. Wind plants are represented by conventional generator models so that the baseline model has zero wind penetration and resembles the current system's dynamic response. The baseline model is then validated against synchro-phasor measurement by adjusting governor deadband and governor ratio using the approach described in the previous chapter. The calibrated baseline model has

similar frequency response level as that of the real EI system. The wind case is built on the calibrated baseline case. The sole difference is that the wind plants are represented by wind dynamics models instead of conventional generators. The impact of wind generation on EI dynamic performance can be therefore illustrated. It should be pointed out that the wind farm locations, as shown in Figure IV-1, are realistic based on detailed planning studies. Transmission upgrades showed in Figure IV-2 are made accordingly to accommodate the new generation.

3.6 Frequency Response Study

Frequency response is the reaction of a power system to a sudden imbalance between generation and load. Such an imbalance can be caused by load shedding or a generation trip, which leads to a large frequency excursion. To ensure power system security and reliability, such frequency excursions need to be arrested and frequency restored to the nominal value. For an under-frequency event caused by a generation trip, various dynamics and controls are in place to mitigate the impact over different time scales. Immediately after a generation trip, synchronous generators have the inherent capability to resist the drop in system frequency. By sacrificing the kinetic energy stored in rotor shafts, synchronous generators provide inertial response instantly for the first two seconds instantly after a disturbance (Figure IV-3). The amount of inherent resistance to frequency deviation is measured by system inertia, which is the sum of inertia of individual interconnected generators and synchronous machines. System inertia, in conjunction with lost capacity in MW, dictates the rate of change of frequency during the initial frequency drop.
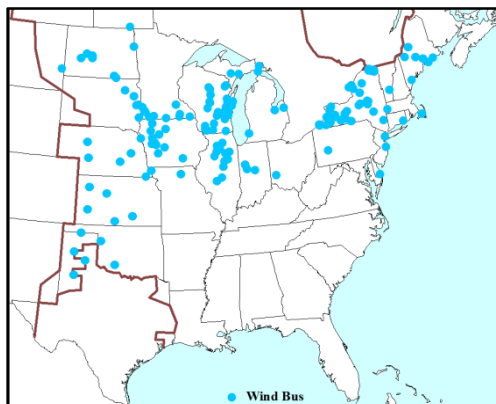
Figure IV-1 Online Wind Farm Locations
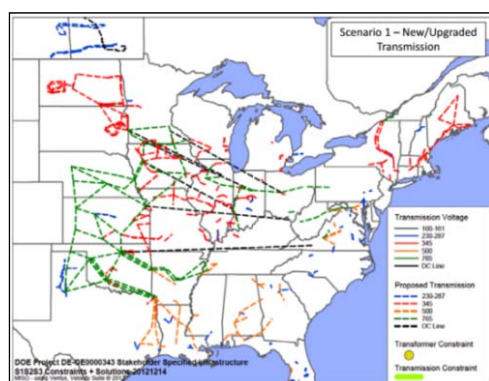
Figure IV-2 Transmission Upgrades
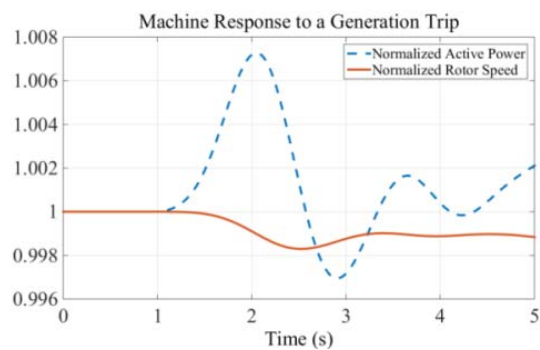
Figure IV-3 Machine Inertial Response

The frequency decline cannot be arrested until a new balance between generation and load is met. The balance is realized by primary frequency control and load response. Active turbine governor control monitors a generator's rotor speed and when a frequency excursion occurs and causes rotor speed outside a pre-set deadband, adjusts the turbine's mechanical power output. The feedback control is closed through a droop curve (Figure IV-4), which characterizes the relationship between frequency change and power output increment. Primary frequency control is implemented at the plant level and, due to deadband and actuating time delay, the response time varies from a fraction of a second to several seconds in length. Additionally, load can respond to generation trips. Frequency dependent load, including direct-driven motors, consumes less power at lower grid frequency. It is reported in [53] that a typical load damping effect is between 1% to 1.5% change in load for a 1% change in frequency. Another aspect of load response is the voltage dependence. Generation loss is usually accompanied by voltage depression in local areas. The load reduction due to voltage decline alleviates the instant power mismatch before voltage is restored. From a typical EI dynamic simulation case, the voltage dependent load could contribute 15% of lost MW capacity (Figure IV-5).

Inertial response, primary frequency response, and load response can stabilize frequency decline at an off-nominal value. To restore frequency to nominal or pre-disturbance frequency, secondary frequency control is deployed to release the primary frequency reserve for potential subsequent event. The restoration process is facilitated by Automatic Generation Control (AGC). By collecting system data including system frequency, actual interchange on tie lines, and generator outputs from Supervisory
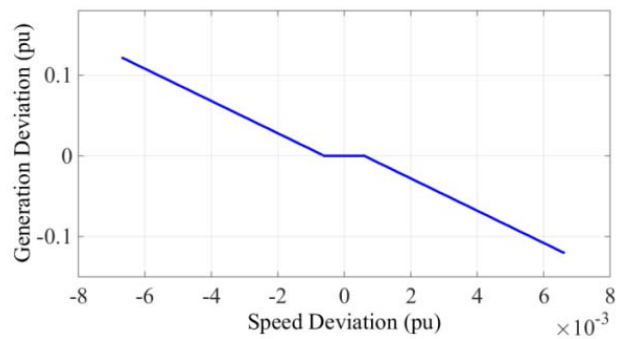
Figure IV-4 A Typical Droop Curve with 36 mHz Deadband and 5%Sspeed Regulation
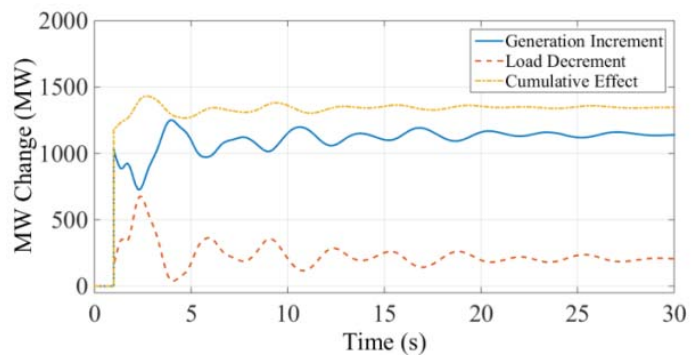
Figure IV-5 Frequency Response Contribution from Generators and Voltage Dependent Load

Control and Data Acquisition (SCADA) systems, operators are able to determine the power balance of a balancing area (BA). If a generation loss occurs within the BA, a negative Area Control Error (ACE) will appear immediately.

To maintain scheduled power interchange and system overall frequency, incremental generation control commands are assigned to committed AGC units to eliminate the deficiency. Due to SCADA time resolution, communication delay, and the potential interference with governor responses, the AGC program has longer response time, ranging from 20 to 30 seconds or even longer [48]. Replacement of a large generation loss is done through a combination of secondary and tertiary (reserve deployment) control. This typically takes 5-15 minutes.

The average EI frequency response is 2,467 MW/0.1 Hz, comparing to 1,179 MW/0.1 Hz for WECC and 586 MW/0.1 Hz for ERCOT. The signature is unique in that the frequency nadir is roughly equal to the settling frequency and exhibits a 'Lazy L' shape [4], as shown in Figure IV-6.
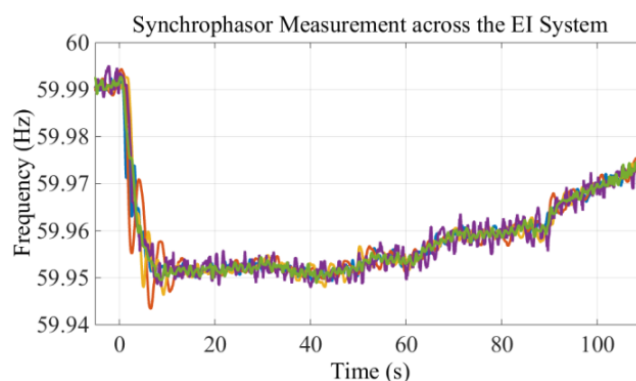
Figure IV-6 Typical EI Frequency Response Measurement

.

From zero to eight seconds, the system frequency continues declining. The inertial response attempts to slow down the descent, while governor response systems begin to react after deadbands are surpassed.

After eight seconds, a settling frequency is reached due to the combined efforts of governor response and load response. This settling frequency does not experience notable change until 30 seconds, when the frequency starts to slowly decline. This phenomenon is associated with governor response withdrawal. The withdrawal stems from the outer-loop control at plant level, which slowly counters the governor response and restores turbine mechanical output to the pre-scheduled value [36]. Beginning at 45 seconds, the AGC program begins to take effect and eventually brings the frequency back to a near nominal value. From the actual measurements, it is observed that multiple dynamics, including inertial response, governor response, load response, governor response withdrawal, and AGC, come into play in various time scales and to some extent overlap each other. From a frequency stability viewpoint, the following aspects are of paramount importance:

- Adequacy of system inertia. Reduced system inertia leads to sharper immediate frequency drop, especially at locations near the disturbance. First step under frequency load shedding, which is prevailingly set at 59.5 Hz in the EI [54], should not be triggered at any locations.

- Adequacy of governor response. It is well known that nuclear reactors and large coal plants are operated under base load mode and thus do not provide governor response. Additionally, steam units in sliding pressure mode are not able to

support frequency decline [42, 53]. Non-responsiveness also occurs on generating units with excessive governor deadband [55]. The deadband width in EI ranges up to hundreds of mHz [4], while a 1000 MW generation loss causes on average less than 50 mHz frequency deviation. According to EI and WECC experience, significantly less governor response is actually online than estimated in planning models [4, 34, 53]. Many control schemes remove the frequency input to the governor when operating in an AGC or MW set point mode. Therefore, maintaining a safe level of governor response online is critical to interconnection security.

- Intentional governor deadband is adopted in turbine control schemes to avoid excessive controller actions and turbine mechanical wear during normal system frequency variations [48]. It is implemented at generator level as shown in Figure 6. According to [55], intentional governor deadband has a significant impact on the frequency response of the EI, whose frequency deviation is so small that a deadband size over 60 mHz will cause turbine governors to bypass most under-frequency events. Even a smaller deadband width could result in reduced governing response. Therefore, the setting and modeling of governor deadband deserve discretion.

- Sustained governor response. This occurs in the EI when the frequency starts to slowly slide downward after primary frequency control has stabilized the deviation. This phenomenon is due to the sluggish resetting effect of governor outer-loop control which eventually brings the turbine governor output set-point

back to pre-scheduled values [40]. The frequency response withdrawal can cause

further frequency depression at any time during the time span of 20 to 60 seconds.

A sustained governor response is desirable before AGC restores frequency.

This study is focused on the first 20 seconds after generation trip, during which the

inertial response and governor response take place and system frequency is stabilized.

The dynamic model used for the EI 2030 high wind scenario contains 70,117 buses,

8,337 machines, 83,860 transmission lines, and 38,461 loads. Gas, nuclear, and wind are

the top three energy sources at the snapshot (Figure IV-7).
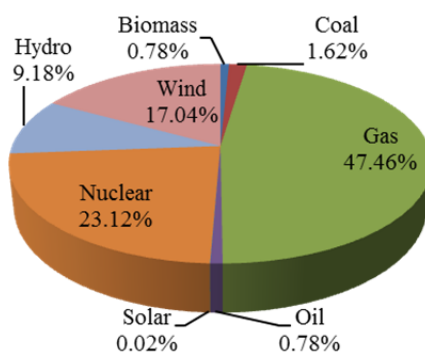
Figure IV-7 Generation Portfolio by Fuel Type

The total system inertia is 4,984,285 MVA·s. Individual wind farms are aggregated

into single wind machine models at their point of interconnection. After converting a very

small portion of wind farms into conventional generators or negative loads because of

low power factors, the remaining 726 wind farms, responsible for 95.42 GW generation,

are modeled by Doubly Fed Induction Generator (DFIG) based wind machine models

(type 3). This essentially captures the constant active power output feature of both type 3 and type 4 wind turbines.

To study the impact of reduced inertial response and governor response due to wind penetration, a No-wind case is created by replacing wind machine dynamic models with synchronous generator models. The No-wind case is used as the reference to reflect the frequency response level of current EI system. The No-wind case is calibrated against synchrophasor measurements by adjusting active governor capacity and governor deadband. It should be clarified that no attempt is made to match the behavior of individual units since the purpose of this study is to validate and examine the system-level frequency signatures. All synchrophasor data were collected by FNET/GridEye, a frequency monitoring system jointly operated by the University of Tennessee, Knoxville, and the Oak Ridge National Laboratory [39].

To offset the degradation of frequency response caused by wind generation, emulated wind inertial and governor response are proposed [17, 56]. By temporarily borrowing kinetic energy from individual wind turbines, wind farms are capable of providing artificial inertial response. Additionally, by reserving a certain margin, wind farms are also able to ramp up quickly to offer governor response. Globally, some grids, such as ERCOT, Ireland, and Hydro Quebec, have required newly built wind plants to have wind inertia or wind governor capability [57-59]. Vendors, including Siemens and GE, provide commercial solutions. Previous studies have shown the effectiveness of wind active power control [40, 60]. To enable wind governing functionality, instead of operating at maximum power output, a certain reserve, typically 5%, is required at all times. The

opportunity cost may not be acceptable by investors without economic incentives. Besides, holding a permanent renewable generation margin seems to partially defeat the purpose of greenhouse gas reduction, especially in large grids where resources for primary frequency reserve are readily available. Therefore, this study looks at the alternative measures, i.e., increasing active governing units and decreasing governor deadband.

The EI power flow and dynamic models and database are prepared by the Multiregional Modeling Working Group (MMWG) under the Eastern Interconnection Reliability Assessment Group (ERAG). The models are widely used in the industry to perform inter-regional transmission reliability assessment studies and are used as the dynamic parameter database for this study. It has been noticed that the MMWG models, which are primarily built for transient (first-swing) analysis, over-estimate the frequency response [22, 40, 53, 55]. The reasons stem from several factors. A notable number of generating units with governor models are not responsive to actual under frequency events due to the plant control mode that blocks under-frequency governor control. Excessive governor deadband also partially or completely defeats governor response. The lack of modeling for outer-loop control leads to further discrepancy after 20 to 30 seconds. Therefore, in order to produce credible simulation results, the No-wind model is calibrated against current system measurements by adjusting active governor capacity and governor deadband. The wind impact is identified by modeling wind generation based on the calibrated No-wind model.

The frequency response in the EI typically stabilizes before 20 seconds. Within this time scale, two major factors dictate settling frequency: active governor capacity and governor deadband. Active governor capacity is the sum of generators in MW that actually provide governing response. The ratio of active governor capacity versus total system capacity is defined as governing fraction, K_t [41]. The governing fraction is around 80% in the MMWG models while the actual value is estimated to be one quarter to one third of that. Governor deadband is another pivotal factor because of the narrow frequency deviation in the EI. To avoid excessive movements of turbine mechanical parts during normal frequency fluctuation, a droop curve is set outside the deadband. Units with over-large deadband do not respond to frequency decline. Units with small and moderate deadband width show less pronounced governing performance than without. According to a NERC report [4], half of the deadband settings in the EI are over 100 mHz. The results of a separate survey on 137 units in the EI, after excluding 33 outliers (deadband width < 2 mHz), is shown in Figure IV-8. Among the 104 units, more than half have deadband width over 50+ mHz and thus rarely react to frequency decline in the EI, with an average frequency response of 2,467 MW/0.1 Hz or 1,234 MW/50 mHz. The rest, with small and mid-sized deadband, start to respond roughly halfway to the settling frequency. The close alignment between frequency deviation and deadband in conjunction with the non-uniformity of deadband settings leads to profound non-linearity of system aggregated frequency response, as shown in Figure IV-9.

Equation (4-1) represents the governor response of a single generator while Equation (4-2) shows the aggregated frequency response of entire system, where S_i is the MVA
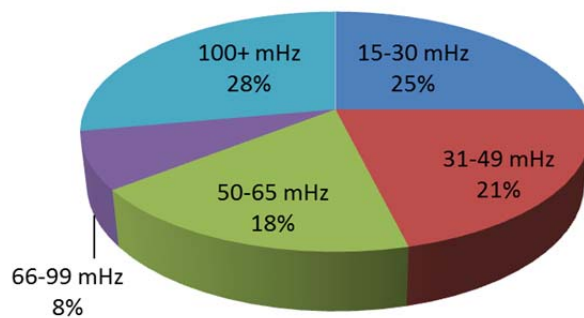
Figure IV-8 Deadband Settings for 104 EI Units

$$\Delta P_i = g_i(\Delta f) \tag{4-1}$$

$$\Delta P_{sys} = (\textstyle\sum_i g_i(\Delta f) \cdot S_i)/S_{sys} \tag{4-2}$$
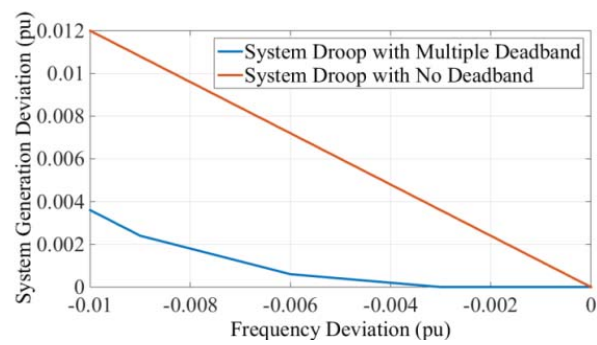
Figure IV-9 Aggregated System Droop Curve

base of the machine *i*. The deadband has the effect of creating non-linear and reduced frequency response, which is not properly modeled in the interconnection-level transient stability simulation models. The deadband effect also tends to explain the observation that statistically frequency response is less if the pre-disturbance frequency is over 60 Hz [4]. Therefore, by accounting for non-responsive governor and governor deadband, the simulated frequency response shall exhibit closer correlation with the real EI system.

Governor deadband is not modeled in most dominant turbine governor models, including TGOV1, IEEEG1, GAST, and HYGOV. In order to represent deadband, non-deadband models are converted to the following types: WSIEG1, GGOV1, and URGS3T. The model specifications can be found in [8].

The goal in validating the No-wind model is to develop a realistic baseline case that reflects the system average frequency response performance. Therefore, a uniform deadband width is assumed to resemble the overall deadband effect. No attempt is made to validate the behavior of individual generators. To adjust the No-wind model, two actual events are selected as reference. The chosen events must be reasonably close to the model in terms of total generation capacity and the lost MW.

Active governor capacity and deadband width are fine tuned to closely match with both Cases 1 and 2. The finalized parameters are shown in Table IV-1. Simulation results are shown as below.

Figure IV-10 indicates the generation trip and observation locations for Case 1. Figure IV-11and Figure IV-12 show measurement and simulation at two different locations. Case 2 is illustrated in Figure IV-13, Figure IV-14, and Figure IV-15.

Table IV-1 Reference Cases

Case Name	Event Time	Tripped Unit	Lost Capacity (MW)
Case 1	2013/06/28 17:29:42 UTC	Watts Bar Unit 1, TN	1,100
Case 2	2013/03/12 18:51:50 UTC	Saint Lucie Unit 1, FL	982

Figure IV-10 Case 1 Locations
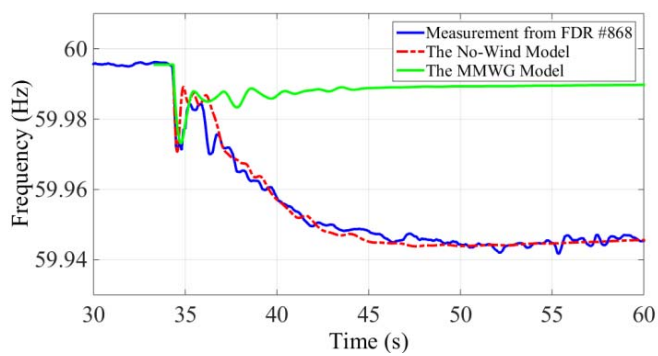
Figure IV-11 Frequency Response in Tennessee
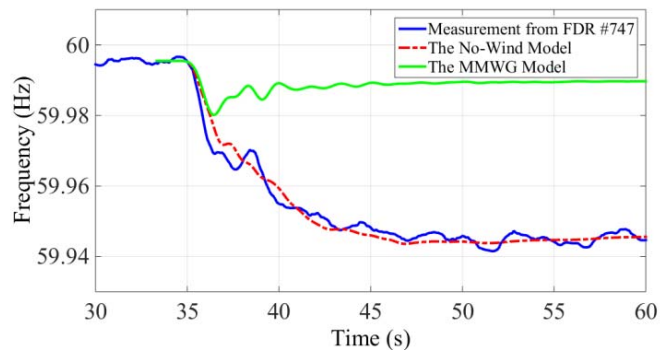
Figure IV-12 Frequency Response in Minnesota
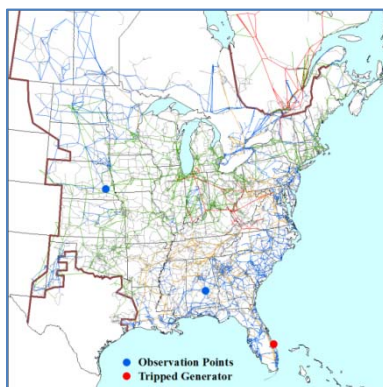
Figure IV-13 Case 2 Locations
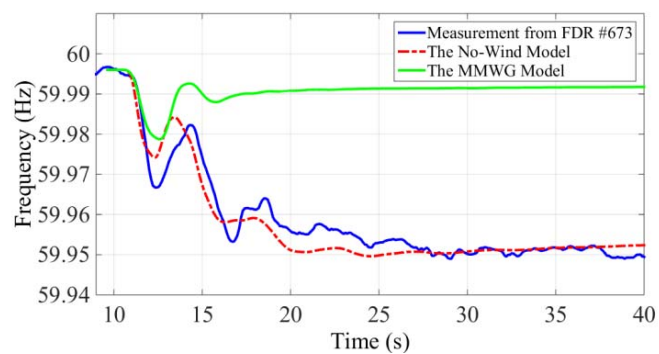
Figure IV-14 Frequency Response in Alabama
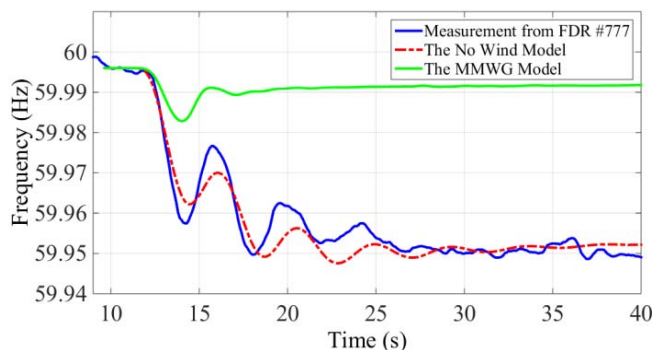
Figure IV-15 Frequency Response in Nebraska

From the simulation results above, the validated No-wind model shows enhanced correlation with actual measurements in frequency response over the MMWG model. No effort is made to tune the oscillations, which are associated with system loading conditions, load models, excitation system settings, power system stabilizers, and so forth.

Comparing against the No-wind model, the Wind model loses 4.63 GW of responsive governor capacity. To further investigate the risk of active governor capacity reduction, a Reduced K_t model is created, which simulates the loss of one third of the active governor capacity due to increased wind penetration and fossil fuel plant retirement. Further, this study proposes two mitigation measures to compensate the frequency response degradation due to wind penetration. All scenarios are listed in Table IV-2.

The simulation results for Cases 1 and 2 are summarized in Table IV-3. From the simulation results in Figure IV-16 and Figure IV-17, the impact of reduced inertial response is not profound and far from triggering the first level of under frequency load

Table IV-2 Developed Dynamic Models

Model Name	Description	Active Governor Capacity (GW)	Deadband Width (mHz)
No-wind	Wind plants are modeled by conventional generators to approximate the current system. This model is calibrated against measurements.	64.69	39
Wind	Wind plants are modeled by double-fed induction generator based units. Instant wind generation is 95.42 GW. No supplementary active power control. Voltage regulation mode.	60.06	39
Reduced K_t	Modified Wind model. Further reduce active governor capacity.	44.29	39
Increased K_t	Modified Wind model. Increase active governor capacity as a mitigating measure.	124.40	39
Reduced DB	Modified Wind model. Reduce governor deadband as mitigating measure.	60.06	29

Table IV-3 Settling Frequency and Frequency Response for Cases 1 and 2

Case Name	No-wind	Wind	Reduced K_t
Case 1	59.945 Hz 2318 MW/0.1 Hz	59.941 Hz 2149 MW/0.1 Hz	59.935 Hz 1938 MW/0.1 Hz
Case 2	59.951 Hz 2047 MW/0.1 Hz	59.948 Hz 1919 MW/0.1 Hz	59.945 Hz 1806 MW/0.1 Hz
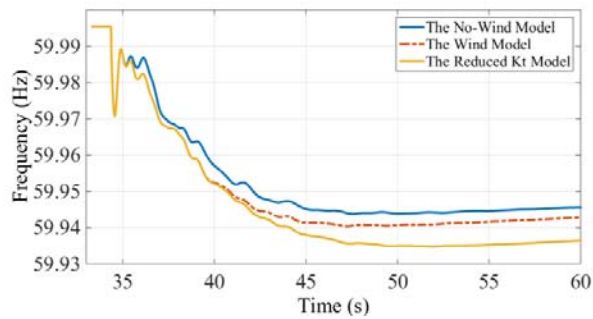
Figure IV-16 Frequency Response in TN Case 1
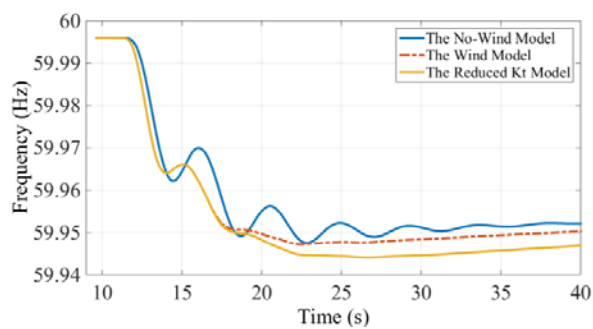
Figure IV-17 Frequency Response in NE Case 2

shedding. Wind penetration and fossil fuel plant retirement lead to broadened frequency deviation. In Case 1, the settling frequency is 59.935 Hz. In Case 2, the settling frequency is 59.945 Hz. Losing one third of responsive governing response can lead to up to 16% frequency response decline. However, even in the worst case, which is 1806 MW/0.1 Hz, the frequency response is far above the IFRO at 1002 MW/0.1 Hz [54].

Two mitigation measures are examined, i.e., increasing active governor capacity and decreasing governor deadband width. In the Increased K_t model, the active governor capacity reaches 124.40 GW, compared to 44.29 GW in the Reduced K_t model. The Reduced DB model has an equal amount of active governor capacity as the Wind model but the deadband width is reduced by 10 mHz. Figure IV-18 and Figure IV-19 show the mitigating effects of the two measures in both Cases 1 and 2. The frequency response is summarized in Table IV-4.

It is observed that increasing active governor capacity or reducing governor deadband have the potential to retain or even improve frequency response, despite the 17% wind penetration. This observation makes practical sense because large interconnected power grids have adequate synchronized generating resources. By imposing strict frequency control standards, such as ERCOT has done [61], or offering economic incentives [62], the degradation from renewables could be minimized and higher renewable penetration levels incorporated.

In this study, the impact of wind generation on frequency response is studied for the EI 2030 system. Dynamic models are built based on the planning studies carried out by
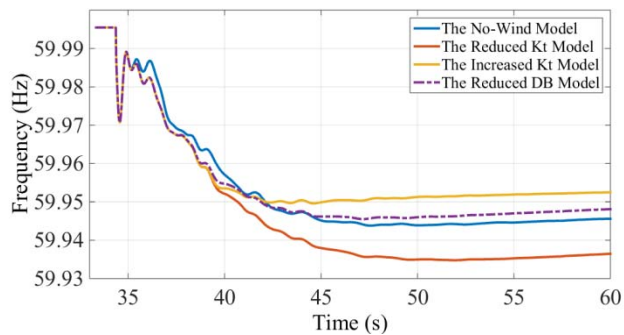
Figure IV-18 Frequency Response in TN Case 1
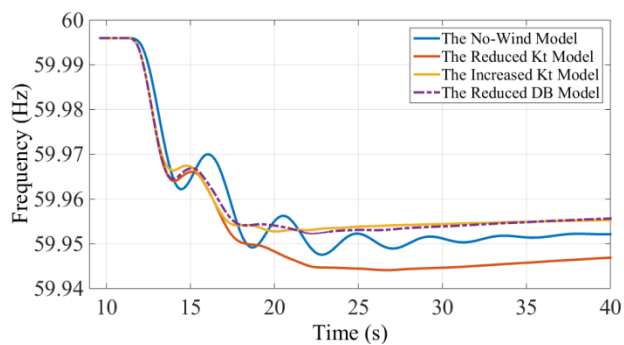
Figure IV-19 Frequency Response in NE Case 2

Table IV-4 Settling Frequency and Frequency Response

Case Name	No-wind	Reduced K_t	Increased K_t	Reduced DB
Case 1	59.945 Hz 2318 MW/0.1 Hz	59.935 Hz 1938 MW/0.1 Hz	59.952 Hz 2686 MW/0.1 Hz	59.947 Hz 2412 MW/0.1 Hz
Case 2	59.951 Hz 2047 MW/0.1 Hz	59.945 Hz 1806 MW/0.1 Hz	59.954 Hz 2193 MW/0.1 Hz	59.954 Hz 2193 MW/0.1 Hz

EIPC. The wind penetration level reaches 17%. To ensure the accuracy of simulation results, a No-wind model is calibrated against measurements of two real events. By adjusting active governor capacity and governor deadband, the No-wind model shows close resemblance to the real system. The wind impact is further illustrated by comparing between the No-wind model and Wind models. Two mitigating measures on frequency response degradation are studied, i.e., increasing active governor capacity and reducing governor deadband.

From the previous analysis and simulation results, the following conclusions can be drawn:

- Under the studied condition, 17% wind generation causes an average 10% reduction in frequency response. But due to the abundance of primary frequency control resources, the declined frequency response is above the Interconnection Frequency Response Obligation and would not endanger system security.

- Maintaining a reasonably high active governor capacity and tightening governor deadband limit are both effective ways to improve frequency response performance under high renewable conditions.

- Modeling governor deadband and validating governor response could largely enhance the accuracy of current EI dynamic models. It would be desirable to validate the system response at the plant level.

This study is limited in its scope. More operating and dispatch conditions, including light spring and heavy summer cases, should be inspected. Although the IFRO is not violated, the performance of each balancing authority needs to be further investigated.

Because of the abundance of potential primary frequency control reserves, larger interconnections generally suffer less degradation in frequency response. Imposing strict standards or creating ancillary service markets could be viable approaches to ensure reliability while steadily increasing renewable generation mix.

This study also exposes the imminent need to improving the accuracy of the EI dynamics models on frequency response prediction. Refined modeling practices on non-responsive governors, governor deadband, outer-loop control, and load models would greatly enhance model credibility. Newly approved NERC standards on model validation would definitely boost this effort [29, 30].

3.7 Inter-area Oscillation and Rotor Angle Stability Study

Wind generation is gaining significant momentum as a new source of electric generation in the United States. Improved turbine technology and reduction in cost slashed the national average levelized price of wind Power Purchase Agreements (PPAs) to a historic low of 2.35 cents per kWh in 2014. With this competitive price, wind constituted 24% of electric generating capacity additions in the same year [63]. By the third quarter of 2015, the cumulative capacity of wind generation in the U.S. reached 69,471 MW [64] and is steadily moving towards the federal goal of 20% wind energy by 2030 [51].

Despite its economic and environmental competitiveness, the stability implications of wind generation must be studied with scrutiny. Type 3 and 4 wind turbines designs are decoupled from the grid side frequency and therefore are exempt of rotor angle stability issues. However, since wind generators do not contribute inherent inertia and have

different voltage control mechanisms than their conventional counterparts, wind generation can introduce distinct boundary conditions for the remaining synchronous generators and thus change their rotor angle stability margin. Moreover, wind generation features rigid active and reactive power regulation. Without additional damping control functions, wind generators only lightly interact with the rest of the system. With the de-commissioning and re-dispatch of conventional generators, system oscillation modes could experience dramatic change. The impact of wind generation on rotor angle and oscillation stability is therefore of interest for power system operation and planning and has been widely studied. By comparing generator rotor angle deviation in the New England 39-bus system, it is concluded in [65] that the displacement of synchronous generators with wind units could improve rotor angle stability. The improvement is directly influenced by reactive power control. A similar study is carried out on a 9-bus system in [66]. By comparing maximum angle separation and the transient stability index, it is discovered that wind generators with unity power factor and terminal voltage control modes can undermine rotor angle stability. As for power system oscillation, in [67] the contribution of wind generators to inter-area oscillation damping is studied on a 12 GW Southeastern Europe system with an instantaneous wind penetration level of 21%. Simulation indicates that double fed wind generators are contributing positive damping to inter-area modes. In [68] a 581 GW 22,000-bus system with a 0.8% wind penetration level is studied. By looking at the sensitivity of the eigenvalue with respect to inertia, the authors conclude that the damping ratio could either increase or decrease with additional wind generation. In [69] the oscillation modes are studied for a series of

Western Electricity Coordinating Council (WECC) planning models in 2010, 2020, and 2022. The total generation is up to 178 GW. The converter control-based generators (CCBGs) make up 0.00%, 2.74%, and 20.22% of generation, respectively. It is found that CCBGs have low participation in the traditional inter-area modes but can introduce new modes. Those new modes may even be poorly damped without properly tuned wind control parameters.

This study is part of an effort to develop and analyze dynamic models for the U.S. Eastern Interconnection (EI) in year 2030. Previous efforts have covered dynamic model development [70], model validation [55], and frequency response [71]. This study looks at the effects of 17% wind penetration on the rotor angle stability of synchronous generators and inter-area oscillation damping. Different than previous studies on rotor angle and oscillation stabilities, this work used a realistic large-scale planning model, i.e., the EI 2030 dynamic models, for simulation. The detailed models include over 70,000 buses and 8,000 generators. The total generation capacity is 560 GW. The baseline model represents governor deadband and is validated against synchrophasor measurements for improved simulation accuracy. A large number of simulation cases are carried out to support the conclusions.

The dynamic models used in this study were developed based on power flow models created by the Eastern Interconnection Planning Collaborative. This U.S. Department of Energy funded project models the impact of various policy options, technological advances, and economic factors on the power grid. Two power flow scenarios for year 2030, i.e., the High-wind and the Business-as-usual scenarios, were further examined by

the research team at the University of Tennessee (UTK) and the Oak Ridge National Laboratory (ORNL). To analyze the stability impact of high wind penetration, the dynamic models were created. The dynamic modeling process involved parameterization of dynamic device models, a dynamic simulation initialization check, and N-1 dynamic contingency simulation. After the dynamic models were adjusted to be stable, actual events were duplicated to check the degree of correlation between simulation and measurement. The synchrophasor measurements used were collected by FNET/GridEye and have a sampling rate of ten points per second [72]. The system validation work indicated that the predicted EI frequency response was stronger than the true value, largely because a key parameter, governor deadband, was not standardly represented in interconnection-level models. By inserting and adjusting governor deadband, simulation could show improved alignment with true response [55, 73, 74]. The simulation models used in this study were indirectly validated to measurement by displacing wind generators with conventional ones to resemble current system behavior.

The stability impact of wind generation is multi-folded. Higher wind penetration usually comes with an upgraded transmission network, which enhances system stability per se. Higher wind penetration also implies re-dispatch of power flow and de-commissioning and de-loading of conventional generators. This change of system operating condition translates into a shift of stability performance. Lastly, the control mechanisms and reactions to system disturbances differ dramatically between wind and synchronous generators. The scope of this study is limited to the latter aspect. The two comparison cases, i.e., the baseline case and the high-wind case, are built upon the power

flow scenario with 17% instantaneous wind generation. The total generation is 560 GW.

The majority of wind plants are located in the footprint of Southwest Power Pool and

Midcontinent Independent System Operator. Except for the wind generator models, the

two dynamic cases are identical. The high-wind case represents wind farms with the

General Electric (GE) wind machine model, while the baseline case models the wind

farms with paired synchronous generator and exciter models. Some units are also

equipped with turbine governor and power system stabilizer models. The frequency

response of the baseline case is calibrated against the current system by adjusting active

governor ratio and governor deadband. Since the only difference between the two

dynamic cases is the dynamic wind farm models, the difference in system dynamic

behavior can be traced directly to the difference between wind and conventional

generators.

There are 726 wind farms online, generating 95.42 GW in the initial operating

condition. Wind farm locations are marked in Figure IV-20. Each wind farm is

represented by a GE wind turbine generator (WTG) model [75]. With proper setup, this

model can be used to represent either Type 3 doubly-fed asynchronous generators or

Type 4 full converters. When properly parameterized, the GE wind WTG model can not

only simulate GE-specific WTGs but also the generic WTGs, whose dynamic behaviors

are completely dominated by converter controls.

More generic and accurate WTG dynamic models have been developed, such as

WECC second generation wind turbine models [76], and the refinement in WTG

modeling will continue. The use of the GE WTG is valid because this model essentially

captures the characteristics of converter-based generators, which have no inherent inertia and tightly regulated active and reactive power output. As the purpose of the impact study is to evaluate the most severe but realistic conditions, it is assumed that all WTGs have no additional active power control functionality like artificial inertia control and wind governor response. Reactive power regulation is set to the voltage control mode, in which the voltage of a designated bus is regulated to a pre-defined reference. One can expect that the ideal reaction of the WTGs to a disturbance is to keep active power unchanged and maintain the voltage magnitude of the terminal or a remote bus.

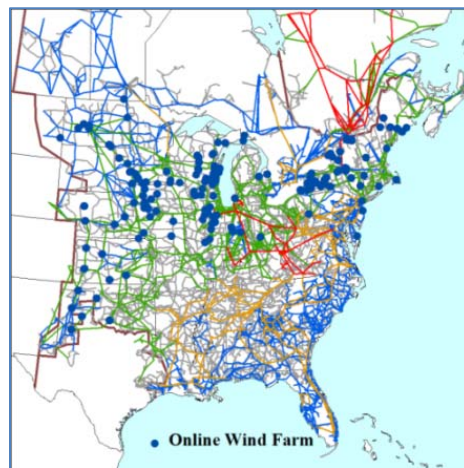Figure IV-20 Online Wind Farm Locations

Generator rotor angle stability is the ability of a synchronous generator to maintain synchronism when subjected to a severe disturbance. Instability is usually in the form of aperiodic angular separation due to insufficient synchronizing torque. The phenomenon is also referred to as first swing stability and usually occurs within the first three seconds

following a disturbance [3]. The dynamics of rotor angle stability are depicted by

Equations (4-3) and (4-4).

$$P_e = \frac{E_r E_I}{X_{eq}} \sin\theta \qquad (4\text{-}3)$$

$$P_m - P_e = \frac{H}{\pi f_0} \frac{d^2\delta}{dt^2} \qquad (4\text{-}4)$$

Where:

P_e: Electric power output　　　　　　　　P_m: Mechanical power input

E_r: Voltage magnitude on the receiving side

E_I: Generator internal voltage　　　　　　X_{eq}: Equivalent reactance

θ: Power transfer angle　　　　　　　　δ: Rotor angle

H: Generator turbine inertia　　　　　　　f_0: Nominal frequency

When a fault occurs near a generator, its electric power output immediately drops due to depressed voltage magnitude. Since the mechanical power input on the generator shaft does not change during the first swing period, the imbalance between the input mechanical power and output electrical power accelerates the shaft speed and tends to break synchronism with the rest of the system. If the protection relays operate properly, the fault will be cleared quickly enough that the generator remains synchronized. However, if fault clearing is delayed, the generator could lose synchronism despite the action of protection relays. This happens because the post-fault power transfer capability may not be adequate to deliver the excessive energy accumulated on the shaft during the fault period. The maximum fault clearing time for a generator to remain synchronized is defined as the critical clearing time (CCT). CCT is a direct measure of a generator's rotor angle stability margin. CCT may change depending on initial system conditions,

generator controls, and disturbance locations. It is also closely linked to boundary conditions. Stronger receiving end voltage support and smaller power transfer reactance can raise rotor angle stability margin and thus increase CCT.

To evaluate the rotor angle stability impact of wind generation, a standardized CCT calculation process was developed as follows. Most synchronous generators are usually connected to an external system through a single transformer or line. Then, a parallel branch is added. The impedances of the branch pair are kept equal and adjusted to be equivalent to the original branch so that power flow does not change. After applying a fault on one branch, the fault is cleared by tripping the faulted branch as shown in Figure IV-21. By examining the angle difference between the generator terminal bus and the external system bus, synchronism can be determined. Through repeated dynamic simulation, the CCT is obtained. Note that the CCT step used in this study is half a cycle.
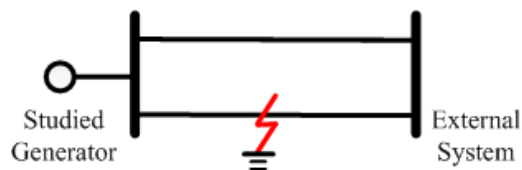
Figure IV-21 Branch Fault Setup

The matrix pencil method is used for estimating oscillation modes in simulation data. The matrix pencil method approximates an oscillatory signal by a summation of exponentially varying sinusoids [77]:

$$y(t) = \sum_i^n a_i \exp(b_i t) \cos(\omega_i t + \phi_i) \qquad (4\text{-}5)$$

Where:

$y(t)$: The oscillatory signal

n: The number of oscillation modes

a_i: The initial amplitude of oscillation mode i

b_i: The damping coefficient of oscillation mode i

ω_i: The oscillation frequency of oscillation mode i

ϕ_i : The initial phase of oscillation mode i

In the matrix pencil method, a Hankel matrix is first formed from *y(t)*. Then, singular value decomposition (SVD) is used to extract singular values that are greater than a user-defined threshold. The remaining singular values are discarded. Last, by QR decomposition, a least square equation is solved to obtain *a_i, b_i, ω_i,* and *ϕ_i*.

34 conventional generators are selected for rotor angle stability study. Those 34 units are geographically located across the system as shown in Figure IV-22.

Figure IV-22 Locations of Studied Synchronous Generators

As previously mentioned, fictitious parallel branches are created on generator terminal buses. A fault is applied on a parallel branch to trigger a severe disturbance. By

incrementally increasing the fault clearing time, the rotor angle of a subject generator will eventually diverge with the angle of the external system and the CCT is obtained. Table IV-5 summarizes the CCT comparison of the 34 generators between the baseline and high-wind cases.
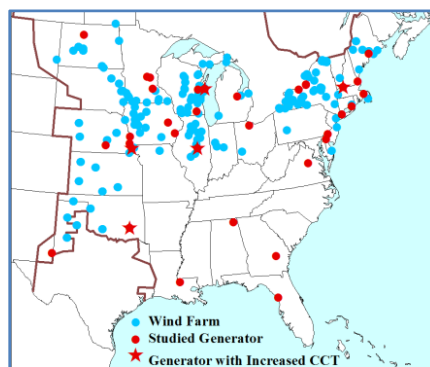
Table IV-5 Comparison of CCTs (Unit: Half Cycle)

Generator #	Baseline	High-wind	Generator #	Baseline	High-wind
1	116	116	18	24	24
2	11	11	19	17	17
3	17	17	20	21	21
4	15	15	21	28	28
5	138	138	22	26	26
6	35	35	23	19	19
7	**36**	**37**	24	25	25
8	16	16	25	18	18
9	26	26	**26**	**13**	**14**
10	**19**	**20**	27	187	187
11	35	35	28	21	21
12	24	24	29	174	174
13	77	77	30	30	30
14	27	27	31	20	20
15	21	21	32	23	23
16	**17**	**18**	**33**	**24**	**25**
17	199	199	34	203	203

It is observed that WTGs have no discernible impact on CCT in 29 out of 34 generators. For the remaining five generators, which are located in or near wind generation areas, WTGs increase CCT by a half cycle. Those generators are marked by a star in Figure IV-22. To explore the physical explanation, an in-depth analysis is conducted on Case 33, shown in Figure IV-23.

The generator rotor angle responses are plotted in Figure IV-24. The fault clearing time is the CCT of the high-wind case. As expected, the subject generator in the high-
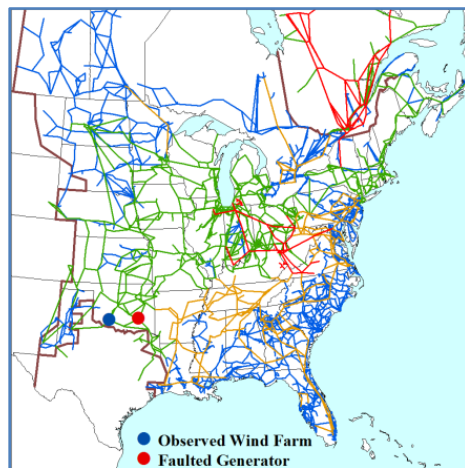
Figure IV-23 Generator Locations for Case 33
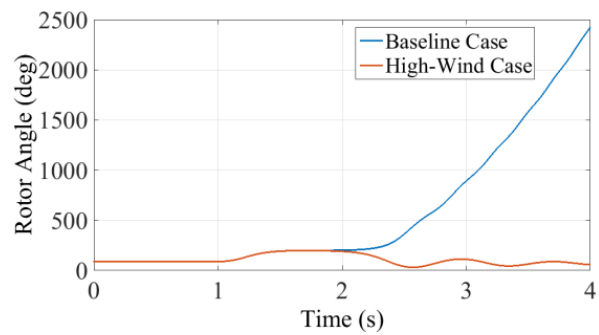
Figure IV-24 Rotor Angle Response

wind case stays synchronized but loses stability in the baseline case. Since CCT is directly tied to power transfer strength and boundary conditions, the difference is traced back to the contribution of WTGs. Figure IV-25 plots the reactive power responses of a nearby wind plant.
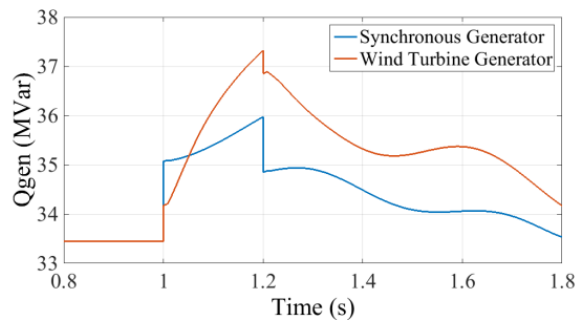
Figure IV-25 Reactive Power at a Nearby Wind Plant

In the high-wind case, the wind plant is represented by a WTG, while in the baseline case the same plant is modeled by a synchronous generator with excitation. The comparison indicates that the WTG provides faster and stronger reactive support than its conventional counterpart and thus increases transfer capability throughout the first swing.

To excite inter-area oscillation modes, 28 generators are tripped across the system. The matrix pencil method is used to calculate bus frequency oscillation modes at 16 observation points across the system. A sample case is plotted in Figure IV-26 and Figure IV-27. The tripped generator is located in the state of Georgia. The studied inter-area oscillation frequency is in the range of 0.15 to 0.20 Hz. The comparison of oscillation damping ratio is plotted in Figure IV-28.

Figure IV-26 Frequency Response of the Baseline Case
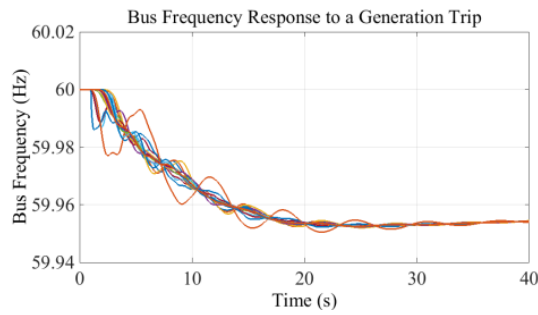
Figure IV-27 Frequency Response of the High-wind Case
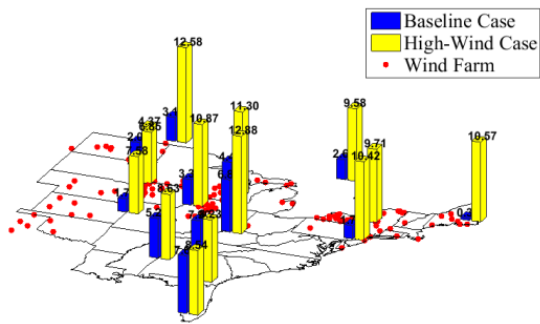
Figure IV-28 Damping Ratio Comparison

In this sample case, the high-wind case shows an average 434% increase in inter-area oscillation damping ratio, 1% increase in oscillation frequency, and 9% increase in oscillation magnitude. Due to the data volume, detailed results are not listed in full in this paper. By average the high-wind case increase the inter-area oscillation damping ratio by 183%, frequency by 7%, and magnitude by 9%.
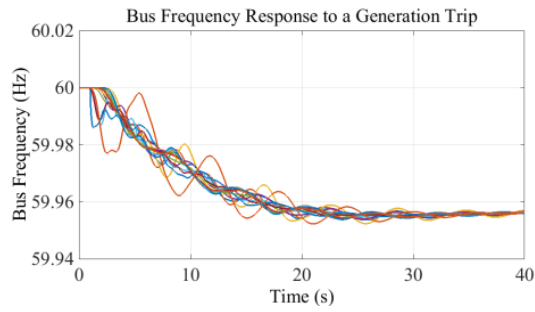
It is physically intuitive that WTGs can increase inter-area oscillation frequency and magnitude due to the reduction of system inertia. To further confirm that WTGs' improvement in damping is always the case, a separate simulation test is conducted on the classical two-area system [11]. With the rest of the system kept identical, one of the four generators is modeled by: 1) High-gain excitation; 2) low-gain excitation with a power system stabilizer (PSS); and 3) a WTG in terminal voltage control mode, respectively. Figure IV-29 compares the simulation results and inter-area oscillation modes.

Case	Oscillation Frequency	Oscillation Damping	Oscillation Magnitude
#1: High-gain exciter	0.79 Hz	4.76 %	0.0018
#2: Low-gain exciter with PSS	0.81 Hz	-1.16 %	0.0060
#3: WTG	0.94 Hz	3.40 %	0.0340

Figure IV-29 Inter-area Oscillation Analysis of the Two-area System

In Case #1, the studied generator contributes negative inter-area damping due to the high excitation gain. In Case #2, the decrease of the excitation gain and the installation of a PSS result in positive damping contribution. The damping ratio of Case #3 falls betwee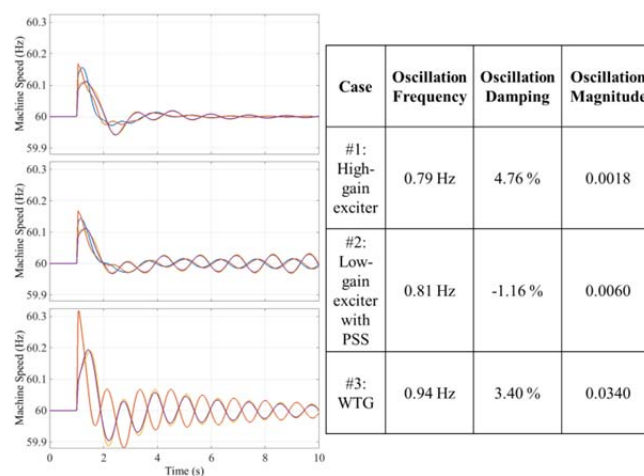n the first two cases, indicating that wind penetration can either enhance or undermine the inter-area damping ratio. This depends on the overall contribution of replaced synchronous generators, as WTGs only lightly react to inter-area oscillations. The conclusions from the two-area system are consistent with that of the detailed EI model but with more discernable difference in simulation.

To assess the impact of wind penetration on rotor angle stability and inter-area oscillation in the EI system, this study looked at critical clearing time and inter-area oscillation damping. From the comparison between the baseline and high-wind cases, dynamic simulation results indicate the following:

- At the 17% penetration level, wind generation has no impact on rotor angle stability for synchronous generators distant to wind generation regions. Nearby generators may be slightly affected with improved stability margin. The improvement is likely linked to the fact that WTGs can provide faster and stronger reactive power support during the first swing and raise power transfer capability.

- WTGs are only lightly engaged in oscillations because of their strict output power regulation. Depending on the damping contribution of displaced synchronous units, wind penetration can either increase or decrease inter-area oscillation damping, but it is certain that wind penetration will increase inter-area oscillation

frequency due to the reduction of system inertia. For the same reason, inter-area oscillations can exhibit higher oscillation magnitude.

This study on the stability impact of wind penetration is far from comprehensive. Future work can be improved in three directions: First, the coverage of a full spectrum of operating conditions, like spring light and summer peak, will give a wider range of performance variation. Second, simulating a much higher percentage of wind penetration, say 60%, can better identify the risks and benefits introduced by WTGs. Last, a larger simulation pool containing thousands of cases would provide more solid conclusions. Ongoing research will address these issues.

3.8 Summary

This chapter concentrates on the stability impact of wind generation on the EI 2030 grid. The study scope ranges from frequency response, inter-area oscillation, and rotor angle stability. By comparing the difference of dynamic performance between the baseline and high-wind cases, it is revealed that:

- The frequency response degradation due to the 17% wind penetration is slight and acceptable. The degradation can also be offset by increasing governor ratio and decreasing governor deadband.

- Compared with the baseline case, the high-wind case exhibits increased inter-area oscillation frequency and magnitude. This phenomenon is associated with the reduction of system inertia. Inter-area oscillation damping is also improved in the EI 2030 cases, although a separate test on the two-area system indicates that trend can go both ways.

- Rotor angle stability of the conventional generators near wind farms seems slightly improved. The improvement is likely to be associated with the voltage control of wind generators.

Since the studied dynamics models only represent a snapshot of a certain system operating condition, more comprehensive studies that include different loading conditions and wind penetration levels are desirable.

V.   Stability Impact of High Solar Penetration on the EI System

Solar generation is experiencing an exponential growth in the U.S. In 2015, the solar PV deployments reached an all-time high of 7,260 MW, up 16% over 2014 and 8.5 times the amount installed five years earlier. When accounting for all distributed and centralized projects, solar accounted for 29.4% of new electric generating capacity installed in the U.S. in 2015, which is only second to that of wind generation [78]. Looking ahead, the U.S. DOE projected that solar technologies would satisfy roughly 14% of U.S. electricity demand by 2030 and 27% by 2050 [5]. With 25.6 GW operating capacity by the end of 2015 and a rapid deployment trend, solar generation is no longer a negligible generation technology. Its stability impact deserves a thorough and comprehensive investigation.

In late 2015, the joint research team from the University of Tennessee, Knoxville, Oak Ridge National Laboratory, and National Renewable Energy Laboratory, was awarded by the DOE SunShot Initiative a three year project to study the effect of increased solar PV generation on frequency response of the three U.S. interconnections and possible mitigation measures. This chapter describes the model development process to build a series of high PV penetration models for the EI system. Preliminary impact studies are also included.

4.1 Baseline Model Building

The key of a credible simulation study is its accuracy. Simulation results based on inaccurate models could lead to problematic conclusions. When it comes to frequency response studies on the U.S. interconnections, the correlation between actual

measurements and simulation results reflects the truthfulness of the simulated model and the credibility of the simulation study. As noticed both by the academia and industry, the original EI Multi-regional Modeling Working Group (MMWG) models that are widely used in the industry exhibit frequency response at a level that is much higher than actual performance. Such inaccuracy tends to conceal the potential risk of frequency response degradation associated with PV penetration. Therefore, building a credible baseline case is critical to the correctness of the end results and conclusions of the entire project.

Interconnection frequency response varies depending on system operating conditions. A large number of factors, including the amount of online generating capacity that has responsible governor response, individual unit governor settings, and load characteristics, can contribute to frequency response. Therefore, it is not surprising to observe in Figure V-1 that the EI beta value falls into a broad range over time, according to NERC [79].

The EI 2030 high wind high build-out model described in Chapter 2 is selected as the baseline model, based on which higher PV penetration will be achieved. This model is chosen for several reasons. First, the EI 2030 model has the most accurate wind farm locations and transmission expansion plans. As mentioned earlier, the steady state study was conducted by all major EI planning coordinators with a bottom-up approach. The network topology and generator commitment will be the closest to the future high wind scenario. Second, the EI 2030 model was indirectly validated through measurement by replacing all wind generators. Therefore, the simulation accuracy is a level higher than any current available EI MMWG models. On the flip side, the EI 2030 model is only a snapshot of the real system, which can operate in thousands of different conditions.

Therefore, the goal of calibrating the baseline case is to match up the system frequency response characteristic under the condition which the case represents.
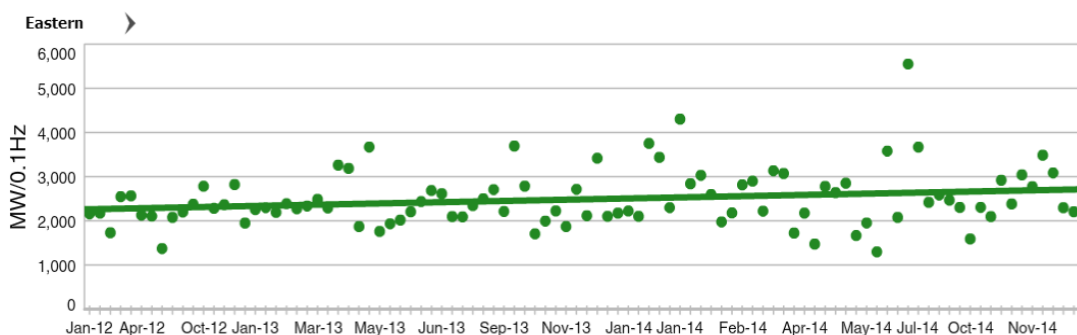

Figure V-1 EI Frequency Response Records

The model calibration process involves two steps: Case selection and parameter tuning. Nuclear generation trip events are preferred because the generation trip time and MW amount are public on the U.S. Nuclear Regulatory Commission website. More importantly, since nuclear units are usually base loaded and operating at a fixed MW level, it is more likely to find that the same unit is dispatched at the same MW value. Thus, an equal amount of MW generation loss can be replicated in the model. Using confirmed cases by the industry is also viable. In addition to selecting events with the right amount of MW loss, the pre-disturbance system condition is another critical factor. Ideally, the model to be validated should capture the exact pre-disturbance system condition, including unit commitment, power dispatch, load capacity, transmission topology, and so forth. However, reconstructing a pre-disturbance system model requires complete system measurement and information and involves a substantial amount of model building work. Such demanding requirements cannot be materialized in the EI

system. As a compromise, the measured pre-disturbance system total load is obtained to make sure the loading condition is comparable to that of the model to be validated. The hourly historical load data of the U.S. power grids can be found from the U.S. Federal Energy Regulatory Commission (FERC) Form No. 714.

Once proper actual events are selected for model validation, FNET/GridEye synchrophasor measurements can be retrieved based on event time. The GPS coordinates of the Frequency Disturbance Recorder (FDRs) should also be obtained to identify the locations of measurement. Simulation results from nearby buses in the dynamics model will be later chosen for comparison with measurement.

After selecting actual events and collecting measurement, parameter tuning can be performed. Assuming a clean dynamics model without any initialization errors is prepared beforehand, there are three major parameters that need adjustment. They are governor deadband, governor ratio, and system inertia. As discussed in Chapter 3, inserting governor deadband to represent turbine governors' non-responsiveness around 60 Hz can highly improve simulation accuracy of the EI system. Since individual deadband data are not available, an average deadband of 33-42 mHz is assumed. Settling frequency is equally determined by governor ratio. A larger number of generators with responsive governor response translate into a stronger frequency response and reduced settling frequency deviation. System inertia has bare influence on settling frequency but largely dictates the inertial slope. It can occur that the modeled system has higher system inertia than the real system and therefore slightly scaling down generator inertia can help

better match the inertia slope. Large inertia tuning down (>50%) is not recommended due to potential numerical divergence caused by unrealistically low machine inertia value.

Governor deadband and governor ratio are adjusted at the same time in order to show best match in settling frequency with multiple events. System inertia is scaled up or down as the final step to align the inertia slope.

Two case studies are shown below. The first case is the McGuire Unit 1 generation trip that occurred in North Carolina on February 21, 2013, 14:57:06 UTC.

The comparison between simulation and measurement in Figure V-2, Figure V-3, and Figure V-4 indicates satisfactory correlation.

The second case is the North Anna Unit 2 in Virginia that was tripped on May 28, 2013, 19:07:54 UTC. Comparison is shown in Figure V-5

Figure V-6, and Figure V-7.

In the finalized base model, the governor deadband is 36 mHz. The generation capacity with responsive governor response is 185 GW or 33% of total generation capacity. The total system inertia is 4976 GVA·s.

To further confirm the accuracy of the base model, a more exhaustive simulation test is conducted. This test includes 32 generation trip events. The largest generators by MW at major balancing areas are selected for the test. After the inclusive simulation test, settling frequency and beta value are calculated. A snapshot of the generation trip simulation results is plotted in Figure V-8. The average beta value of the 32 cases is 2634 MW/0.1 Hz, while the measured EI average beta value is 2363 MW/0.1 Hz [4]. Considering the variation of the EI frequency response, 11% difference is satisfactory.
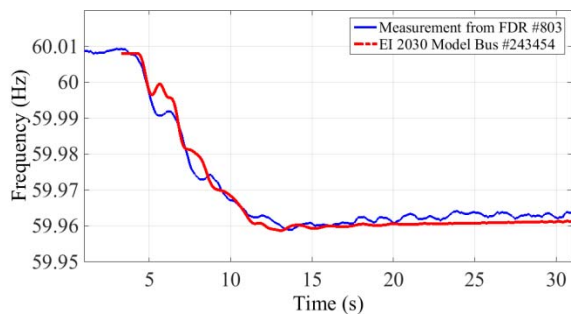
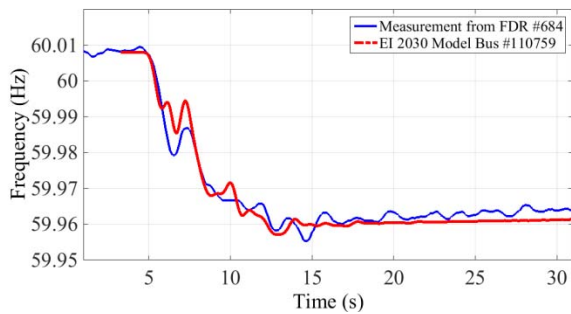Figure V-2 Model Validation Case #1: Observation in Ohio

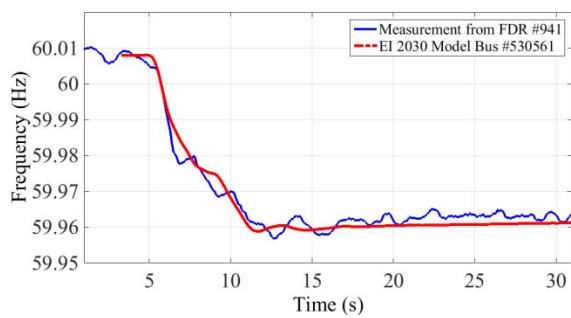Figure V-3 Model Validation Case #1: Observation in Massachusetts

Figure V-4 Model Validation Case #1: Observation in Kansas
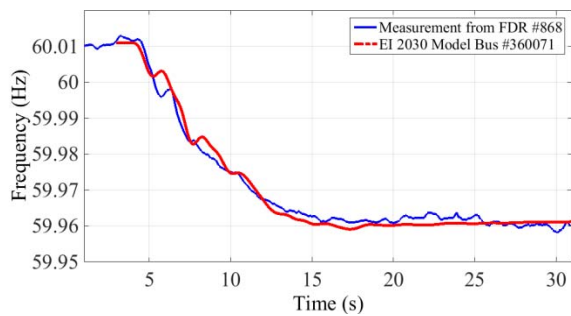
Figure V-5 Model Validation Case #2: Observation in Tennessee
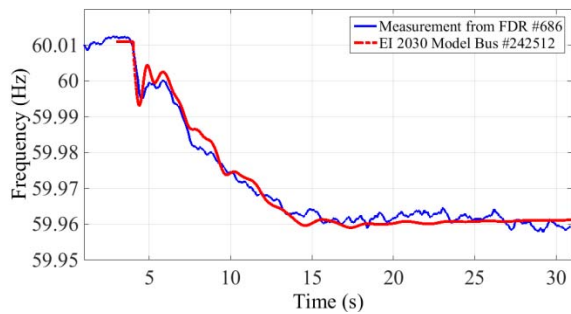

Figure V-6 Model Validation Case #2: Observation in Virginia
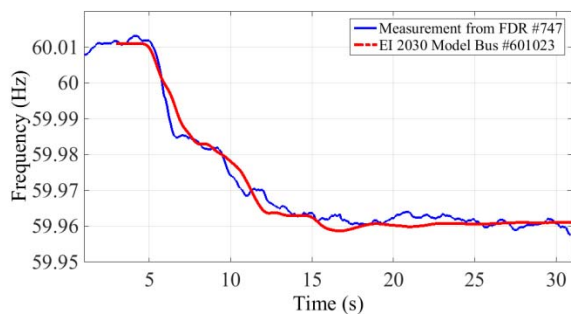

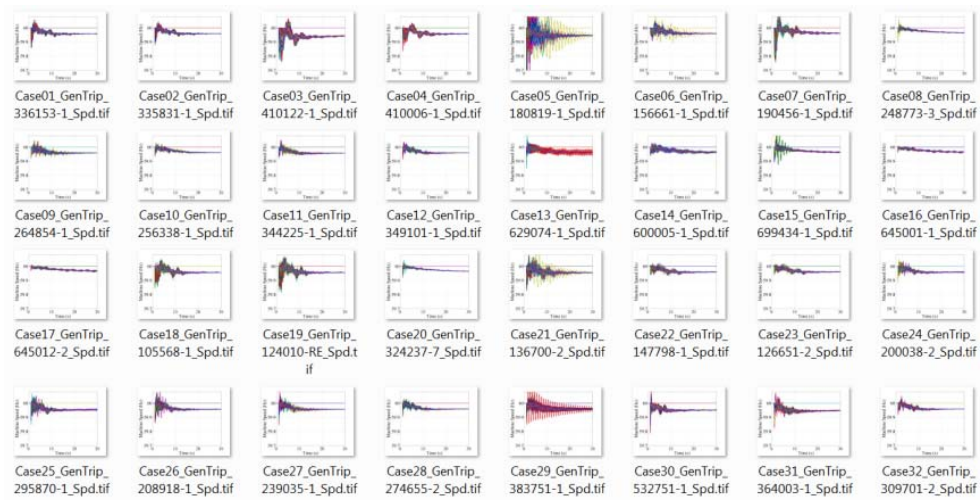Figure V-7 Model Validation Case #2: Observation in Minnesota

Figure V-8 Generation Trip Test

Although the base case matches certain actual events and its average beta value is close to the real system, one particular governor setting cannot match every single event. Figure V-9 shows the Saint Lucie Unit 1 generation trip event that occurred on March 12, 2013, 18:51:50 UTC. The settling frequency has 9 mHz mismatch.
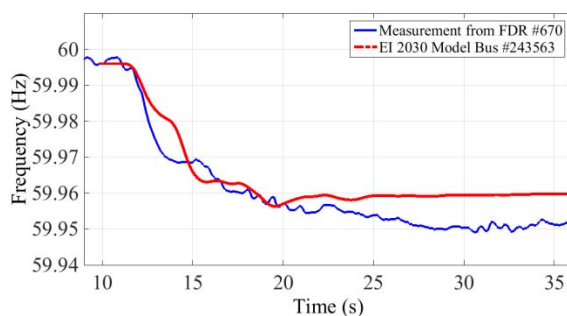

Figure V-9 Generation Trip Occurred in Florida

4.2 Integrating PV Generation

The GE Photovoltaic Converter model is selected to represent the dynamic behavior of PV plants. This model is preferred for two reasons. First, the GE PV model in PSS/E is a user-defined model and thus is not subject to the upper limit on the number of built-in wind and solar models. The limit is 560 in PSS/E 33. The 80% solar case has 2,433 PV units and cannot be achieved only by built-in PV models. Second, the GE PV model is one of the most well prepared PV dynamics models available for grid studies. The vendor has been putting substantial efforts to improve and validate the model [80]. Its accuracy is therefore accountable. It is true that the GE PV model is not a generic model that represents any PV unit's dynamic behaviors. However, the model captures the major

frequency response characteristic of converter based generators, which is inertia and governor non-responsive.

The GE PV model is a built for bulk power system studies and focuses on how a solar plant reacts to grid disturbances. Very fast dynamics associated with the inverter controls are simplified with algebraic equations. The model is intended for positive sequence electromechanical simulation rather than short circuit or electromagnetic simulations. The PV plant model consists of two device models, i.e. the inverter model and the electrical control model. The inverter model injects active and reactive current in response to control commands given by the electrical control model. The inverter model also integrates high and low voltage protective functions. The electrical control model feedbacks terminal voltage and gives active and reactive current commands accordingly. The reactive control strategies include voltage regulation, fixed Q, and fixed power factor. The model structure of the GE PV model is shown in Figure V-10 [80].
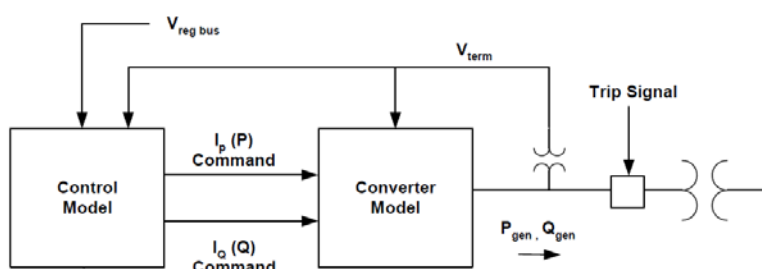

Figure V-10 The Structure of the GE PV Model

To create high PV penetration scenarios up to 80% and regional 100%, a portion of conventional generators are converted to PV plants and modeled by the GE PV model. The selection is based on power factor. Since PV plants are operated at a relatively high

power factor (> 95%), a screening process is performed to select units with high power factor as candidates.

The major simulation challenge of modeling high PV penetration is the numerical divergence. When the PV penetration reaches a certain level, the numerical integration can fail to solve. The numerical divergence can fall into two types. The first type results in network divergence warnings by PSS/E, which means the numerical integration at a certain time step cannot converge within the pre-set number of iterations. Severe network divergence can even lead to program crashes. The other type of numerical divergence does not cause network divergence warnings but high frequency oscillations in simulation results. An example is shown in Figure V-11. The numerical high frequency oscillation is fundamentally different than physical oscillations. The oscillation frequency of numerical oscillations ranges from 14-20 Hz and is above the frequency bandwidth of time-domain electromechanical simulation software. Besides, the numerical oscillation frequency is dependent on simulation time step and can even disappear when time step is small enough.
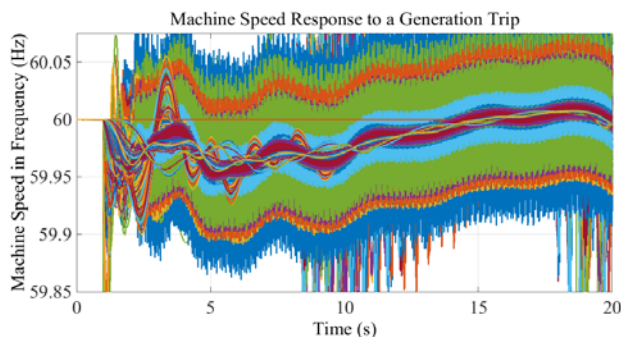

Figure V-11 Numerical High Frequency Oscillation

Although both types of numerical divergence can output simulation results, their accuracy is compromised. To ensure simulation accuracy, extensive simulation tests were conducted to identify the root cause of the numerical divergence. It is found that numerical divergence is likely to occur when converter based renewable dynamics models reach a certain penetration level regionally. By re-locating PV generators from high penetration areas to less penetrated areas, a higher penetration level can be reached interconnection wide.

A series of high penetration level cases are created based on previously measurement validated base case. The PV penetration levels include 20, 40, 60, and 80%. The PV plant locations are plotted in Figure V-12, Figure V-13, Figure V-14, and Figure V-15.

Extensive generation trip cases, including the largest single generator in major EI balancing areas, are conducted at each penetration level. No numerical divergence exists in the finalized model series.

4.3 Preliminary Frequency Response Study

As discussed in the last chapter, adding renewable energy in the power grid can result in declining frequency response. The purpose of this SunShot Initiative project is to evaluate the impact of PV generation on interconnection frequency response and find out at what penetration level the interconnection frequency response obligation will be violated. With the measurement calibrated base model and the high PV penetration model series, a preliminary frequency response impact study is presented below.
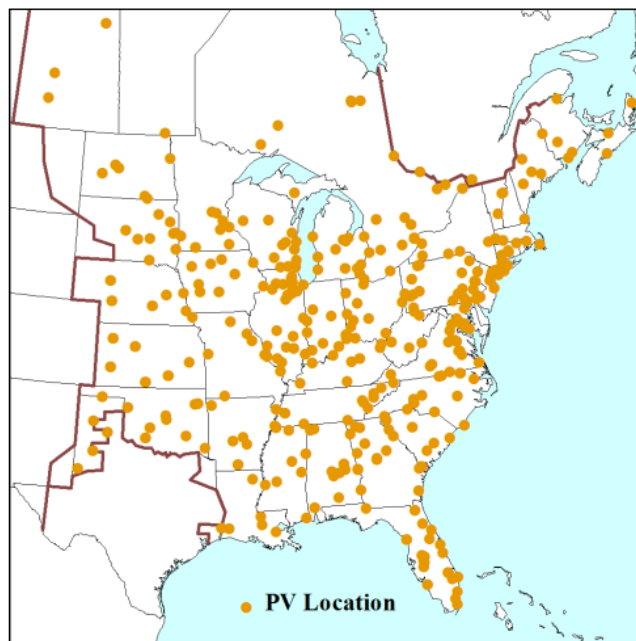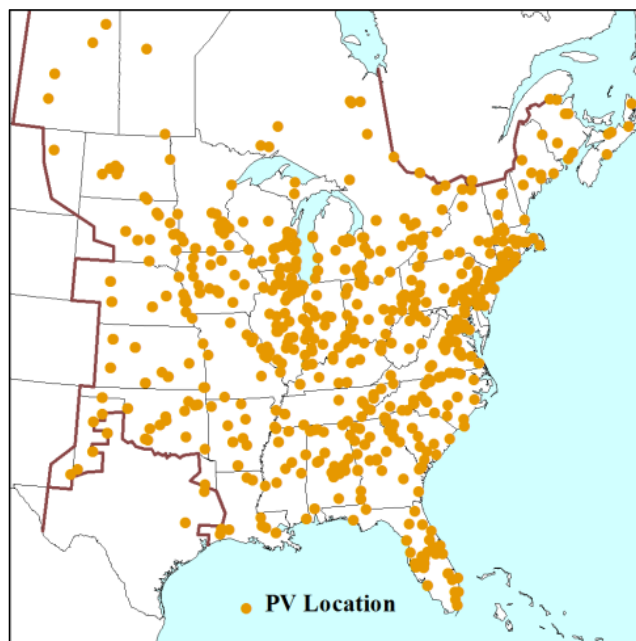
Figure V-12 20% PV Penetration Map
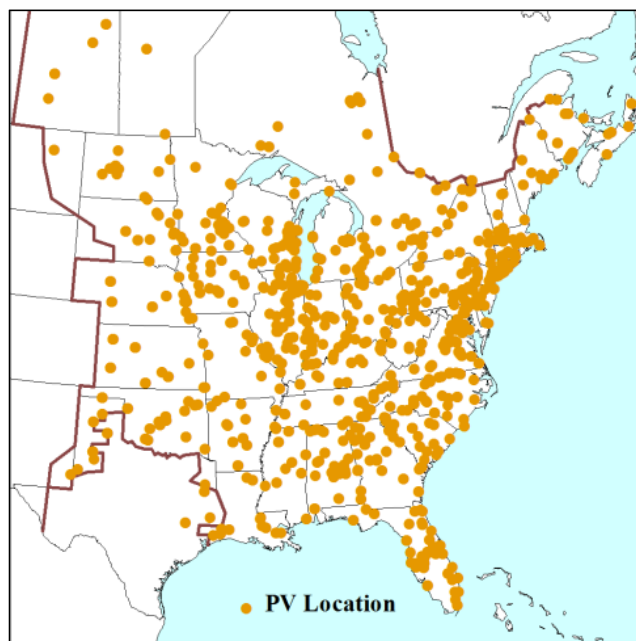

Figure V-13 40% PV Penetration Map

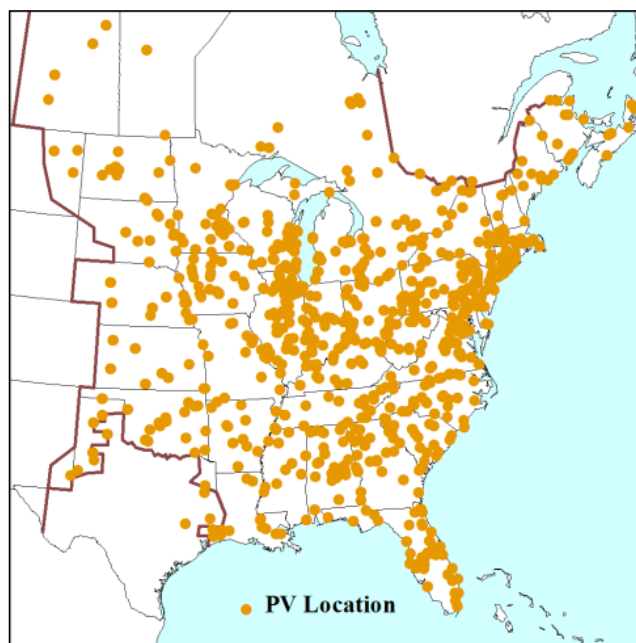Figure V-14 60% PV Penetration Map

Figure V-15 80% PV Penetration Map

Frequency response is provided by generator governor response and load response. It varies by different operating conditions and the MW generation loss. To get an accurate measure of frequency response, extensive generation trip tests were conducted to calculate the average β value. 32 generation trip cases were run. The selected generators are the largest two generators in each balancing area and have at least 500 MW loading. β value is calculated for each generation trip case by dividing MW loss over frequency deviation. An average β value is then obtained from the 32 cases and represents the frequency response of a certain PV penetration level.

The simulation results for five different PV scenarios are summarized in Table V-1 and Figure V-16. It is observed that the inertia and the governor capacity decline linearly as PV penetration increases. The frequency response reduces steadily. At roughly 75% PV penetration, frequency response falls to the interconnection frequency response obligation.

Table V-1 Frequency Response at Different PV Levels

PV %	Frequency Response (MW/0.1Hz)	Inertia (GVA·s)	Governor Capacity (GVA)
0	2634	4976	263.54
20	2421	4299	204.14
40	2117	3618	142.05
60	1683	2965	85.15
80	911	2297	26.49

4.4 Inter-area Oscillation Study

Solar generation is characterized as inertia-less and barely being engaged with oscillations. The early study in this thesis on wind generation indicates power converter based generators could lead to higher inter-area oscillation frequency and improved damping. An impact study on the increased PV generation in the WECC system used planning models and built augmented high renewable cases by displacing conventional generations. The highest PV case reaches 24 GW. This study discovers that higher PV penetration will result in an upward trend in oscillation frequency due to reduced system inertia. The oscillation damping is unaffected although some modes may exhibit damping decrease [81]. A separate study on the WECC system models PV generation, including utility scale PVs and rooftop PVs, up to 50%. This study shows that higher PV penetration can lead to decreased damping [82]. This section is investigating the impact of increasing PV on the inter-area oscillation of the EI system.
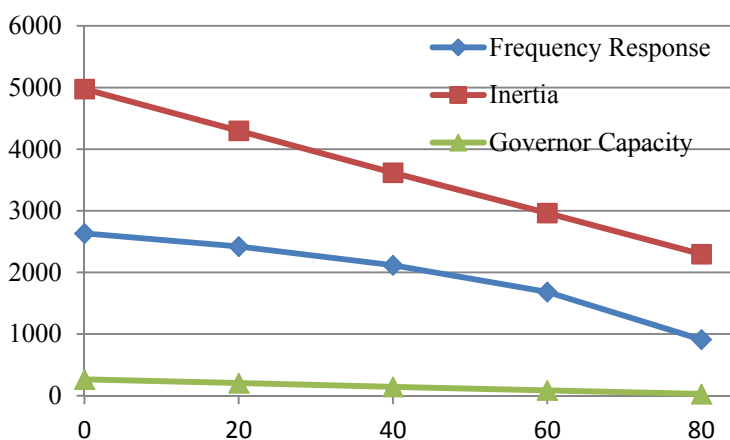

Figure V-16 Frequency Response at Different PV Levels

The inter-area oscillation pattern is depicted as the three areas, i.e. Midwest, Northeast, and Florida, oscillating against the central area. The oscillation frequency ranges around 0.2 Hz. To better observe the inter-area oscillation behavior, bus frequency at the four areas are selected for modal analysis. Since the central area is largest in capacity and the other three areas are oscillating against it, the bus frequency from the central area is chosen as the reference. Bus frequency difference is preferred than bus frequency to observe and quantify inter-area oscillation, because bus frequency provides better observability and therefore it is less numerically challenging for modal analysis algorithms to reach accurate estimations. A comparison of oscillation observability is shown in Figure V-17and Figure V-18.

Four generation trip cases are studied. The tripped generators are located in Vermont (VT), Illinois (IL), Minnesota (MN), and Florida (FL), respectively. This way the findings would not be biased on generation trip locations. The exact locations of generation trips and selected observation buses are shown in Figure V-19. Matrix Pencil Method is used to calculate oscillation frequency and damping. A separate program is employed to calculate first swing magnitude.

The oscillation calculation divides into three steps. First, a generation trip event is created in different PV levels, including 0%, 20%, 40%, 60%, and 80%. The selected bus frequency is output. Two sample simulations are demonstrated in Figure V-20 and Figure V-21. The simulation time is extended to 40 seconds to fully capture the damping dynamics.
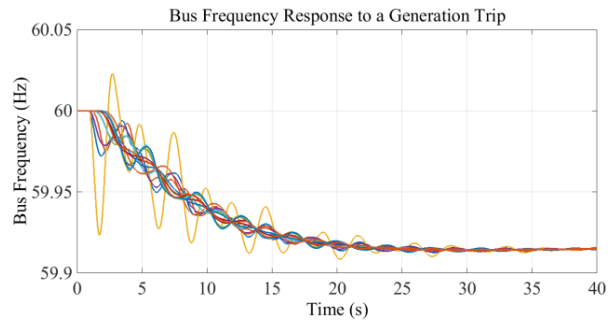
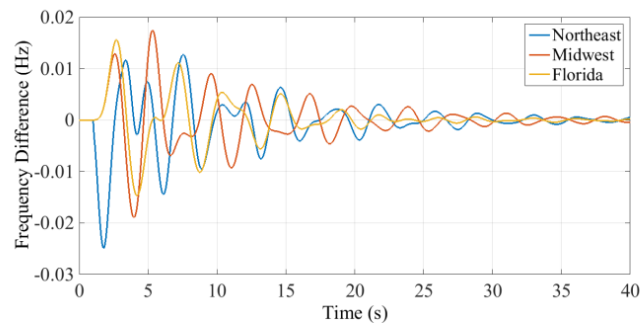Figure V-17 Oscillation Observed from Bus Frequency

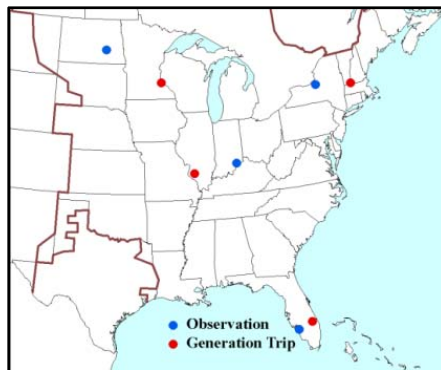Figure V-18 Oscillation Observed from Bus Frequency Difference

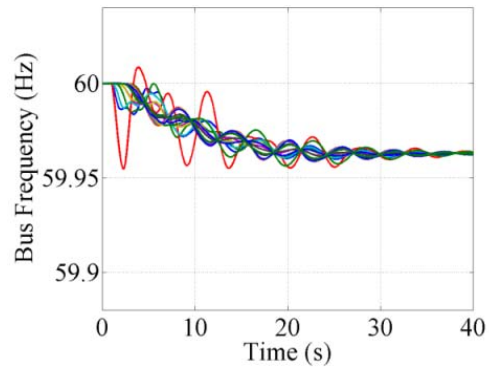Figure V-19 Generation Trip and Observation Locations

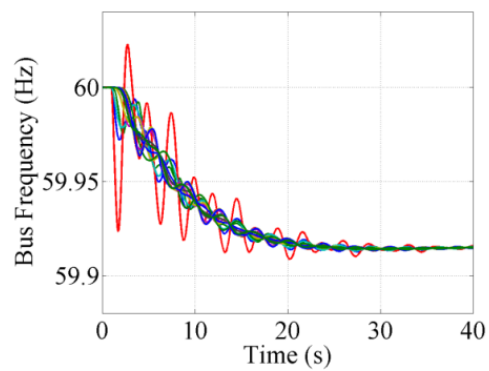Figure V-20 Bus Frequency Response to a Generation Trip in the 0% PV Case

Figure V-21 Bus Frequency Response to a Generation Trip in the 80% PV Case

Second, bus frequency difference is obtained by subtracting the reference frequency in the central area from the other three areas to get the inter-area oscillations. An example plot is shown in Figure V-22. Third, Matrix Pencil Method is applied on the three bus frequency difference channels, i.e. Northeast, Midwest, and Florida. Oscillation frequency, damping, and first swing magnitude are obtained for the three channels and there are totally five PV penetration cases.
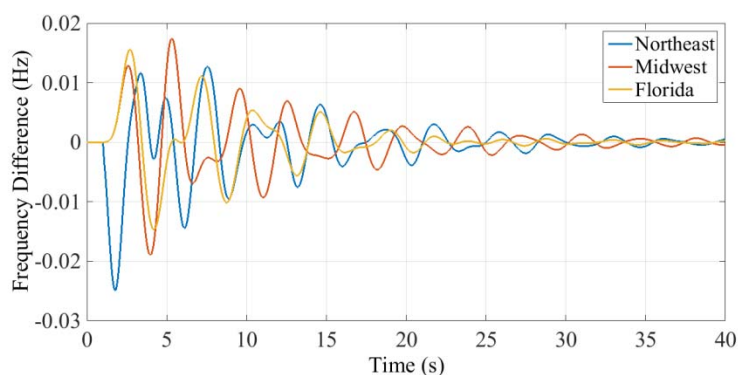
Figure V-22 Bus Frequency Difference

Four generation trip cases are studied and their oscillation patterns are summarized below. Figure V-23, Figure V-24, and Figure V-25 present a generation trip in Vermont (VT).

It is noted that every 20% PV penetration poses a 0.02 Hz increase in inter-area oscillation frequency. Damping peaks between 20% to 40% and then decreases as PV penetration grows. First swing magnitude increases monotonically. The increase in oscillation frequency and first swing magnitude is related to the inertia reduction. Similar

patterns are observed on another three cases and consistent among different observation locations.

Figure V-26, Figure V-27, and Figure V-28 show a generation trip that occurs in Illinois (IL).

Figure V-29, Figure V-30, and Figure V-31show a generation trip that occurs in Florida (FL).

The last case shows a generation trip in Minnesota (MN) in Figure V-32, Figure V-33, and Figure V-34.

The oscillation trend can also be observed from time domain simulation in Figure V-35.

It is consistent and evident from the studied four cases:

• Reduced inertia increases inter-area oscillation frequency.

• With increased PV penetration, the inter-area oscillation damping in the studied EI model improves and then deteriorates.

• Lower system inertia also leads to larger inter-area oscillation first swing magnitude.

The fact that reduced inertia results in higher inter-area oscillation frequency in the EI system is further confirmed in other systems, such as the Kundur two area system, ERCOT, and WECC. Figure V-36 presents the upward trend in oscillation frequency regarding to system inertia reduction. The change rate of oscillation frequency over inertia percentage reduction is roughly the same throughout different systems.

Figure V-23 Inter-area Oscillation Frequency of the Generation Trip in VT

Figure V-24 Inter-area Oscillation Damping of the Generation Trip in VT

Figure V-25 Inter-area Oscillation First Swing Magnitude of the Generation Trip in VT

Figure V-26 Inter-area Oscillation Frequency of the Generation Trip in IL

Figure V-27 Inter-area Oscillation Damping of the Generation Trip in IL

Figure V-28 Inter-area Oscillation First Swing Magnitude of the Generation Trip in IL

Figure V-29 Inter-area Oscillation Frequency of the Generation Trip in FL

Figure V-30 Inter-area Oscillation Damping of the Generation Trip in FL

Figure V-31 Inter-area Oscillation First Swing Magnitude of the Generation Trip in FL
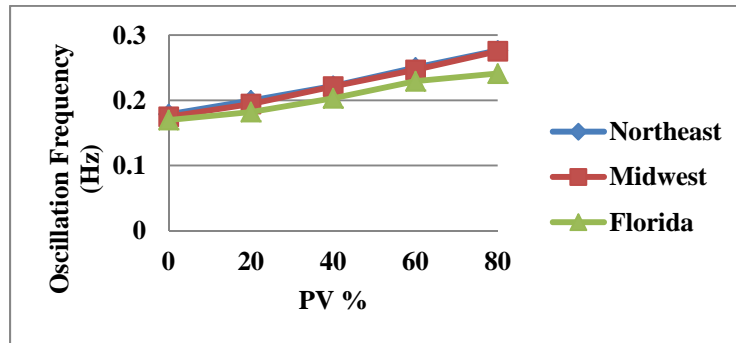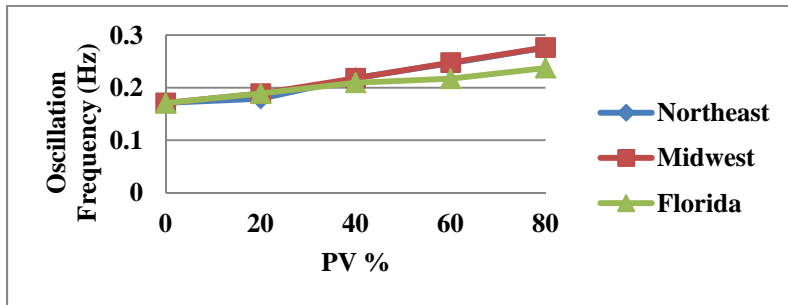
Figure V-32 Inter-area Oscillation Frequency of the Generation Trip in MN
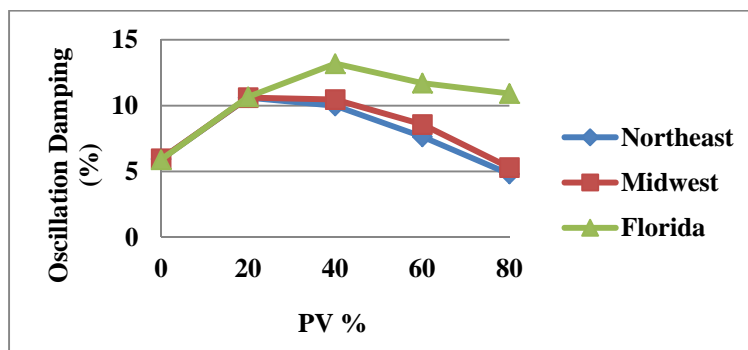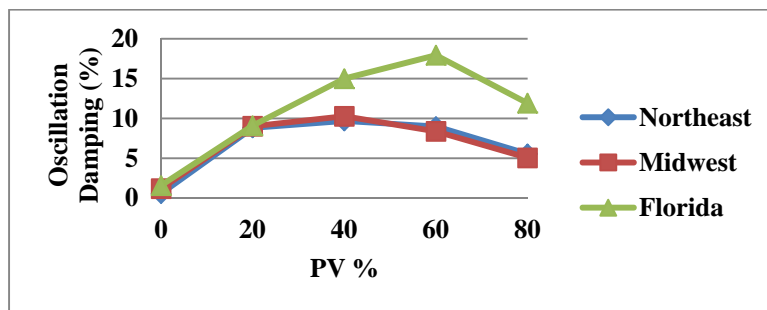

Figure V-33 Inter-area Oscillation Damping of the Generation Trip in MN
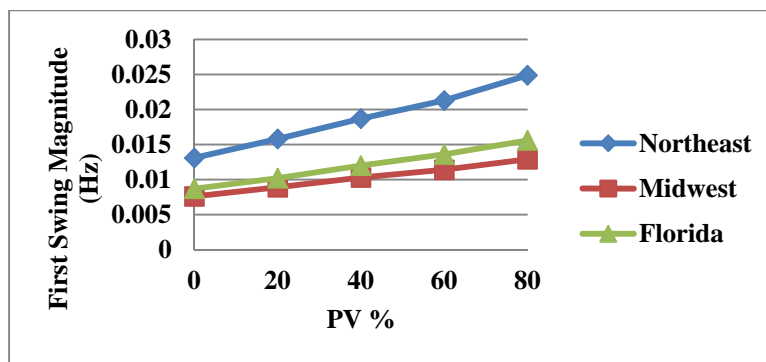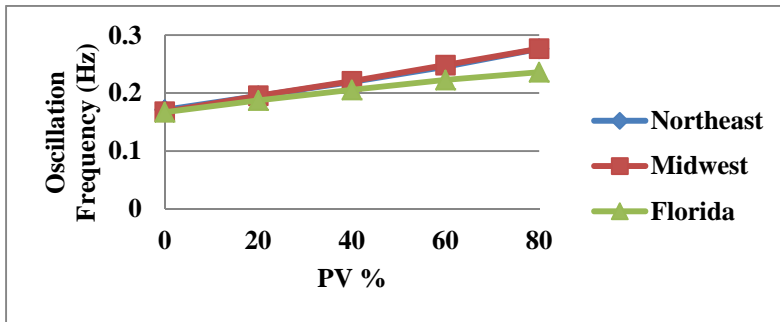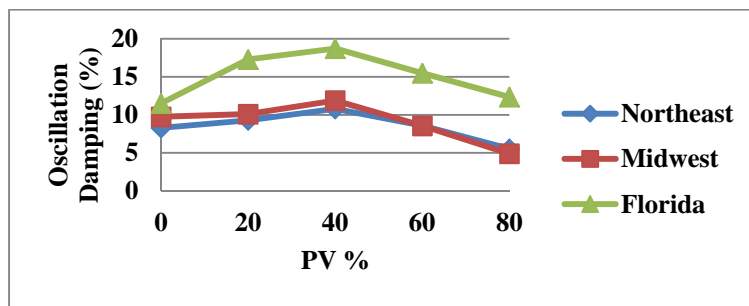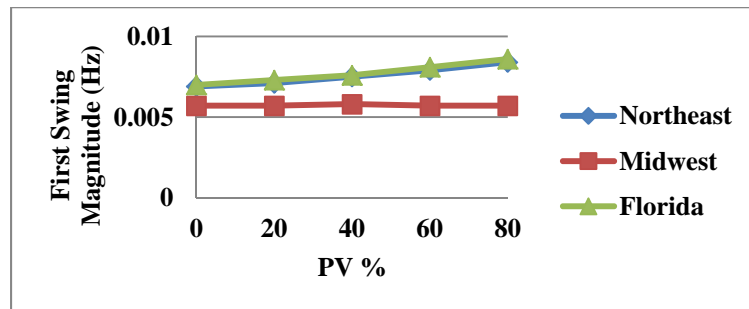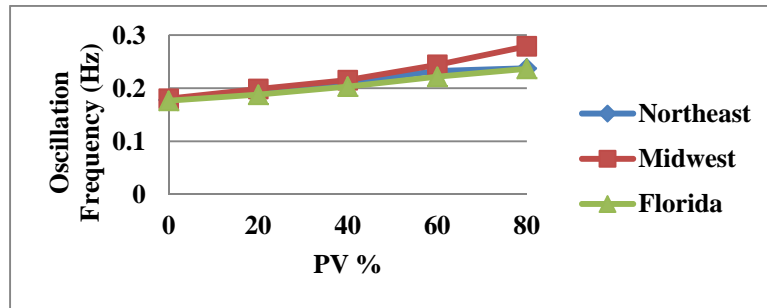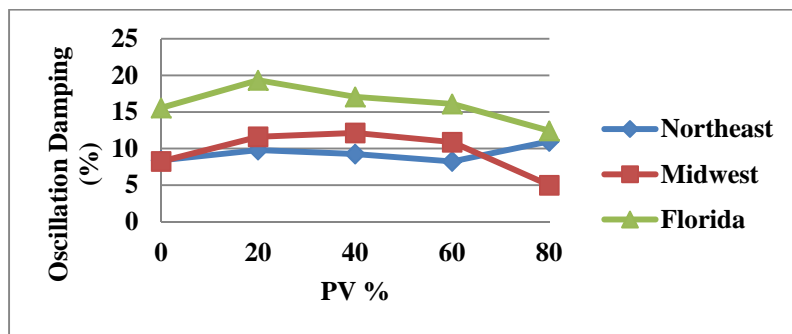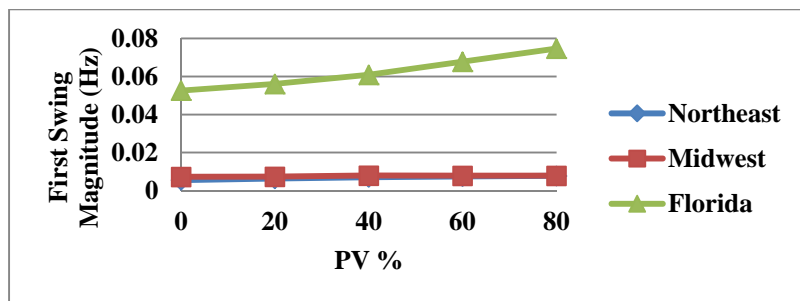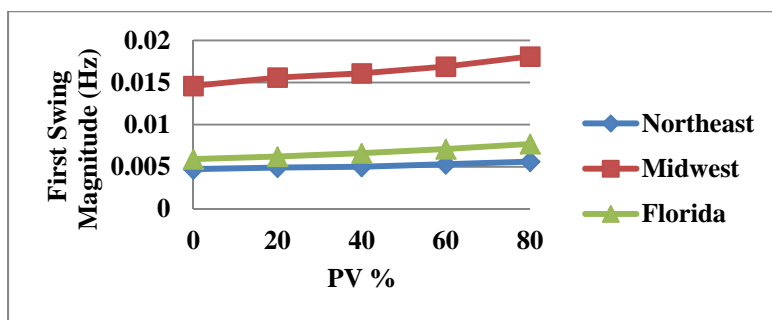

Figure V-34 Inter-area Oscillation First Swing Magnitude of the Generation Trip in MN
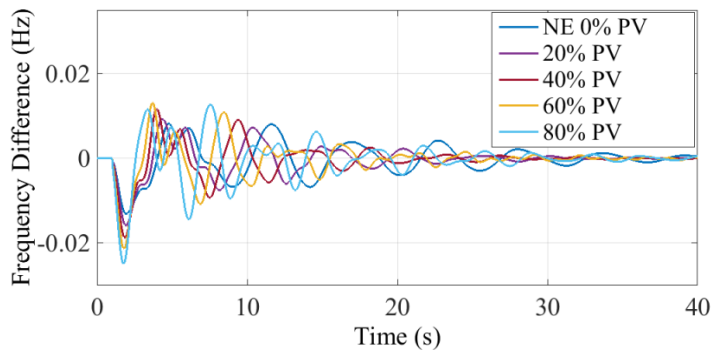
Figure V-35 Inter-area Oscillation Trend with higher PV penetration
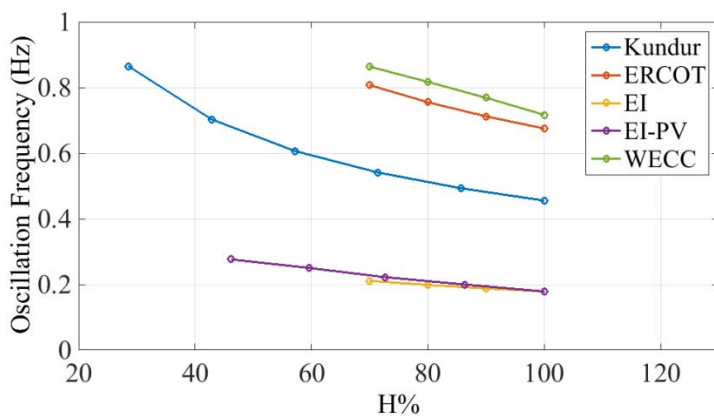
Figure V-36 Inter-area Oscillation Frequency Related to System Inertia

To understand the oscillation damping pattern, additional studies are carried out to examine the relationship between oscillation damping and PV generator voltage control modes. A new model series is built, in which PV generators are switched from voltage regulation mode to constant Q control mode. Similar peaking pattern is also observed among constant Q control cases. It is discerned that PV constant Q control tends to improves inter-area oscillation damping. Damping comparison is shown in Figure V-37. A sample time domain comparison is plotted in Figure V-38. The improved damping due to voltage control mode is noticeable.

This study consolidates the observation that increased level of PV generation will raise up inter-area oscillation frequency due to the loss of system inertia. The first swing magnitude also tends to amplify for the same reason. Results on inter-area oscillation damping present that damping reaches maxima at 20-40% levels. The results also imply that higher PV penetration can either increase or decrease damping. Future efforts are needed to answer further questions such as under what conditions PV and wind would improve or compromise system damping.

4.5 Summary

This high solar penetration study exemplifies an advanced approach to perform interconnection level dynamic simulation studies. Efforts are made to ensure numerical convergence and validate simulation results against measurement. High renewable penetration models are built based on the validated base case. A comprehensive simulation test is conducted to make sure findings are consistent.
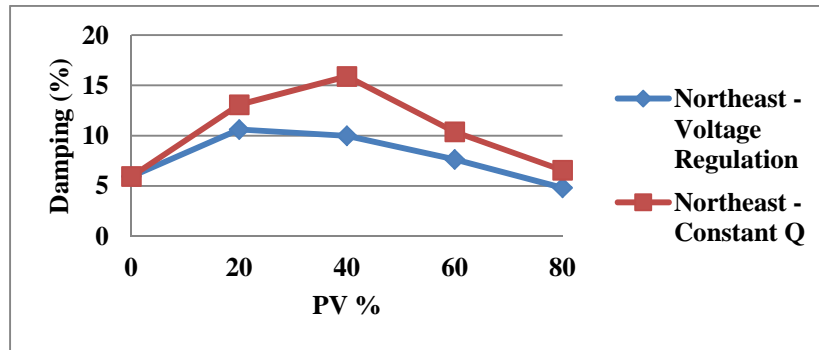
Figure V-37 Inter-area Oscillation Damping in different PV Voltage Control Modes
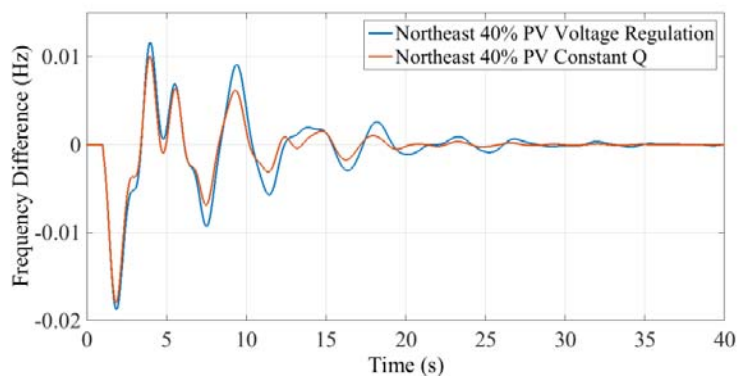
Figure V-38 Time Domain Comparison of Different PV Voltage Control Modes

The frequency response and inter-area oscillation studies give some preliminary observation on the impact of high solar penetration. Degraded frequency response and inter-area oscillation damping deserve further investigations through more extensive simulations under various operating conditions. Mitigation measures should also be studied and tested.

VI.   Dynamic Model Reduction on the U.S. Power Grids

Dynamic model reduction is used in many applications, such as dynamic security assessment and system control design, where a simplified model is needed to satisfy computational or software constraint. In the last three decades, three methods have been proposed to reduce the dynamic model [83]. The modal method is based on the state-space model. By analyzing eigenvalues, eigenvectors, and participation factors, this method selects less damped modes to represent the overall response of the system [84-87]. The coherent method identifies generators that swing together after a perturbation and aggregates coherent machines into one large generator. The associated networks and control devices are aggregated accordingly. The coherent method is also based on modal analysis to recognize coherent generators [88-91]. The measurement or simulation-based method uses an equivalent model, such as gray box, to represent the system. Algorithms like the least-squares algorithm are utilized to identify the best set of parameters [92].

The model reduction study in this chapter documents the effort to build highly simplified U.S. power system models and represent the interconnection level information and behavior such as topology, inter-area oscillation, and frequency response.

5.1 The U.S. 12-machine System

Tightly coupled groups of generators connected by long transmission lines can often exhibit inter-area oscillations. Analysis of FNET measurements provides insights into the oscillation modes of the bulk power system. For example, Figure VI-1shows four inter-area oscillation modes in the EI system detected by FNET. It is noted that there are four coherent regions in the EI system.

After obtaining the number of coherent regions, clustering analysis is performed to aggregate each region into a large generator and a load. To finalize the capacities and boundaries of the coherent regions, a detailed system model is used. One generator is tripped at a time, and the frequency responses at buses corresponding to the locations of FNET Frequency Disturbance Recorders (FDRs) are recorded. By applying the k-means clustering algorithm to the frequency responses, buses are grouped into coherent regions. Figure VI-2 shows the flow chart of the *k*-means clustering algorithm. Figure VI-3 shows the clustering result of the EI system.
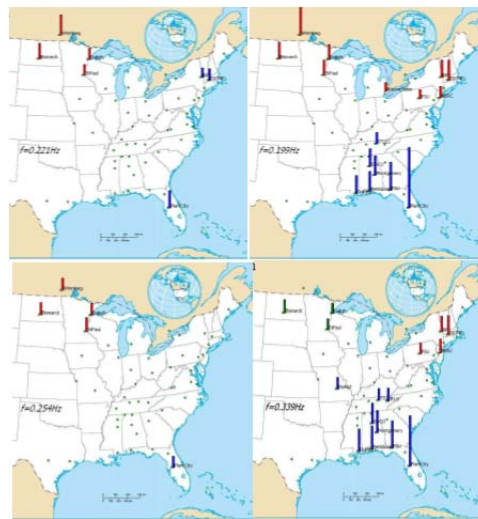
Figure VI-1 Measured Inter-area Oscillation in the EI System

After clustering coherent regions, each interconnection in North America is represented by four generator-load clusters. Besides, to simulate HVDC transmission
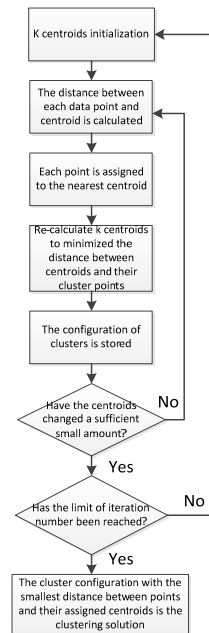
Figure VI-2 *K*-means Clustering Algorithm Flow Chart
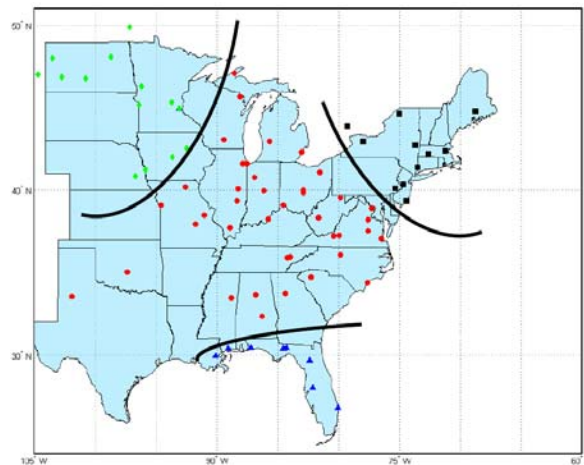
Figure VI-3 Clustering of the EI System

lines, line commuted converters (LCC) are used to link between every two

interconnections. The structure of the proposed large-scale system testbed is shown in

Figure VI-4. In the testbed, weak AC transmission, which has higher reactance and

lower charging, is used to represent the weak electric coupling between regions.

To obtain the total generation and load capacities for every coherent region, a Python

program was coded to sum up the capacities based on detailed system models. The

equivalent generation and load capacities are listed in Table VI-1.

Since the total generation capacity of a coherent region is much larger than that of a

single generator, it is not appropriate to use one generator to represent the generation in

one region. Therefore, a scaling factor of 100:1 is applied to both generation and load.

The testbed model in PSS/E is shown in Figure VI-5.
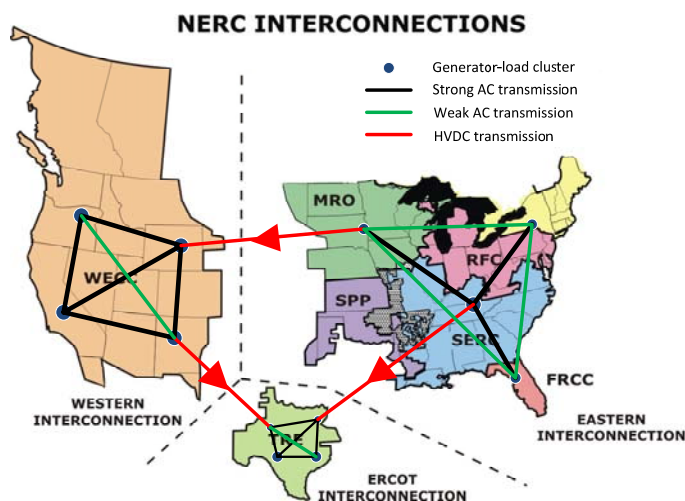
Figure VI-4 Simplified Model Structure

Table VI-1 Generation and Load Capacity of Coherent Regions

Interconnection	Area	Generation Capacity (GW)	Load Capacity (GW)
EI	Central	434.23	431.76
EI	Northwestern	35.08	35.15
EI	Northeastern	81.89	82.05
EI	Florida	39.54	41.79
WECC	Washington	77.60	70.91
WECC	Wyoming	11.88	11.00
WECC	New Mexico	27.28	21.45
WECC	California	37.55	50.93
ERCOT	Northern	15.64	11.11
ERCOT	Houston	9.74	8.02
ERCOT	Southern	1.99	9.24
ERCOT	Western	5.98	4.99
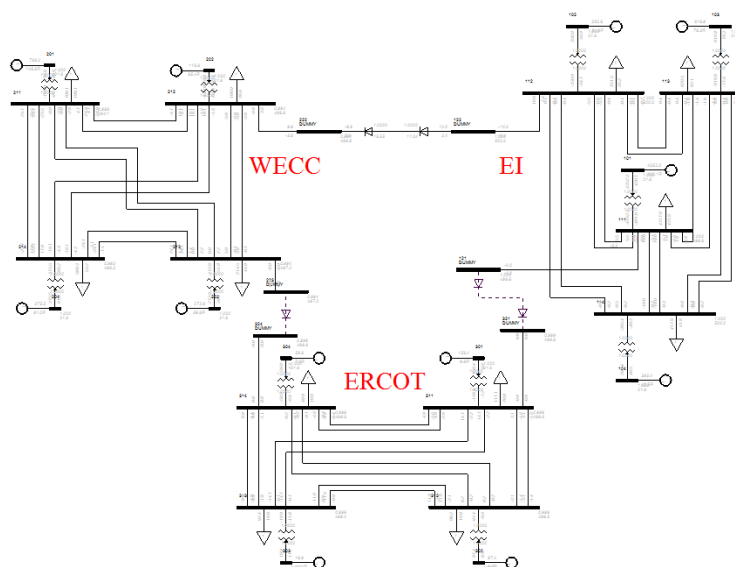
Figure VI-5 Model Structure in PSS/E

To study the dynamic characteristics of the large-scale model, generator, exciter, and governor models are used. All the generators are modeled as round rotor generator with simplified exciter model and steam turbine governor.

To assess the validity of the large-scale model, dynamic simulation is performed. A line fault is created between two coherent regions in the EI system at 1.0 s, and then cleared at 1.2 s. The line fault causes a voltage drop on the HVDC rectifier AC bus, therefore the HVDC shut down during on-fault period. Since the EI system is modeled to output power to the other two interconnections, the line fault results in generation loss within WECC and ERCOT. The generator speed deviation is shown in Figure VI-6 and Figure VI-7.

5.2 The EI 266-bus System

The Eastern Interconnection is the largest synchronized power grid in North America. Simulating the dynamic behavior of such large power grid can be challenging because of model availability, the complexity and volume of the model, and the quality of the dynamics data set. In this study, the goal is to develop a simplified dynamics model for the EI system that conceptually represents the topology and inter-regional behavior. Later, this model was connected with simplified WECC and ERCOT models via HVDC lines. Together, the simplified continental power system models give approximate representation of the national power grid and serve as a major testbed to evaluate transmission overlay plans, renewable impact, and HVDC based frequency controls. This section describes the process of developing the 266-bus EI dynamics model.
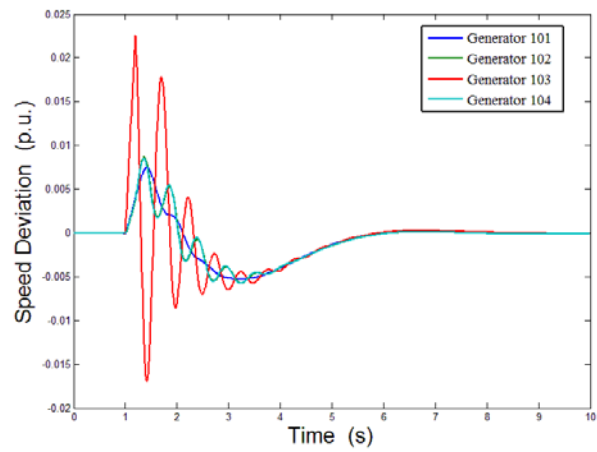
Figure VI-6 Generator Speed Deviation in EI
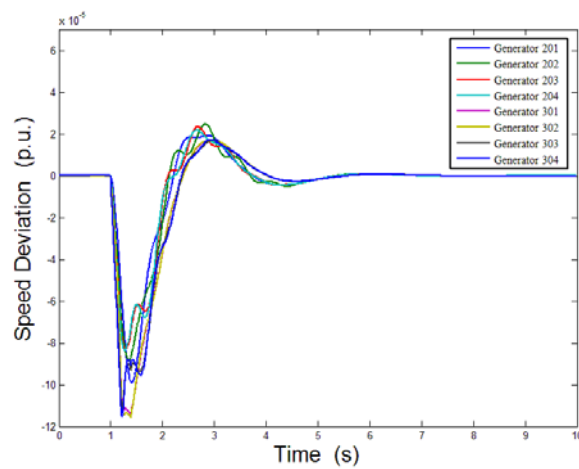
Figure VI-7 Generator Speed Deviation in WECC and ERCOT

The model reduction is based on the concept of balance area, which is a metered segment of the grid where power transfer is maintained. In a balance area, balancing of generation and load is managed by an entity called balancing authority. The balancing authority dispatches generators in order to meet demands. If a mismatch occurs, a real-time value called area control error (ACE) will appear non-zero and Automatic Generation Control (AGC) will be activated to eliminate the control error. There are over one hundred balancing authorities in varying size in North America as shown in Figure VI-8. [93].
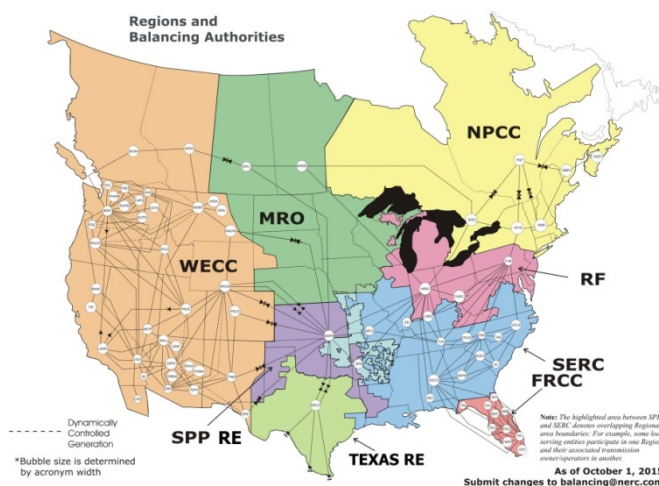
Figure VI-8 Regions and Balancing Authorities in North America

The simplified EI model is obtained through three procedures. First, the generation and load within each balance area is aggregated and represented by a single machine/load cluster (Figure VI-9). Second, equivalent transmission lines are added between balancing areas which have energy interchange. The transmission line impedance is assigned so that the power exchanges between balancing areas are retained. Finally, dynamics models and

parameters for generators are prepared. Testing simulation is conducted and proper

dynamics model adjust is done to ensure the validity of the model. The finalized model is

shown in Figure VI-10. It has 133 generator/load clusters and 266 buses. Generic

generator models are used for dynamic simulation. A testing line fault case is presented

in Figure VI-11. Numerical convergence and reasonable system response are reached.
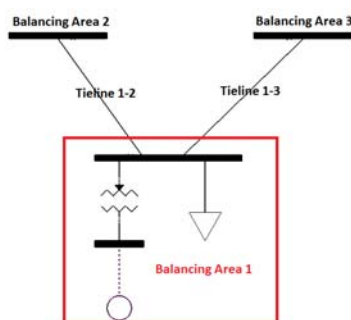
Figure VI-9 A Single Machine/Load Cluster

Figure VI-10 The Structure of the 266-bus System
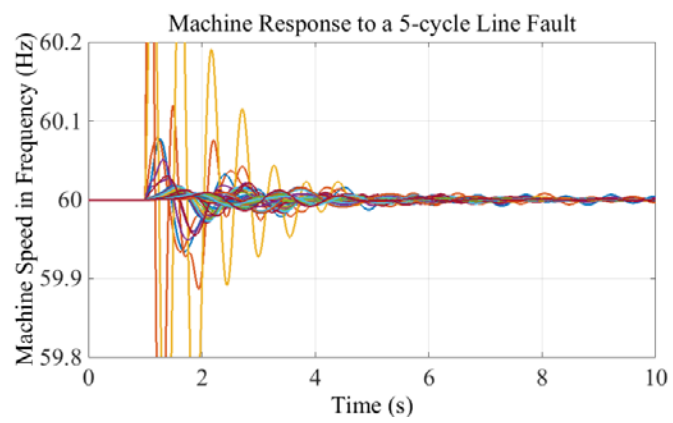
Figure VI-11 System Response to a Line Fault

VII.   Conclusions, Contribution, and Future Work

Extensive power system dynamics modeling, simulation, and renewable integration studies were conducted and the following findings are concluded:

- The numerical performance and simulation accuracy of the EI dynamics models, along with other large-scale power system models, has the potential to be improved. Models that capture the system's critical dynamic behavior will help make better operation and planning decision.

- The impact of governor deadband on the frequency response of the EI system is significant. By representing the deadband effect, enhanced correlation between simulation and measurement can be achieved.

- From the EI 2030 high wind case, the frequency response degradation due to wind generation is acceptable and can be mitigated. Wind penetration could also result in improved rotor angle stability and inter-area oscillation damping.

- Preliminary solar studies indicate that high PV penetration dynamic models can be subject to numerical divergence. Solar generation can also contribute to frequency response degradation and reduced inter-area oscillation damping.

Major contribution of this work includes:

- A systematic approach to develop and validate interconnection-level dynamics models.

- Recognition of governor deadband as a major frequency response factor.

- The application of synchro-phasor measurement in power system dynamics model validation.

- Dynamic stability impact studies of high wind and PV penetration on the EI system.

- Model reduction on the U.S. power grids.

Future work can focus on a more comprehensive renewable impact study by building and analyzing models in different loading conditions, including peak, shoulder, and light cases. Frequency response, rotor angle stability, and oscillations can be studies. Mitigation measures for improved frequency response and damping can be further explored.

Improving dynamics model accuracy is a continuous effort. With the new NERC standards on power system model validation, more industry interests will be drawn to use synchro-phasor measurement to calibrate system models. The ultimate solution to building high accuracy dynamics models is to develop a master dynamic model database and constantly verify and adjust device models against actual events in different system operating conditions.

References

[1]   "Phase 1 Report: Formation of Stakeholder Process, Regional Plan Integration and Macroeconomic Analysis," Eastern Interconnection Planning Collaborative, 2011.

[2]   "Phase 2 Report: DOE Draft – Part 1 Interregional Transmission Development and Analysis for Three Stakeholder Selected Scenarios," Eastern Interconnection Planning Collaborative, 2012.

[3]   P. Kundur, J. Paserba, V. Ajjarapu, G. Andersson, A. Bose, C. Canizares, N. Hatziargyriou, D. Hill, A. Stankovic, C. Taylor, T. Van Cutsem, and V. Vittal, "Definition and classification of power system stability IEEE/CIGRE joint task force on stability terms and definitions," *IEEE Transactions on Power Systems,* vol. 19, pp. 1387-1401, 2004.

[4]   "Frequency Response Initiative Report," North American Electric Reliability Corporation, Atlanta US, 2012.

[5]   "SunShot Vision Study," United States Department of Energy, 2012.

[6]   "2015 Long-Term Reliability Assessment," The North American Electric Reliability Corporation, 2015.

[7]   "Multiregional Modeling Working Group Procedural Manual Version 14," Eastern Interconnection Reliability Assessment Group, 2015.

[8]   "PSS/E 33.1.1 Program Application Guide Volume 2," Siemens Power Technologies International, 2012.

[9]   P. M. Anderson and A. A. Fouad, *Power System Control and Stability*. Ames: The Iowa State University Press, , 1977.

[10]   B. Stott, "Power system dynamic response calculations," *Proceedings of the IEEE,* vol. 67, pp. 219-241, 1979.

[11]   P. Kundur, *Power System Stability and Control*. New York, NY, USA: McGraw-Hill, 1994.

[12]   IEEE, "IEEE Recommended Practice for Excitation System Models for Power System Stability Studies," in *Std. 421.5-1992*, ed, 1992.

[13]   I. C. Report, "Dynamic Models for Steam and Hydro Turbines in Power System Studies," *IEEE Transactions on Power Apparatus and Systems,* vol. PAS-92, pp. 1904-1915, 1973.

[14]   R. P. Schulz, "Modeling of governing response in the Eastern Interconnection," in *Power Engineering Society 1999 Winter Meeting, IEEE*, 1999, pp. 561-566 vol.1.

[15]   L. Chen, P. N. Markham, and Y. Liu, "Wide-area dynamic model validation using FNET measurements," in *2012 IEEE PES Innovative Smart Grid Technologies (ISGT)*, 2012, pp. 1-7.

[16]   L. Pereira, J. Undrill, D. Kosterev, D. Davies, and S. Patterson, "A new thermal governor modeling approach in the WECC," in *Power Engineering Society General Meeting, 2003, IEEE*, 2003, p. 1.

[17]   J. Milanovi, x, K. Yamashita, S. Martinez, S. Djoki, and L. Korunovi, "International industry practice on power system load modelling," in *PES General Meeting | Conference & Exposition, 2014 IEEE*, 2014, pp. 1-1.

[18]   J. M. Undrill and T. F. Laskowski, "Model Selection and Data Assembly for Power System Simulations," *IEEE Transactions on Power Apparatus and Systems,* vol. PAS-101, pp. 3333-3341, 1982.

[19]   "Standard load models for power flow and dynamic performance simulation," *IEEE Transactions on Power Systems,* vol. 10, pp. 1302-1313, 1995.

[20]   F. Milano, *Power System Modeling and Scripting*: Springer, , 2010.

[21]   Y. Zhang, P. Markham, T. Xia, L. Chen, Y. Ye, Z. Wu, Z. Yuan, L. Wang, J. Bank, J. Burgett, R. W. Conners, and Y. Liu, "Wide-Area Frequency Monitoring Network (FNET) Architecture and Applications," *IEEE Transactions on Smart Grid,* vol. 1, pp. 159-167, 2010.

[22]   J. H. Eto, "Use of frequency response metrics to assess the planning and operating requirements for reliable integration of variable renewable generation," Lawrence Berkeley National Laboratory, Berkeley, CA, USA, 2010.

[23]   D. N. Kosterev, C. W. Taylor, and W. A. Mittelstadt, "Model validation for the August 10, 1996 WSCC system outage," *IEEE Transactions on Power Systems,* vol. 14, pp. 967-979, 1999.

[24]   B. Agrawal and D. Kosterev, "Model Validation Studies for a Disturbance Event That Occurred on June 14 2004 in the Western Interconnection," in *Power Engineering Society General Meeting, 2007. IEEE*, 2007, pp. 1-5.

[25]   "Final Report on the August 14, 2003 Blackout in the United States and Canada: Causes and Recommendations," U.S.-Canada Power System Outage Task Force, 2004.

[26]   "Mandatory Reliability Standards for the Bulk-Power System," United States of America Federal Energy Regulatory Commission Order No. 693, 2007.

[27]   "Verification of Models and Data for Generator Excitation Control System or Plant Volt/Var Control Functions," North American Electric Reliability Corporation (NERC) , 2013.

[28]   "Verification of Models and Data for Turbine/Governor and Load Control or Active Power/Frequency Control Functions," North American Electric Reliability Corporation (NERC) , 2013.

[29]   "Steady-State and Dynamic System Model Validation," North American Electric Reliability Corporation (NERC) , 2014.

[30]   "Data for Power System Modeling and Analysis," North American Electric Reliability Corporation (NERC) , 2014.

[31]   L. T. G. Lima, "Dynamic model validation for compliance with NERC standards," in *2009 IEEE Power & Energy Society General Meeting*, 2009, pp. 1-7.

[32]   J. W. Feltes and L. T. G. Lima, "Validation of dynamic model parameters for stability analysis; industry need, current practices and future trends," in *Power Engineering Society General Meeting, 2003, IEEE*, 2003, pp. 1-1301 Vol. 3.

[33]   J. F. Hauer, W. A. Mittelstadt, K. E. Martin, J. W. Burns, H. Lee, J. W. Pierre, and D. J. Trudnowski, "Use of the WECC WAMS in Wide-Area Probing Tests for Validation of System Performance and Modeling," *IEEE Transactions on Power Systems,* vol. 24, pp. 250-257, 2009.

[34]   D. Kosterev and D. Davies, "System model validation studies in WECC," in *IEEE PES General Meeting*, 2010, pp. 1-4.

[35]   D. Kosterev, A. Meklin, J. Undrill, B. Lesieutre, W. Price, D. Chassin, R. Bravo, and S. Yang, "Load modeling in power system studies: WECC progress update," in *Power and Energy Society General Meeting - Conversion and Delivery of Electrical Energy in the 21st Century, 2008 IEEE*, 2008, pp. 1-8.

[36]   L. Pereira, D. Kosterev, D. Davies, and S. Patterson, "New thermal governor model selection and validation in the WECC," *IEEE Transactions on Power Systems,* vol. 19, pp. 517-523, 2004.

[37]   J. Undrill, L. Pereira, D. Kosterev, S. Patterson, D. Davies, S. Yang, and B. Agrawal, "Generating unit model validation: WECC lessons and moving forward," in *2009 IEEE Power & Energy Society General Meeting*, 2009, pp. 1-5.

[38]   "Power System Model Validation," North American Electric Reliability Corporation (NERC) 2010.

[39]   L. Yilu, "A US-wide power systems frequency monitoring network," in *2006 IEEE Power Engineering Society General Meeting*, 2006, p. 8 pp.

[40]   N. W. Miller, M. Shao, S. Pajic, and R. D'Aquila, "Eastern Frequency Response Study," GE Energy, Schenectady2013.

[41]   J. Undrill, "Power and frequency control as it relates to wind-powered generation," John Undrill LCC, 2010.

[42]   B. P. Vitalis, "Constant and sliding-pressure options for new supercritical plant," *Power*.

[43]   G. Kou, J. Culliss, P. Markham, Y. Liu, S. Hadley, J. Stovall, and T. King, "Developing generic dynamic models for the 2030 Eastern Interconnection grid," in *2014 IEEE PES T&D Conference and Exposition*, 2014, pp. 1-5.

[44]   A. Ellis, D. Kosterev, and A. Meklin, "Dynamic Load Models: Where Are We?," in *2005/2006 IEEE/PES Transmission and Distribution Conference and Exhibition*, 2006, pp. 1320-1324.

[45]   "Composite load model for dynamic simulations Report 1.0," Western Electricity Coordinating Council (WECC) Modeling and Validation Work Group (MVWG), 2012.

[46]   Y. Zhang, Y. Liu, L. Chen, and J. Guo, "Visualization of distribution level voltage magnitude pattern trend in EI system using FNET data," in *2014 IEEE PES T&D Conference and Exposition*, 2014, pp. 1-5.

[47]   "New thermal turbine governor modeling for the WECC," Western Electricity Coordinating Council (WECC) Modeling and Validation Work Group (MVWG), 2002.

[48]   T. F. o. T.-G. Modeling, "Dynamic models for turbine-governors in power system studies," IEEE Power & Energy Society, 2013.

[49]   "Global Wind Energy Outlook 2014," Global Wind Energy Council, 2014.

[50]   "U.S. Wind Industry Fourth Quarter 2014 Market Report," American Wind Energy Association2015.

[51]   "20% Wind Energy by 2030: Increasing Wind Energy's Contribution to U.S. Electricity Supply," The U.S. Department of Energy, July 2008.

[52]   "Annual Energy Outlook 2014," [4]   U.S. Energy Information Administration, 2014.

[53]   "Interconnected power system response to generation governing: present practice and outstanding concerns," IEEE Power & Energy Society, 2007.

[54]   N. A. E. R. C. (NERC), "BAL-003-1 Frequency Response and Frequency Bias Setting," ed, , 2014.

[55]   G. Kou, P. Markham, S. Hadley, T. King, and Y. Liu, "Impact of Governor Deadband on Frequency Response of the U.S. Eastern Interconnection," *IEEE Transactions on Smart Grid,* vol. PP, pp. 1-1, 2015.

[56]   E. Ela, "Active Power Controls from Wind Power: Bridging the Gaps," National Renewable Energy Laboratory, Denvor, CO, 2014.

[57]   "Primary Frequency Response Requirement from Existing WGRs," Electric Reliability Council of Texas (ERCOT), 2010.

[58]   "EirGrid Grid Code Version 5.0," EirGrid, 2013.

[59]   "Transmission Provider Technical Requirements for the Connection of Power Plants to the Hydro-Quebec Transmission System," Hydro-Quebec, 2009.

[60]   N. W. Miller, "Western Wind and Solar Integration Study Phase 3–Frequency Response and Transient Stability," GE Energy Management, 2014.

[61]   N. A. E. R. C. (NERC), "BAL-001-TRE-1 Primary Frequency Response in the ERCOT Region," ed, , 2012.

[62]   E. Ela, V. Gevorgian, A. Tuohy, B. Kirby, M. Milligan, and M. O. Malley, "Market Designs for the Primary Frequency Response Ancillary Service—Part I: Motivation and Design," *IEEE Transactions on Power Systems,* vol. 29, pp. 421-431, 2014.

[63]   R. Wiser and M. Bolinger, "2014 Wind Technologies Market Report," Lawrence Berkeley National Laboratory, Berkeley, California2015.

[64]   "U.S. Wind Industry Third Quarter 2015 Market Report," American Wind Energy Association, 2015.

[65]   E. Vittal, M. O. Malley, and A. Keane, "Rotor Angle Stability With High Penetrations of Wind Generation," *IEEE Transactions on Power Systems,* vol. 27, pp. 353-362, 2012.

[66]   M. Edrah, K. L. Lo, and O. Anaya-Lara, "Impacts of High Penetration of DFIG Wind Turbines on Rotor Angle Stability of Power Systems," *IEEE Transactions on Sustainable Energy,* vol. 6, pp. 759-766, 2015.

[67]   G. Tsourakis, B. M. Nomikos, and C. D. Vournas, "Contribution of Doubly Fed Wind Generators to Oscillation Damping," *IEEE Transactions on Energy Conversion,* vol. 24, pp. 783-791, 2009.

[68]   D. Gautam, V. Vittal, and T. Harbour, "Impact of Increased Penetration of DFIG-Based Wind Turbine Generators on Transient and Small Signal Stability of Power Systems," *IEEE Transactions on Power Systems,* vol. 24, pp. 1426-1434, 2009.

[69]   J. Quintero, V. Vittal, G. T. Heydt, and H. Zhang, "The Impact of Increased Penetration of Converter Control-Based Generators on Power System Modes of Oscillation," *IEEE Transactions on Power Systems,* vol. 29, pp. 2248-2256, 2014.

[70] G. Kou, Y. Liu, S. Hadley, and T. King, "Developing dynamic models for the 2030 Eastern Interconnection grid," in *2014 IEEE PES General Meeting Conference & Exposition*, 2014, pp. 1-5.

[71] G. Kou, M. Till, T. Bilke, S. Hadley, Y. Liu, and T. King, "Primary Frequency Response Adequacy Study on the U.S. Eastern Interconnection Under High-Wind Penetration Conditions," *IEEE Power and Energy Technology Systems Journal,* vol. 2, pp. 125-134, 2015.

[72] Y. Liu, L. Zhan, Y. Zhang, P. N. Markham, D. Zhou, J. Guo, Y. Lei, G. Kou, W. Yao, and J. Chai, "Wide-Area-Measurement System Development at the Distribution Level: An FNET/GridEye Example," *IEEE Transactions on Power Delivery,* vol. 31, pp. 721-731, 2016.

[73] J. C. Mantzaris, A. Metsiou, and C. D. Vournas, "Analysis of Interarea Oscillations Including Governor Effects and Stabilizer Design in South-Eastern Europe," *IEEE Transactions on Power Systems,* vol. 28, pp. 4948-4956, 2013.

[74] S. Stavrinos, A. G. Petoussis, A. L. Theophanous, S. Pillutla, and F. S. Prabhakara, "Development of a validated dynamic model of Cyprus Transmission system," in *7th Mediterranean Conference and Exhibition on Power Generation, Transmission, Distribution and Energy Conversion (MedPower 2010)*, 2010, pp. 1-11.

[75] K. Clark, N. Miller, and J. Sanchez-Gasca, "Modeling of GE Wind Turbine-Generators for Grid Studies," General Electric International, Inc., 2010.

[76] P. Pourbeik, "Specification of the Second Generation Generic Models for Wind Turbine Generators," Western Electricity Coordinating Council, 2014.

[77] M. L. Crow and A. Singh, "The matrix pencil for power system modal extraction,"*, IEEE Transactions on Power Systems,* vol. 20, pp. 501-502, 2005.

[78] "U.S. Solar Market Insight 2015 Year in Review," Solar Energy Industries Association, 2016.

[79] *Interconnection Frequency Response*. Available: http://www.nerc.com/pa/RAPA/ri/Pages/InterconnectionFrequencyResponse.aspx

[80] N. W. Miller, R. Walling, M. Shao, and J. MacDowell, "Modeling of GE Solar Photovoltaic Plants for Grid Studies," Schenectary, NY, 2011.

[81] R. Elliott, R. Byrne, A. Ellis, and L. Grant, "Impact of increased photovoltaic generation on inter-area oscillations in the Western North American power system," in *2014 IEEE PES General Meeting | Conference & Exposition*, 2014, pp. 1-5.

[82] S. Eftekharnejad, V. Vittal, G. T. Heydt, B. Keel, and J. Loehr, "Small Signal Stability Assessment of Power Systems With Increased Penetration of Photovoltaic Generation: A Case Study," *IEEE Transactions on Sustainable Energy,* vol. 4, pp. 960-967, 2013.

[83] U. D. Annakkage, N. K. C. Nair, Y. Liang, A. M. Gole, V. Dinavahi, B. Gustavsen, T. Noda, H. Ghasemi, A. Monti, M. Matar, R. Iravani, and J. A. Martinez, "Dynamic System Equivalents: A Survey of Available Techniques," *IEEE Transactions on Power Delivery,* vol. 27, pp. 411-420, 2012.

[84] I. J. Perez-arriaga, G. C. Verghese, and F. C. Schweppe, "Selective Modal Analysis with Applications to Electric Power Systems, PART I: Heuristic Introduction," *IEEE Transactions on Power Apparatus and Systems,* vol. PAS-101, pp. 3117-3125, 1982.

[85] G. C. Verghese, I. J. Perez-arriaga, and F. C. Schweppe, "Selective Modal Analysis With Applications to Electric Power Systems, Part II: The Dynamic Stability Problem," *IEEE Transactions on Power Apparatus and Systems,* vol. PAS-101, pp. 3126-3134, 1982.

[86] S. E. M. d. Oliveira and J. F. d. Queiroz, "Modal dynamic equivalent for electric power systems. I. Theory," *IEEE Transactions on Power Systems,* vol. 3, pp. 1723-1730, 1988.

[87] S. E. M. d. Oliveira and A. G. Massaud, "Modal dynamic equivalent for electric power systems. II. Stability simulation tests," *IEEE Transactions on Power Systems,* vol. 3, pp. 1731-1737, 1988.

[88] W. W. Price, A. W. Hargrave, B. J. Hurysz, J. H. Chow, and P. M. Hirsch, "Large-scale system testing of a power system dynamic equivalencing program," *IEEE Transactions on Power Systems,* vol. 13, pp. 768-774, 1998.

[89] J. H. Chow, R. Galarza, P. Accari, and W. W. Price, "Inertial and slow coherency aggregation algorithms for power system dynamic model reduction," *IEEE Transactions on Power Systems,* vol. 10, pp. 680-685, 1995.

[90] R. J. Newell, M. D. Risan, L. Allen, I. S. Rao, and D. L. Stuehm, "Utility Experience With Coherency-Based Dynamic Equivalents Of Very Large Systems," *IEEE Transactions on Power Apparatus and Systems,* vol. PAS-104, pp. 3056-3063, 1985.

[91] L. Wang, M. Klein, S. Yirga, and P. Kundur, "Dynamic reduction of large power systems for stability studies," *IEEE Transactions on Power Systems,* vol. 12, pp. 889-895, 1997.

[92] A. M. Stankovic and A. T. Saric, "Transient power system analysis with measurement-based gray box and hybrid dynamic equivalents," *IEEE Transactions on Power Systems,* vol. 19, pp. 455-462, 2004.

[93] "Balancing and Frequency Control," North American Electric Reliability Corporation (NERC), Princeton, NJ, 2011.

Vita

Gefei "Derek" Kou received his B.S. from Tianjin University in 2011. He later received M.S. and Ph.D. in Electrical Engineering from the University of Tennessee, Knoxville, in 2014 and 2016. His research concentration is on power system dynamic modeling and renewable integration. He is a member of the IEEE Power & Energy Society.